Rice University

Key steps towards carbon nanotube-based conductors

by

Yao Zhao

A THESIS SUBMITTED
IN PARTIAL FULFILLMENT OF THE
REQUIREMENTS FOR THE DEGREE

Doctor of Philosophy

Approved, Thesis Committee:

Enrique V. Barrera, Committee Chair
Professor of Mechanical Engineering &
Materials Science

Pulickel M. Ajayan
Professor of Mechanical Engineering &
Materials Science

Jun Lou
Assistant Professor of Mechanical
Engineering & Materials Science

Ed Billups
Professor of Chemistry

Houston, Texas

August 2011

Abstract

Key steps towards carbon nanotube-based conductors

By

Yao Zhao

Making a robust carbon nanotube-based conductor as a replacement of copper in electricity grids can initiate a paradigm shift in energy transmission. This dissertation identifies four fundamental factors for making carbon nanotube-based conductors as functionalization, dispersion, concentration and processing. These four factors are discussed in detail by studying four separate systems: nanotube/epoxy composites, nanotube/porous medium density polyethylene (MDPE) composites, nanotube/high density polyethylene (HDPE) composites and pure nanotube cables.

In nanotube/epoxy composites, homogeneous dispersion of nanotubes and a strong interface between nanotubes and epoxy matrix were simultaneously achieved through the development of a novel nanotube functionalization. While the degree of functionalization was high, the process was non-destructive to the mechanical properties of the nanotubes. In addition, the functional groups constructed covalent bonds with the epoxy matrix and also made dispersing the nanotubes much easier. As a result, the composites reinforced by the functionalized nanotubes had better mechanical properties than the samples reinforced by the raw nanotubes.

In nanotube/porous MDPE composites, the degree of nanotube dispersion reached a level of 1 micron for nanotube agglomerate size within the matrix. This successful dispersion

was primarily attributed to creating the porous MDPE. The pore size was tuned to be as small as 1 micron so that the sub-micron long HiPco nanotubes could easily penetrate into the matrix. The nanotube/porous MDPE composites obtained enhancement both in mechanical strength and electrical conductivity compared to the control samples.

In nanotube/HDPE composites, the nanotube conducting networks were studied. Conductivity of the composites with the loading ratio at the percolation threshold was not sufficiently high for conductor applications. Nanotube/HDPE composite wires with higher loading ratios up to 40 wt% were prepared. Key factors for improving the formation of the conducting networks were identified. Through optimization in processing, maximum conductivity of $\sim 10^3$ S/m was achieved.

Pure nanotube cables were prepared by a solid spinning procedure, which showed the potential to make macroscopic cables of various length and thickness. The pure nanotube cables circumvented the bottleneck in improving conductivity for composite systems, in which polymer in-between the nanotubes caused high contact resistance. The pure nanotube cables reached conductivity as high as $\sim 10^6$ S/m. Through iodine doping, conductivity further was enhanced so that the specific conductivity of the doped cables exceeded that of metals such as copper.

As a result of applying the knowledge learned from study of the four fundamental factors, a macroscopic carbon-nanotube cable was created. It reached an unprecedented conductivity as high as $\sim 10^7$ S/m. Mechanically it was more robust than steel, but with 1/6 the weight. This advanced nanotube-based conductor can have a wide spectrum of applications such as transmission lines and low dimensional connecting wires.

Acknowledgements

Firstly, I would like to thank my advisor, Dr. Barrera. Thank you for giving me the opportunity to study at Rice. Thanks for always being supportive along the whole process I pursued the Ph.D. degree. When I started the research, you encouraged me to think outside the box and gave me freedom to choose my own direction. When I wanted to apply what I learned from the lab to the real world, you supported me to do internships with Baker Hughes and Schlumberger. When I would like to extend my research to the next horizon, you sent me to China for research collaborations. Without these rentless supports, I could not finish this dissertation today.

I am grateful to my committee members, Dr. Ajayan, Dr. Lou and Dr. Billups for readily agreeing to be on my committee and your valuable suggestions on my research. Special thanks to Dr. Ajayan and Dr. Robert for helping me out for the nanotube cable project. My sincere thanks to Dr. Lou, Dr. Loos, Dr. Mclellan, Dr. Brotzen and Dr. Yakobson for passing on knowledge through your courses. Thanks to MEMS department staff: Maria, Alicia, Gary, Linda, Lisa, Sherry for your kind love and support.

I would like to thank Barrera group: Jonny, Andres, Luke, Suman, Padraig, Dyvia, Jennifer, Marvin, Sukesh, Xiaobo, Jaime and Laura for your support and friendship. With you being around, I obtained the courage for conquering any difficulty in research. I also would like to appreciate my friends in MEMS department: Xiaoge, Yue Huang, Yang Lu, Hao Lu, Yogi, Wei Gao, Cheng Peng, Jiangnan, Jianxin, Fangbo, Yuanyue, Daneil, Philip, Zheng, Lulu and mingjie for your support and love. Thanks to my friends at Rice and in Houston: Jun Yao, Haiyang, Zhengzong Sun, Hao Sun, Yu Pu, Jingbo, Nina, Yanli,

Rui, Jiajie, Michael, Yaming, C.J. and Jason. You have been my family away from home. Thank you Nanoridge team: Lori, Kyle, Chris for your generous support and helpful discussions. Thanks to James Huang at Boeing Inc. for providing me with insightful suggestions on research. Thanks to Prof. Jinquan Wei, Prof. Hong Lin at Tsinghua University for your help and input on my research and kind host for my trip to Beijing. I would like to thank my bachelor research advisor Prof. Pan at Wuhan University and master research advisor Prof. Sellmyer at University of Nebraska. Without their help, I could not shape my life to this point. Thanks to my special 71-years-old friend, Frank for teaching me knowledge in all aspects of life. You have been my life coach. Of course, I would like to thank my classmates in elementary school and high school: Tracy Wang, Huasong, Xueting, Mingxing, Kai, Wei, Song, and Yao Cheng for your company and encouragement through so many years. Also thanks to my college buddies: Yiqun, Huatao, Xi Zhang, Shaoding, Rui Liu, Xin Li, Xu Zhang, Yong Wang, Yong Zhou, Lei An, Xiao Shen, Ying Jia, Jing Li, Di Wang, Mark Wu, Lei Liao, Jingle, Daowen, Feng Zheng, Yinfu Hu and Liangwen for your love. You guys have been awesome. The wonderful memories with you I would cherish forever. Thanks to my friends at Vancouver and Nebraska: Yi, Zhiyi, Shun, Zhihao, Qing, Xiang, Ning, Yushun, Ah Sui and Nan. Because of you, my life journey was such a pleasant experience. Qing, our ski trips should go on. I hope we can do a helicopter drop one day. Ah Sui, your work and personal ethics always inspired me and helped me grow.

Particularly I would like to thank Qi for the friendship which has been built since when we were born and will last forever.

Lastly, I would like to thank my family. Thanks to all my uncles and aunts, and to my cousins. Whereever I go, your love makes me feel that home is always the warmest place and the harbor for my soul.

Finally, my eternal love and gratitude to my parents. Mom and Dad, you are the most important people in my life. You have been always there and believing in me. Thanks for your unconditional love and support. I love you!

I know how lucky I am to have all of you in my life. This work wouldn't have been possible without all of you. Thank you!

Contents

List of Tables

List of Figures

Nomenclature

CVD	Chemical Vapor Deposition
CNTs	Carbon nanotubes
DGEBA epoxy	diglycidyl ether of biphenol A epoxy
DMA	Dynamical Mechanical Analysis
DMF	Dimethylformamide
DSC	Differential Scanning Calorimetry
DWNTs	Double-walled carbon Nanotubes
EMI	Electromagnetic interference
ESD	Electrostatis discharge
GIF	Gatan Imaging Filter
HiPco	High-pressure carbon monoxide conversion
HDPE	High Density Polyethylene
MDPE	Medium Density Polyethylene
MWNTs	Multi-walled carbon nanotubes
PC	Polycarbonate
SEM	Scanning Electron Miscroscopy
TEM	Transmission Electron Microscopy
TGA	Thermogravimetric analysis
VRH	Variable Range Hopping
XPS	X-ray Photoelectron Spectrum

Chapter 1: Introduction

Fully utilizing the superior properties of nanotubes in nanotube composites has been a grand challenge [1]. To efficiently transfer the strength of nanotubes to the matrix, a strong interface between nanotubes and matrix is required [2-4]. The pristine nanotube has an inert graphene layer as the outer wall [5], which is not easy to construct strong bonds with the matrix. To creat a strong interface, nanotubes are normally functionalized before they are added into the matrix [6-10], especially when enhancing the mechanical properties is the primary objective. However, when electrical conductivity is the primary concern in a composite, functionalization is no longer a good choice because it degrades electrical conductivity of nanotubes in most circumstances [6, 11-12]. Functionalization can be a double-edged sword in making a composite. Whether we need to apply it in processing depends on what function the final product will serve. Here the concept of "function-oriented processing" is brought up; it means that the processing needs to be deliberately designed based on the functions we are looking for. "functioin-oriented processing" is reflected all through from chapter 3 to 6 in four different macroscopic systems covered in this dissertation.

In chapter 3, improving the mechanical performance of epoxy was the major target. Based on this target, amino functionalized nanotubes were added into the epoxy matrix [13]. Choosing amino functional groups was majorly based on two thoughts. First, the amino groups cause nanotubes be better dispersed in the matrix. Second, the amino groups construct robust covalent bonds with the epoxy by ring-opening etherification. Good dispersability and strong bond with the matrix are the prerequisites for realizing the

efficient load transfer from nanotubes to the matrix, and hence achieving the desired mechanical performance in the nanotube/epoxy composites.

In chapter 4, multifunctional composites with high strength and electrical conductivity were pursued [14]. To avoid the degradation in conductivity caused by functionalization, the raw HiPco nanotubes were added into MDPE matrix. The dispersion of the nanotubes was majorly attributed to creating a unique porous structure for MDPE. The pore size, 1micron in diameter, had a good match with the sub-micron average length of the HiPco nanotubes. The nanotubes easily penetrated into the pores, and as a result, the degree of dispersion reached the level of sub-micron. Both the mechanical strength and electrical conductivity were greatly improved in the HiPco nanotube/porous MDPE composites compared to the matrix materials.

In chapter 5, the goal was mass production of nanotube/HDPE composites used as the conducting wires. Here electrical conductivity was the major concern. Due to cost consideration, multiwalled nanotubes (Manufactured by Bayer Inc.) were used as the fillers. The nanotubes were dispersed into the HDPE by the melt mixing, and then the nanotube/HDPE masterbatch was made into the continuous wires by melt spinning. Through study of the conductivity mechanism [15-18], the major difficulty in improving conductivity was identified as minimizing the contact resistance between nanotubes. The origin of the contact resistance was mainly the polymers wrapped around the nanotubes [19-23]. To overcome the difficulty, it triggered the research in chapter 6.

Chapter 6 introduces the preparation of a macroscopic cable purely assembled from nanotubes [24-30]. The nanotube type, processing procedures and the conditioning on the as-prepared cables were found to be critical factors for obtaining high conductivity. The

iodine doped DWNT (double-walled carbon nanotube) cable has conductivity of $6.6*10^6$ S/m. Its specific conductivity, $1.96*10^4$ $S.m^2/kg$ (the ratio of conductivity to density) outperforms all metals except sodium. Due to the superior properties of the cable such as high specific conductivity, corrosion-resistance and high strength, it would have a wide range of applications. Some possible applications for the cables are transmission lines in electricity grids, conducting wires for aerospace or auto industry and low dimensional connecting wires in electronics.

Chapter 7 presents the overall conclusions of this dissertation along with suggestions for the future works. The whole dissertation bears the concept of "function-oriented processing" as the backbone and shows the efforts for making a macroscopic carbon nanotube-based conductor. Filling the gap between the nano and macro extends the application domain of nanotechnology, enables nanotechnology make broader impacts, and provides far-reaching benefits to mankind.

Chapter 2: Background on carbon nanotubes and their applications

Carbon nanotubes have raised great interests from research communities since the pioneering work by Iijima in 1991 [31]. Knowledge on carbon nanotubes has been built up over the last decade through intensive research [5, 32-45]. Early research was focused on preparing the nanobubes and understanding their properties [46-54]. As the more fundamental understandings on nanotubes have been accumulated, developing the applications of nanotubes becomes increasingly important and practical. In general, nanotubes have been applied in two types of systems: microscopic systems such as microsensors, microchips as well as molecular electronics and macroscopic systems such as composites, bucky papers as well as continuous fibers [55-70]. This dissertation is focus on nanotubes' applications in macroscopic systems.

2.1 Nanotube composites

Composites are materials made from two or more constituent materials with significantly different physical or chemical properties which remain separate and distinct at the macroscopic or microscopic scale within the finished structure [71]. There are mainly three types of composites categorized by the matrix materials: polymer matrix, metal matrix and ceramic matrix composites. Nanotubes are considered as the "ultimate filler" in composites because of its high aspect ratio and exceptional physical properties [72-74]. However, there are many challenges in fully taking advantage of the unique properties of nanotubes in composites. Challenges would differ when using different matrix in

composites. The more in-depth discussions of those challenges in the specific systems and the solutions for resolving the challenges will be covered from chapter 3 to chapter 6. The following paragraphs briefly discuss the general challenges due to nanotubes.

Nanotube growth is very sensitive to a variety of factors, such as carbon source, carrying gas, catalyst, temperature, pressure, and reaction time [75-78]. A slight fluctuation in any of these factors during the growth could result in variations in nanotube products. Nanotubes from most suppliers, even those from the same batch, are diverse by length, diameter, wall numbers, and chirality. The diversity causes difficulties in the composite processing. Take making nanotube/HDPE composites by melt mixing as an example, a certain combination of mixing time, temperature and rotation speed is optimal for dispersing nanotubes of a certain length and diameter. If the nanotubes were diverse in length and diameter, it would result that only a portion of nanotubes would have an optimal match with the processing conditions and could be well dispersed. The remaining portion of nanotubes could form agglomerates and degrade the properties. Therefore, the demand for producing uniform nanotubes is pressing.

Other than accurate control of length and diameter, the other challenge is mass production of the pure metallic nanotubes [79-83]. This issue is very critical for making conductive composites because the metallic tube-to-metallic tube contact has much lower resistance than that of the semiconducting tube-to-semiconducting tube contact [17]. If these challenges were overcome, the pace for improving electrical conductivity of

nanotube composites would be boosted. In addition, longer nanotubes are preferred for being used as fillers in conductive composites because fewer nanotube-nanotube contacts would be introduced when using longer tubes than shorter ones to construct a conducting path [19].

For use as mechanical reinforcements, long nanotubes are desirable too [72, 84-87]. The major failure mechanism in the nanotube composites is nanotube pulling-out instead of nanotube fracture [18]. Nanotubes of length over the critical value can be fractured when the composites are broken, however most commercial nanotubes are too short to reach the critical length so that the mechanical strength of nanotubes is not fully transferred to the matrix.

The following gives a summary of the challenges in nanotube growth. By resolving them, both the mechanical and electrical performances of nanotube composites can be greatly enhanced.

- Grow nanotubes with uniform diameter, length as well as wall numbers.
- Produce pure metallic nanotubes at large scale.
- Prepare ultra-long nanotubes massively.

2.2 Macroscopic nanotube fibers

Energy ranks first in the list of grand challenges for next 50 years [20]. The life cycle of energy includes production, storage, transmission and consumption. Researchers have

been trying to resolve the grand challenge in every phase of the energy life cycle. Tremendous efforts have been devoted for producing renewable energy and enhancing the production of traditional energy. A number of batteries, supercapacitors and other devices have been developed for energy storage [21]. Many methodologies have been created for improving the efficiency in using energy. Currently the infrastructure for energy transmission is electricity grids, in which copper is the major carrier. In 2001, Rick E. Smalley proposed that the nanotube cables can be used as a replacement for copper and initiate a paradigm shift in energy transmission [22]. The proposed ideal energy transmission line, so called armchair nanotube quantum wire, is assembled from the pure armchair nanotubes. The nanotubes are packed into a crystal structure, within which all nanotubes are oriented in one direction. Theoretically the ideal structure is predicted to have the following superior properties:

- 10x copper conductivity
- 6x lighter
- Stronger than steel
- Zero thermal expansion

Due to the difficulties in mass production of armchair nanotubes, the macroscopic nanotube cables, either assembled by multi-walled nanotubes or HiPco single-walled nanotubes [24, 27, 103-109], have conductivity far smaller than the expected performance of the ideal "quantum wire". In chapter 6 of this dissertation, the progress made by the author towards carbon nanotube-based conductors will be presented.

For the four projects covered by this dissertation, five types of nanotubes have been used. The key features for those nanotubes are listed in table 2.1.

Table 2.1. Five types of nanotubes used in the research covered by this dissertation and key features about these nanotubes.

Name	Description	Manufacturer	Diameter/length	Metallic or semiconducting	Cost level
XD nanotube	A mixture of 1/3 single-walled and 2/3 multiwalled	Unidym	1 nm~20 nm/NA	Mixture	low
HiPco nanotube	Single-walled	Unidym	~1 nm/sub-micron	Mixture	high
CG nanotube	Single-walled	Southwest	~1 nm/NA	Mixture	moderate
Bayer nanotube	Multi-walled	Bayer	1 nm~30 nm/NA	Mixture	low
Double-walled nanotubes	Double-walled	Tsinghua University	2~3 nm/>10 microns	Mixture	home-made

Chapter 3: Asymmetric diamino functionalization of nanotubes assisted by BOC protection and their epoxy nanocomposites body

3.1 Introduction

3.1.1 Nanotube/epoxy composites

Theoretically, carbon nanotubes have tensile modulus and strength as high as 1 TPa and 150 GPa, respectively. Therefore, carbon nanotubes have been termed the "ultimate fiber" that is promising as a reinforcement in polymer composites [31, 36]. Epoxy resin is the most common class of thermosetting resin used in a wide range of applications because of its high tensile strength, low shrinkage in curing, and good chemical and corrosion resistance [23]. Carbon nanotube/epoxy composites incorporate the properties of both elements and have attracted intense interest among researchers [2, 3, 74, 111-112]. However, fabricating high quality carbon nanotube/epoxy composites is challenging. A carbon nanotubes/epoxy blend usually has a very high viscosity particularly when fabricating composites with high concentration of nanotubes. In the viscous mixture, dispersing nanotubes is difficult. Furthermore, because of the atomically smooth surface of the nanotubes, the lack of interfacial bonding limits load transfer from the matrix to nanotubes. Functionalization on the nanotubes has proven an efficient way to resolve these problems and hence improve the mechanical properties of the nanotube-reinforced composites.

3.1.2 Physical and chemical functionalization on nanotubes

A variety of chemical and physical functionalizations have been developed [24]. Copolymers with a lyophobic and a lyophilic part are usually used in non-covalent functionalizations, in which the lyophobic part adsorbs onto the surface of nanotubes, while the lyophilic part is incorporated into the matrix. The repulsion among the lyophilic blocks overcome the van der Waals forces between the nanotubes and separates the nanotubes. This non-covalent functionalization can reduce nanotube agglomerates and improve interfacial bonding while still retaining nanotubes intrinsic structure, but non-covalent methods are, in general, not as effective in yielding a system that adheres as well as a functionalized system. Oxidation is one of the most widely used covalent functionaliztion methods. A number of functional groups have been produced on oxidized SWNTs, such as hydroxyl, carbonyl, ester, ether and carboxyl [25]. The oxygen-containing functional groups effectively improve the exfoliation and interfacial bonding in the polymer matrix. However, the oxidization process brings defects to the nanotubes and degrades their mechanical properties. The chemical technique available for modifying the nanotube surface without disrupting its tubular structure is very restrictive. To date, several functionalizations of free radical addition were reported and some chemical groups can be grafted onto the sidewall of nanotubes without introducing sidewall defects [26]. Apart from free radical addition, fluorination is another functionalization method without reduction in nanotube length. Fluorine atoms can be very densely adhered to the nanotubes. For single walled carbon nanotubes, the atomic ratio of the fluorine to carbon can be as high as 1:2. The subsequent substitution

reactions derived from fluoronanotubes are efficient so a significant amount of functional groups can be easily attached to the nanotube [27].

It was reported that fluorine atoms on the fluoronanotubes can be substituted by amino groups under mild heating in an ambient environment [27]. Moreover, it is known that amino groups can fuse with the epoxy matrix by ring-opening etherification and create robust covalent bondings [28]. Intuitively, diamine chains with one end linked to the sidewall of a nanotube by a fluorine substitution reaction and the other end covalently bonded to the epoxy is desirable for enhancing dispersion and creating strong interfacial bonding in the epoxy composite. In our work, we initially used a symmetric diamine structured molecule, NH_2-$(CH_2)_6$-NH_2. In the fluorine substitution reaction, both amino groups on the two ends of the molecule react with the fluorines. Then, amino groups are not available for the subsequent etherification reaction with the epoxy matrix (The nanotubes acquired from the reaction with the symmetric diamine molecules are denoted as Di-nanotubes shown in scheme 1). In order to circumvent this problem, we applied an asymmetric diamine molecule, BOC-NH-$(CH_2)_6$-NH_2, as the fluorine substitution agent. The BOC group is commonly used for protecting peptides in the pharmaceutical industry [29]. In the initial stage, almost all the fluorine atoms on the sidewall of the fluoronanotube were removed, and amino groups on the unprotected end were covalently bonded to the nanotube wall. Afterwards, a BOC de-protection reaction was conducted in which BOC groups were dissociated from molecular chains, and the amino groups on the end were exposed for the subsequent etherification reaction with the epoxy matrix (The nanotubes obtained after the fluorine substitution and de-BOC reactions are denoted

as BOC-nanotubes shown in scheme 2). Following the substitution and de-BOC reactions, the functionalized nanotubes were mixed with the epoxy matrix through processing optimization. The resulting composite showed 30 % increase in the tensile strength with 0.5 wt %* loading compared to the neat epoxy resin (The asterisk indicates that the nanotube concentration is held constant yet the total weight % increases as a function of the functionalization used). This enhancement is similar to that reached by Zhu et al.'s previous work [28]. They used a symmetric diamine molecule to graft onto the oxidized nanotubes with carboxyl groups. The excessive amino moieties make the functionalized nanotubes covalently integrate into the epoxy matrix. The composite prepared through this functionalization acquires 30 % increase in tensile strength with 1 wt % loading. In our present work, fewer nanotubes are needed to obtain the similar level of enhancement in the mechanical property. This improvement might be ascribed to the nanotubes that are derived from asymmetric diamine molecules having better dispersion and cross linking with the epoxy matrix.

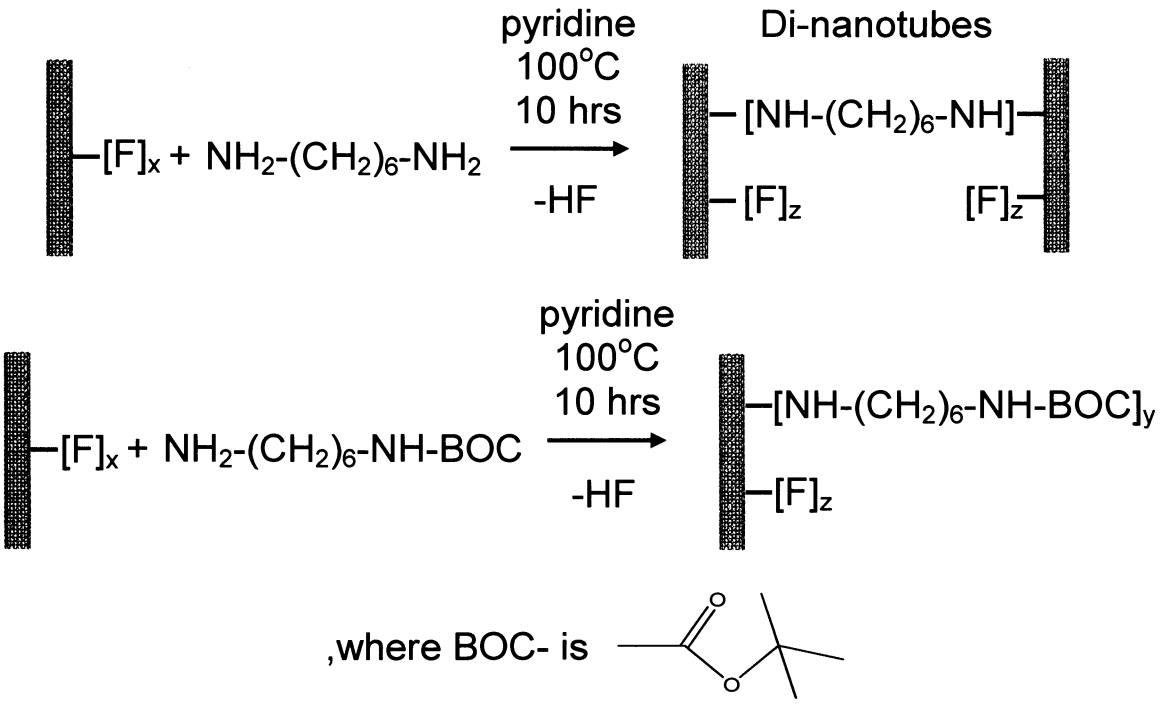

Scheme 3.1. Fluorine substitution reaction by amino molecules, 1,6-diaminohexane or N-Boc-1,6-diaminohexane in the presence of a base catalyst. x>>z.

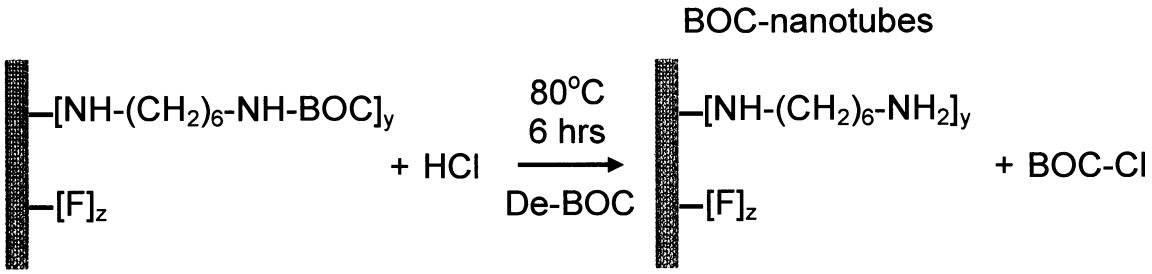

Scheme 3.2. In the de-BOC reaction, BOC as the protection group dissociates from the amino group under mild heating and acid environment.

3.2Experimental

Materials

Carbon nanotubes used in this work were obtained from Unidym, Inc., from Lot # XD 3365 A, which contains about 33 wt % single-walled CNTs and some double- and multi-walled CNTs with less than 5 wt % metal impurities. The epoxy resin was a DGEBA

epoxy (diglycidyl ether of biphenol A)-EPON 862-obtained from Shell Chemicals. This resin was used in combination with the commercial aromatic diamine EPI-CURE W as a curing agent. N-Boc-1,6-diaminohexane, 98 % was purchased from Alfa Aesar and 1,6-diaminohexane was purchased from Sigma-Aldrich.

3.2.1 Nanotube functionalization

Functionalization

A) Fluorination: The fluorination was carried out in a Monel reactor heated to 150°C for 12 h to obtain the approximate $C_{3.7}F$ stoichiometry. The gas-flow ratio for fluorine, hydrogen, and helium was 2:1:30, respectively. B) Fluorine substitution: The mixture of fluoronanotubes and N-Boc-1,6-diaminohexane was added into DMF with a molar ratio of fluorine atoms to amino groups of about 1:5, then pydine was added into the solution. In a typical experiment, 300 mL of DMF and 2.5 mL of pydine would be used if 70 mg of fluoronanotubes were involved in the substitution reaction. The reaction was conducted at 100°C for 10 h, thereafter; the product was washed several times by acetone and collected through filtration. Two types of nanotubes were prepared in this procedure, which are the products after the fluorines were substituted by N-Boc-1,6-diaminohexane and 1,6-diaminohexane individually. (Scheme 1) The nanotubes whose fluorines were substituted by 1,6-diaminohexane were named Di-nanotubes and ready for filling into the epoxy matrix. The other nanotubes were not used until the subsequent de-BOC reaction was accomplished. C) de-BOC reaction: It removes BOC groups and makes the amino groups exposed for the etherification reaction with the epoxy. The nanotubes attached with the BOC-protected functional groups were heated in 4 mol/L hydrochloride acid at 80°C for 6 h with magnetic stirring. (Scheme 2) Afterwards, the de-BOC nanotubes were

washed by saturated bicarbonate solution followed by de-ionized water several times until the residual acid and ions were removed. The final products were named as BOC-nanotubes. All the functionalized nanotubes were dried in the vacuum oven at 80°C overnight before they are added into the composite.

3.2.2 Processing the functionalized nanotube/epoxy composites

Composite processing

Three kinds of composites have been prepared for comparing the reinforcing effect of pristine XD nanotubes, Di-nanotubes and BOC-nanotubes. In the experiment, XD nanotubes, Di-nanotubes and BOC-nanotubes were dispersed in DMF (2 mg/mL) by sonication for 5 min using a high-power CUP-HORN ultrasonic processor and then for 1 h in an ultrasonic bath (40 kHz). Thereafter, the epoxy resin was added, and the solution was stirred for 30 min. DMF was evaporated at 100°C in a vacuum chamber. A 100:26 ratio of EPI-CURE W curing agent was added, and further stirring was performed with a high-shear mixer. The blends of epoxy with the three types of nanotube were degassed for 5 h in a vacuum oven and then cast into an aluminum mold. The curing cycle was 2 h at 100°C under a pressure of 0.3 MPa followed by another 2 h at 160°C. The XD nanotube/epoxy composite were prepared using a 0.5 weight percent (wt %) load of pristine XD nanotubes. In preparation of the Di-nanotube/epoxy and the BOC-nanotube/epoxy composites, the functionalized nanotubes were loaded into the epoxy matrix in the same molar ratio as the XD nanotube/epoxy samples. Since the nanotubes will gain some weight after functionalization, the weight percent of Di-nanotube and BOC-nanotube in the composites are higher than 0.5 wt %. In this paper, we denote this with an asterisk as 0.5 wt %* for the Di-nanotube and the BOC-nanotube. Five dog-

bone-shaped specimens of each kind of composites were cut and polished for tensile testing. Following the same procedure described above, a control sample from pure epoxy resin was also prepared and tested for comparison.

3.2.3 Characterizations on the nanotubes and the nanotube/epoxy composites

Characterization

X-ray photoelectron spectroscopy (XPS) and Thermogravimetric Analysis (TGA) were used to characterize the extent of functionalization of the nanotubes. The heating rate of TGA was 5°C/min. The fracture surface of the nanotube/epoxy composite was imaged using a Philips scanning electron microscope (SEM) at an accelerating voltage of 30 kV. Prior to observation, the specimens were sputter-coated with gold. Tensile testing was performed using a screw driven INSTRON testing machine with a 5 kN load cell according to the ASTM standard D638. Dynamical mechanical analysis (DMA) was performed on a Perkin-Elmer Pyris Diamond DMA instrument at a frequency of 1.0 Hz with the dual-cantilever bend mode. The strain amplitude was set at 0.05%. Testing temperature was set as from 40°C to 200°C at a heating rate of 5°C/min.

3.3Results and discussion

3.3.1 The extent of functionalization characterized by thermogravimetric analysis and X-ray photoelectron spectroscopy

The extent of sidewall functionalization is often estimated from the relative mass loss in a TGA curve. The TGA of the sample shows a steady mass loss between 200°C and 600°C in a manner typical of sidewall functionalization [30]. We also determine the functionalization by the relative intensities of the C and N peaks in the XPS. On the basis

of XPS, for BOC-nanotube, the substituent ratio of C (carbon atoms on the sidewall of the BOC-nanotube and Di-nanotube not including the carbon atoms on the functional groups) to N is calculated as 35:1. For Di-nanotube, this ratio is 19:1. These compare favorably with the ratios calculated from TGA measurements, 35.1:1 (BOC-nanotube) and 21.6:1 (Di-nanotube). The TGA data is shown in Figure 3.1. The details of XPS can be found in Figure 3.2. Using a (6,6) armchair SWNT as an example, a hexagonal belt cut along the circumference of the nanotube contains 36 carbon atoms [31]. Consider the fact that the molar ratio of functional groups to carbon atoms on the sidewall is 35:1; this means the spacing between two adjacent functional groups is approximately the spacing between two adjacent carbon hexagons, 0.369 nm along the nanotube axial direction [5]. In this work, both Di-nanotubes and BOC-nanotubes are start from the XD nanotubes, which contains about 33 wt % single-walled CNTs and some double- and multi-walled CNTs with less than 5 wt % metal impurities. For multiwall nanotubes, only the carbon atoms on the outmost wall are involved in the substituent reaction. In this regard, the average spacing between functional groups on the BOC-nanotube is even closer than 0.369 nm. It is worth noting that most fluorine atoms were removed after the substitution [32]. The XPS data in the supporting information gives evidence for this phenomenon.

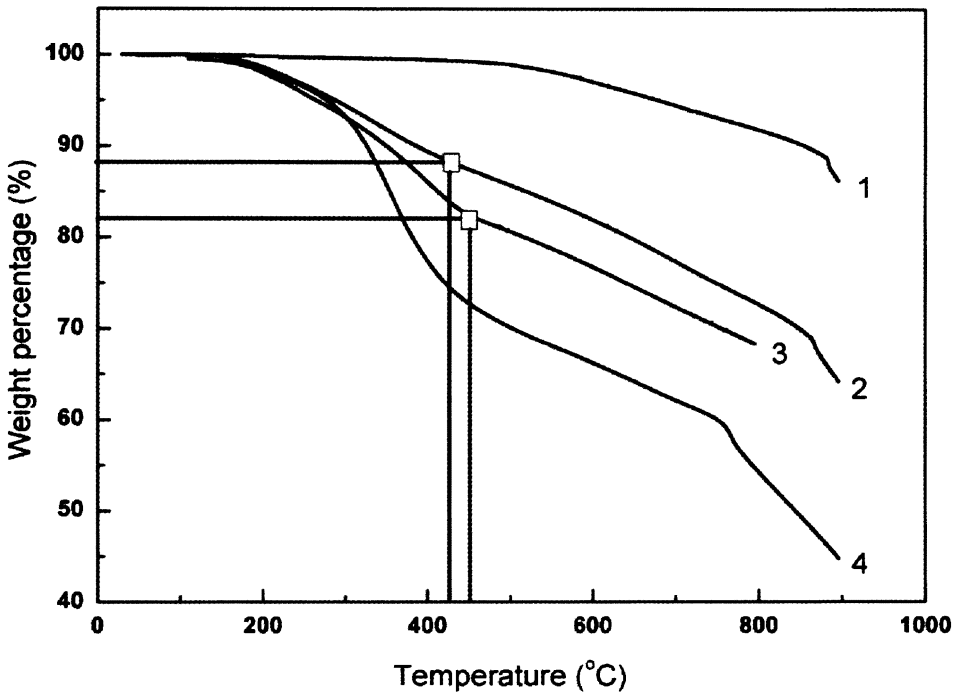

Figure 3.1. TGA curves of XD nanotube (1), BOC-nanotube (2), Di-nanotube (3) and Fluoronanotube (4).

Table 3.1. Tensile properties of nanotube/epoxy composites. The numbers in the parentheses indicate the standard deviation.

Epoxy composites formulation	Young's modulus E [MPa]	Tensile strength σ [MPa]	Elongation [%]	Toughness [MJ/m^3]
Neat epoxy	2320 (56)	73 (2.6)	4.3 (0.18)	2.09 (0.05)
0.5 wt% XD-nanotube	2287 (92)	71 (2.1)	4.4 (0.12)	2.08 (0.03)
0.5 wt%* Di-nanotube	2195 (105)	70 (3.2)	4.8 (0.14)	2.25 (0.04)
0.5 wt%* BOC-nanotube	3052 (95)	91 (2.8)	5.5 (0.2)	3.34 (0.05)

a) Fluoronanotubes

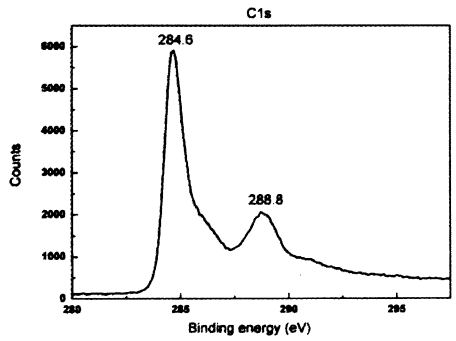

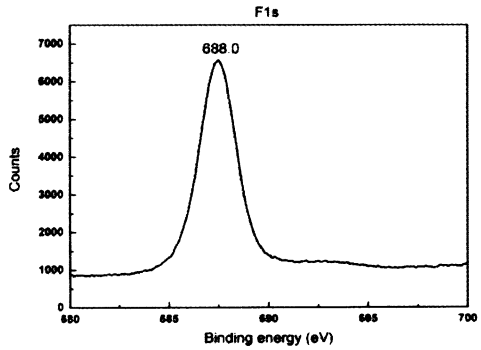

b) Di-nanotubes

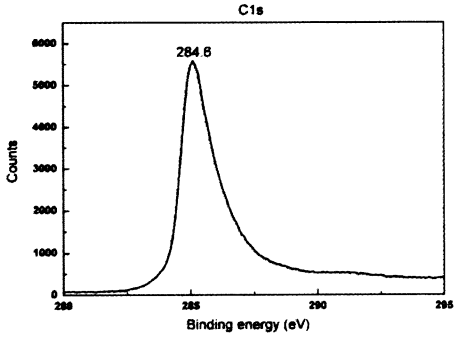

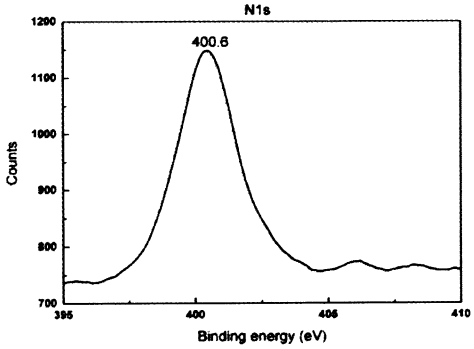

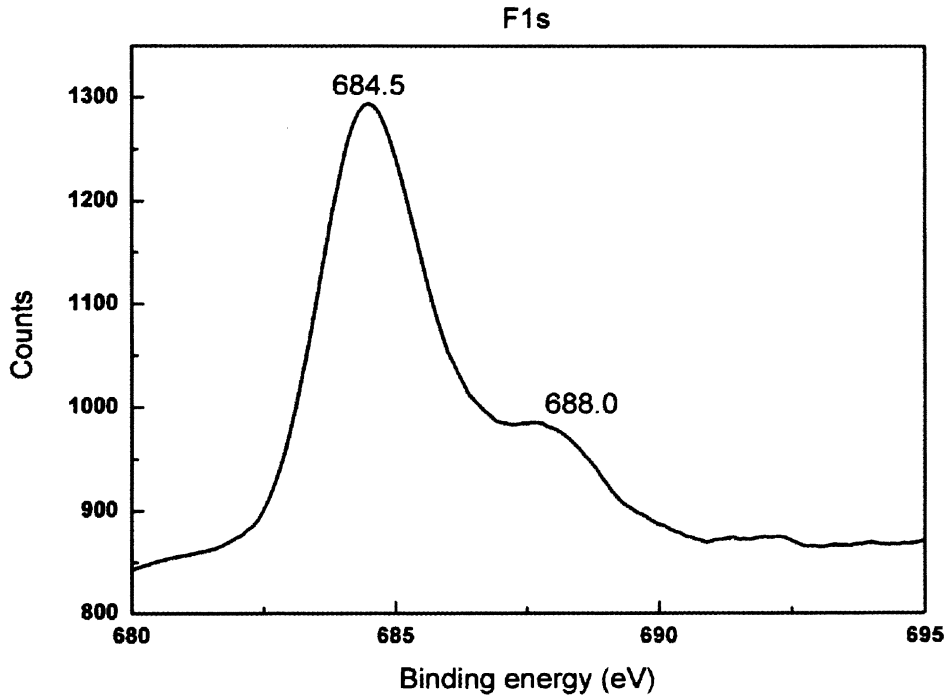

c) BOC-nanotubes

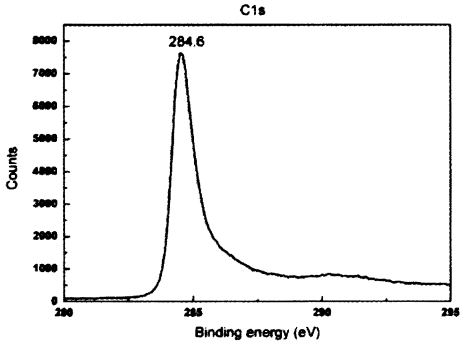

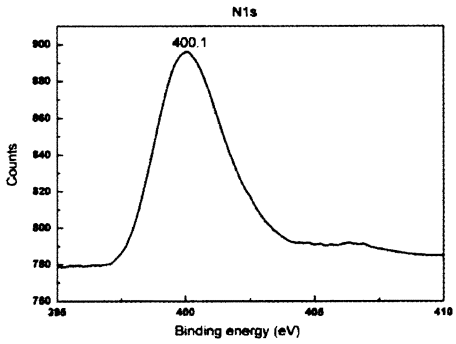

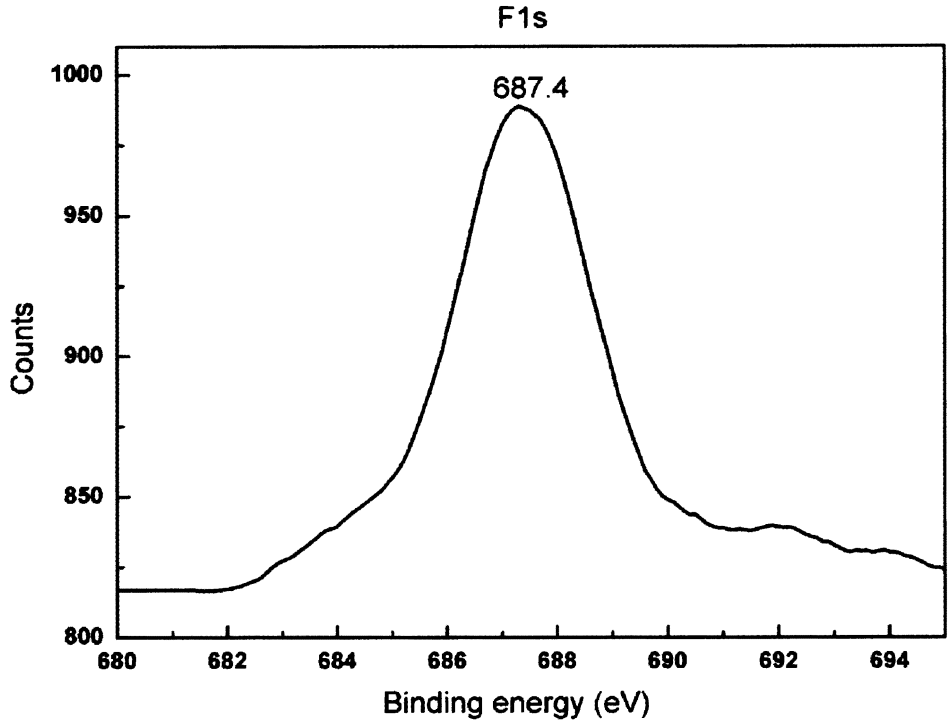

Figure 3.2. High resolution XPS spectra for Fluoronanotubes, Di-nanotubes and BOC nanotubes. a) Fluoronanotubes, atomic ratio of C and F is 76.3% and 20.6%. (N is less than 0.1%, N peak does not appear in the fluoronanotube.) b) Di-nanotubes, atomic ratio of C, N and F is 91.2%, 4.8% and 2.3%. c) BOC-nanotubes, atomic ratio of C, N and F is 94.2%, 2.3% and 2.5%.

3.3.2 Morphology of the nanotubes and the nanotube/epoxy composites

Other than dense functionalization, another merit of the BOC-nanotube is that the nanotube intrinsic structure remains intact in the functionalization process. The fluorine substitution and de-BOC reaction applied in synthesizing the BOC-nanotube were conducted in the DMF at around 100°C and in 4 M HCl at 80°C respectively; these relatively mild conditions can minimize the mechanical degradation during the functionalization process. Figure 3.3 shows that the MWNT structure remains intact through the functionalization process.

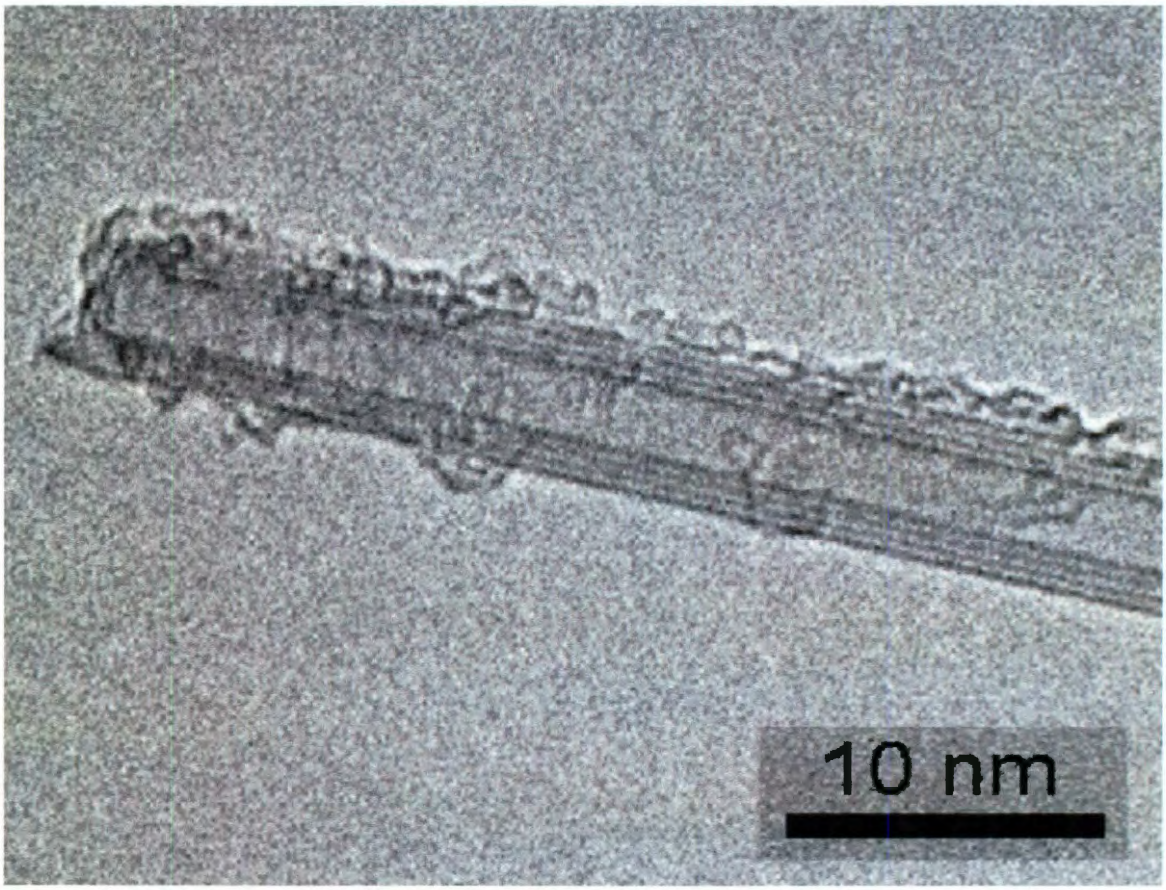

Figure 3.3. High resolution TEM image of a BOC-MWNT with the sidewall structure intact.

Before being mixed with epoxy, the nanotubes were initially dispersed in DMF through bath sonication for 1 h. Figure 3.4 shows that the BOC-nanotubes/DMF solution is a nearly opaque black suspension and remains stable one week with minimal precipitation formed; in contrast, the XD nanotubes and Di-nanotubes are agglomerated a few minutes after the sonication. The amino functional groups were successfully attached to the BOC-nanotubes and play a positive role on the solubility of BOC-nanotubes in DMF. Di-nanotubes and XD nanotubes both show appearance of the agglomerates in DMF, but their agglomerates are induced by different mechanisms. XD nanotubes are entangled by van der Waals forces. For Di-nanotubes, the agglomerates are attributed to an amine-

fluorine reaction that occurs on one nanotube, and another at the end of the same molecule that occurs on another nanotube. The agglomerates of Di-nanotubes and XD nanotubes cause difficulty in dispersing the nanotubes into the matrix, whereas the solubility of the BOC-nanotubes makes better dispersion within the matrix possible.

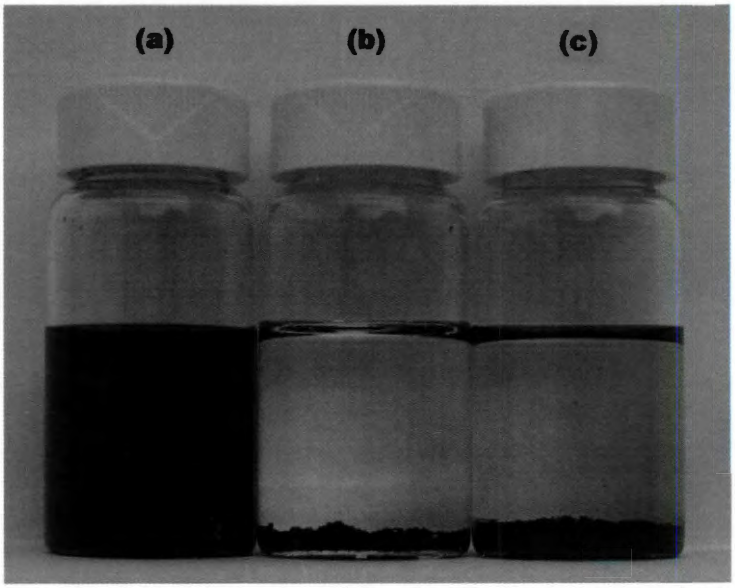

Figure 3.4. Photograph of (a) BOC-nanotubes, (b) Di-nanotubes, and (c) XD nanotubes in DMF, respectively (1 mg for each kind of nanotube dispersed in 15 mL of DMF).

Microscopic characterization was conducted on the fracture surface of composite specimens. It is shown from the SEM image in Figure 3.5a that BOC-nanotubes were homogenously dispersed and tightly embedded in the epoxy matrix. Figure 3.5b shows that the Di-nanotubes form into agglomerates which are caused by the di-amine linking reaction. From Figure 3.5c, we can see that the pristine XD nanotubes are entangled. From Figure 3.5b and 3.5c, it is observed that more nanotubes are pulled out from the epoxy matrix, which reflects better interfacial bonding in the composite filled by BOC-nanotubes shown in Figure 3.5a. The better dispersing ability of BOC-nanotubes and their strong interfacial bonding with the matrix causes the composite loaded with BOC-

nanotube to have superior mechanical properties. The agglomerates and entanglement of the Di-nanotubes and pristine XD nanotubes have no covalent bonding with the matrix at the interface where cracks are more likely to be initialized.

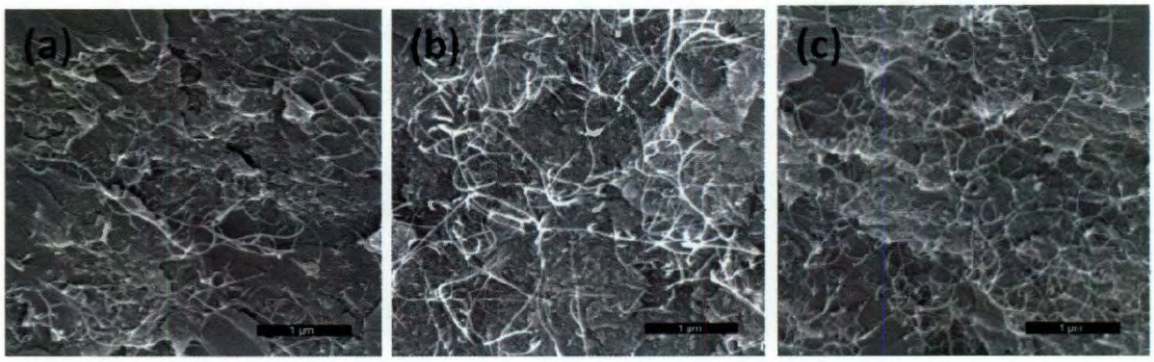

Figure 3.5. SEM images of fracture surfaces of BOC-nanotubes (3.5a), Di-nanotubes (3.5b) and XD nanotubes (3.5c) reinforced composites.

3.3.3 Tensile test and dynamic mechanial analysis

Representative stress-strain responses of composites reinforced by different nanotubes are shown in Figure 3.6. The Young's modulus, the tensile strength at break, the ultimate elongation and the toughness (and corresponding standard deviations) are listed in Table 3.1. It is observed that the tensile strength at break and the Young's modulus of composites reinforced by 0.5 wt %* BOC-nanotubes are increased by around 25 % and 30 %, respectively, relative to the neat epoxy resin. In contrast, the composites reinforced by Di-nanotubes and pristine XD nanotubes show slight degradation in mechanical properties. This degradation might be attributed to the agglomerates, which have atomically smooth surface and limited load transfer with the matrix. The observations coincide with the previous solubility analysis. It is also noticed that the fracture strain of the specimen loaded with the BOC-nanotubes increased by about 20 %, suggesting that

covalent bonding between the BOC-nanotubes and the matrix improves load transfer at the composite interface. By means of this strong covalent bonding at the molecular level with cross linked polymer chains, the unique flexibility and geometric features of the nanotubes will contribute to continuous absorption of energy and result in increased elongation in the epoxy [33].

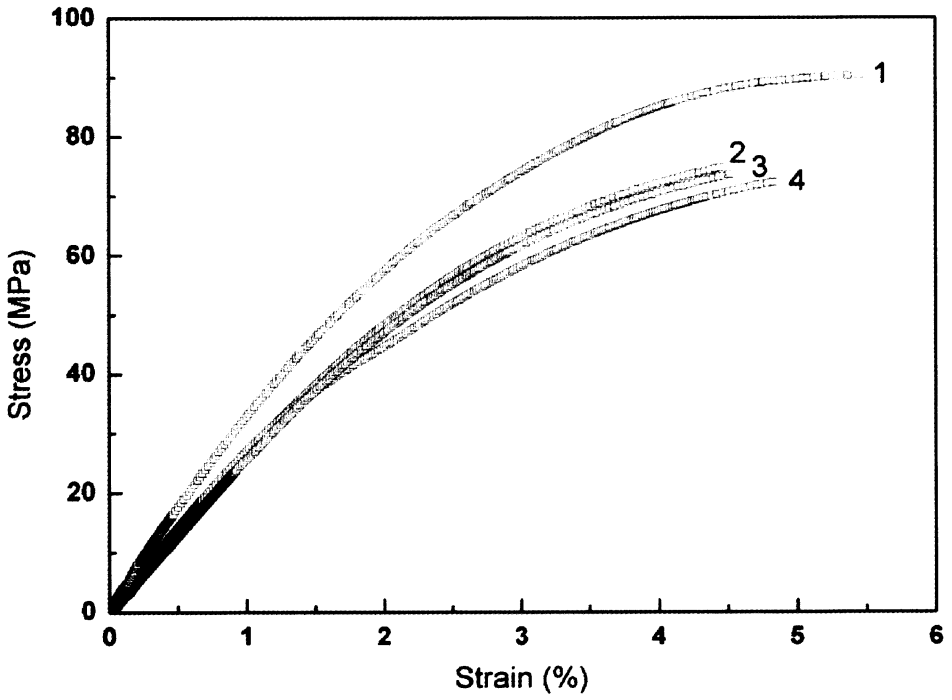

Figure 3.6. Tensile stress-strain curves of (1) a composite loaded with 0.5 wt%* BOC-nanotubes, (2) neat epoxy, (3) a composite loaded with 0.5 wt% XD-nanotubes, and (4) a composite loaded with 0.5 wt%* Di-nanotubes.

DMA was performed to obtain the temperature-dependent properties of materials such as the storage modulus and the tanδ. The dynamic properties reflect the amount of the energy in the composite stored as elastic energy and the amount of energy dissipated during the strain process. These properties are highly dependent on the existence of fillers:

dispersion within the matrix, volume fraction, geometrical characteristics, and load transfer from the filler to the matrix [34]. Figure 3.7 shows the storage modulus of the composite loaded with 0.5 wt %* BOC-nanotubes are higher than the other composites over the temperature range from 40°C to 200°C. For example, at the 40°C, the storage modulus of neat epoxy is 2.73 GPa and that of the nanocomposites with 0.5 wt% XD nanotubes and 0.5 wt%* Di-nanotubes are 2.54 GPa and 2.52 GPa, respectively. However, the BOC-nanotubes/epoxy composite with the same loading results in a storage modulus of 2.98 GPa, about 17.3 % increase compared to the raw XD nanotubes/epoxy composite. The precursors, fluoronanotubes derived from XD nanotubes, have the atomic ratio of carbon to fluorine as 3.7:1. Even more dense functionalization is achievable when using single-walled fluoronanotubes with atomic ratio of carbon to fluorine as 2:1. More concentrated functionalization and intact structure of single-walled nanotubes leave a broad space for improving mechanical properties.

The glass-transition temperature (defined as the temperature at which maximum tanδ is reached) is an indicator of the degree of cross linking in the nanotube-epoxy composite. The higher the glass-transition temperature reflects a higher cross linking density [28] As shown in Figure 3.8, the glass transition temperature for the BOC-nanotube reinforced composite is highest, followed by the Di-nanotube and XD nanotube filled samples; the lowest one is that of the neat epoxy resin. The amino groups on the BOC-nanotubes are protected before they are added into the epoxy matrix and involved in a ring-opening etherification reaction, which increases cross linking density in a BOC-nanotubes/epoxy composite. This in turn raises its glass transition temperature.

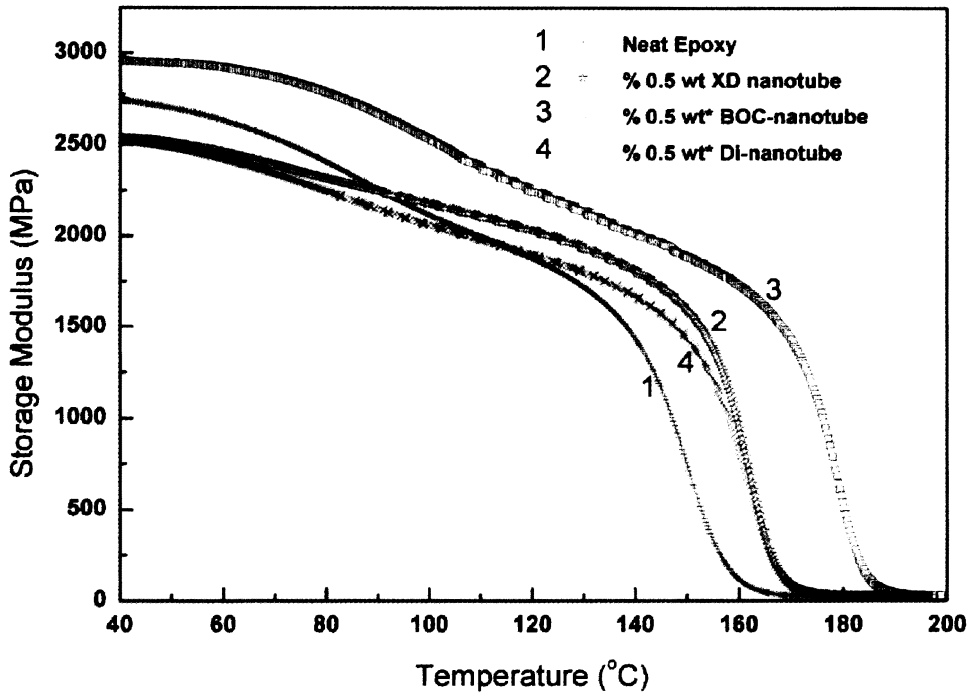

Figure 3.7. Storage modulus measured by DMA as a function of temperature for neat epoxy, composites loaded with 0.5 wt % XD nanotube, 0.5 wt %* BOC-nanotubes and 0.5 wt %* Di-nanotubes.

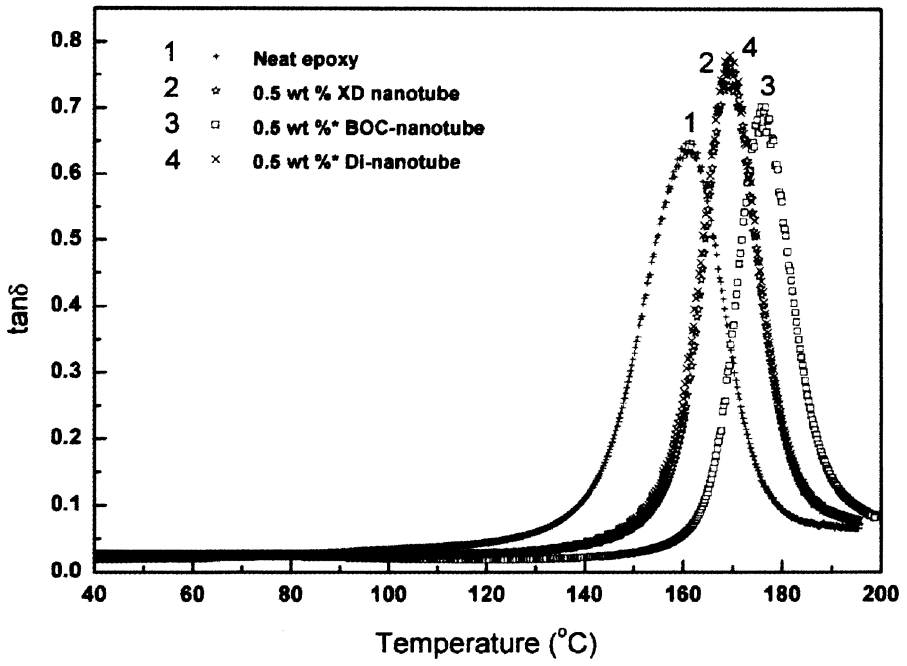

Figure 3.8. The curves of tan δ versus temperature for neat epoxy and composites over the temperature range from 40°C to 200°C.

3.4Conclusions

An epoxy resin composite filled with the amino-functionalized nanotubes was prepared. The nanotubes are integrated into the cross linked epoxy matrix by covalent bonds. The processing involved a BOC-protected diamine molecule as a linking agent. Using a protecting agent does not allow reactions on the amino groups until the epoxy is added. The functionalized nanotubes show homogeneous dispersion within the matrix and construct strong interfacial bonding during the curing process. Through applying the BOC-protected diamines instead of the symmetric peers for functionalizing nanotubes, the agglomerates are reduced and the better mechanical properties of the composites are achieved.

Chapter 4: Porous medium density polyethylene/nanotube composites

A scalable approach was developed for preparing the porous medium density polyethylene (MDPE) powder. Due to high surface area of the porous MDPE and size match between the pores and the nanotubes, nanotubes were easily dispersed into the porous MDPE matrix. The resultant composites showed improved mechanical and electrical properties compared to that of the control samples. Fabrication of the porous MDPE started from the raw MDPE powder. Originally, the powder approximately had a solid spherical structure and an average diameter of 100 microns. After etching in toluene under the optimized pressure and the time duration, the powders on their surface were entrenched with the deep pores. Diameter of the pores was 1.6 microns in average and had a relatively narrow standard deviation. The SWNTs of sub-micron length were selected as the fillers in the system. They readily penetrated into the pores and achieved dispersion in the porous MDPE simply by the sonic agitation in Dimethylformamide (DMF). The resultant porous MDPE/SWNT composite of 2 wt % loading ratio obtained a 54 % increase in tensile strength and a 19 order magnitude enhancement in DC volume conductivity than the raw MDPE. This system demonstrated that a multifunctional composite was created by tuing the features at nanoscale and rationally designing the processing.

4.1 Introduction

Due to the porous structure of the matrix, nanotube dispersion is realized simply by the sonic agitation. In section 4.1.1, the traditional methods for dispersing nanotubes in viscous polymer matrices are discussed followed by a comparison between the traditional methods and the method applied in this work. In section 4.1.2, the discussion will be particularly focus on crystallization behavior of the matrix by itself and by with adding nanotubes. In addition, microscopy study on the interface will be presented. This research sheds a new light on composite processing.

4.1.1 Methods for dispersing nanotubes in thermoplastic matrix

Incorporating carbon nanotubes into a matrix is a promising way to obtain multifunctional composites due to superior electrical, mechanical and thermal properties of carbon nanotubes [5]. However, some challenges are posted on the way for commercializing nanotube-filled composites. One of the challenges is acquiring a large quantity of nanotubes at a low price. This one has been mitigated as the nanotubes fabrication technology has developed [35]. The other challenge is scarcity of processing techniques for properly incorporating nanotubes into a polymer matrix. Melt mixing, solution phase mixing and mixing along with in-situ polymerization are three common methods for dispersing nanotubes into a polymer matrix. Petra Pötschke et al. prepared Polyethylene (PE) /Multiwalled carbon nanotube (MWNT) and Polycarbonate (PC) /MWNT composites by melt mixing, in which agglomerates were broken by shear force and the nanotubes were dispersed by mechanical mixing [36]. Haggenmueller et al. developed a hot-coagulation method, in which the nanotubes were dispersed in dichlorobenzene by the sonic agitation and polyethylene were dissolved in hot

dichlorobenzene. After the two solutions were mixed, the nanotubes and polyethylene coagulate into a composite as dichlorobenzene was evaporated. Within the composite, dispersion of the nanotubes was achieved [37]. Tang et al. synthesized the composites by starting with mixing the nanotubes with the monomers [38]. Then, the polymerization was conducted along with the mixing. Within the resultant polymer/CNT composite, the nanotubes retained the dispersed state as that they had in the monomers.

In this dissertation, a new method for dispersing nanotubes was developed. Using the porous MDPE as the matrix, simply the sonic agitation could make nantoubes penetrate into the pores. Nanotube agglomerate size was restricted by the pore size. By carefully controlling the pore size in micron range, degree of nanotube dispersion in the resultant composite was achieved to micron level.

4.1.2 Crystalization of polyethylene by itself vs. within nanotube/PE composites

Polyethylene is a semicrystalline polymer, which includes both the amorphous and the crystalline phases [39]. Adding nanotubes into polyethylene would change the crystallization behaviors, such as the crystallization ratio and rate as well as the crystal structure and orientation [40]. As a result, the properties of polyethylene by itself and the nanotube/polyethylene composite would be changed. Regarding to the mechanical properties, the higher ratio of the crystallization normally causes the polyethylene become more brittle [41]. With respect to the electrical properties, the crystallization on the surface of the nanotubes would introduce a significant contact resistance, and hence hinder formation of the conductive networks [42]. Understanding the crystallization

behavior of polyethylene in the nanotube filled composite system is important for designing the composites with the desired properties.

Bhattacharyya et al. found that 0.8 wt% nanotubes as the nucleation sites in polypropylene reduced spherulite size (without introducing the nanotubes, polypropylene is inclined to crystallize into a spherical shape) and made the crystallization time halves [19].

Zhang et al. found that carbon nanotubes induced formation of transcrystallinity. Lamellae of its c axis aligned in the long axis direction of nanotubes grew radially from the nanotubes surface [43].

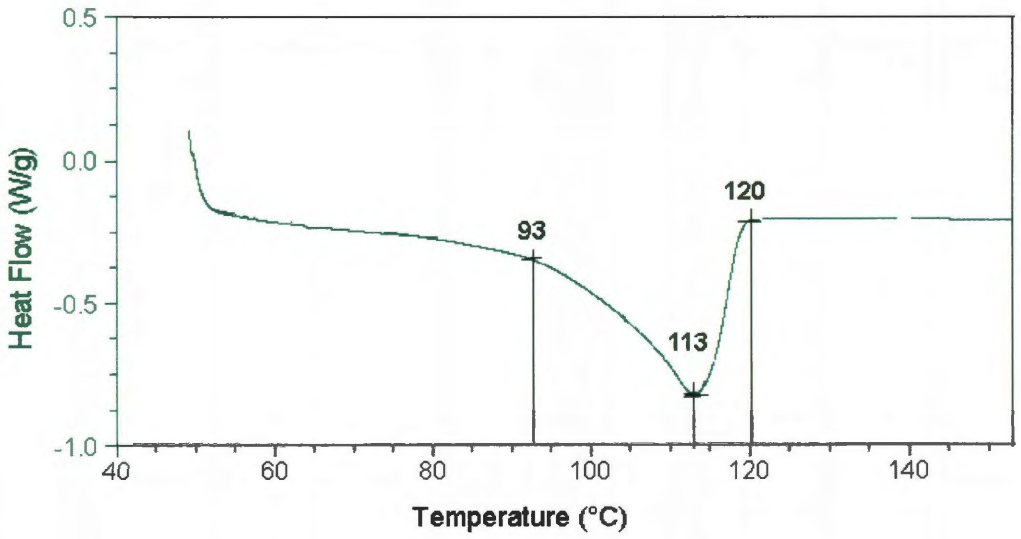

Figure 4.1. DSC curve of the porous MDPE for heat flow as a function of temperature.

Crystallization is an exothermic process. Differential scanning calorimetry (DSC) measures the heat flow (as shown in figure 4.1) as the porous MDPE experiences a phase

change from the molten state to the solid state. From the curve that heat flow as a function of temperature, the nominal melting temperature of the porous MDPE is identified as 113°C.

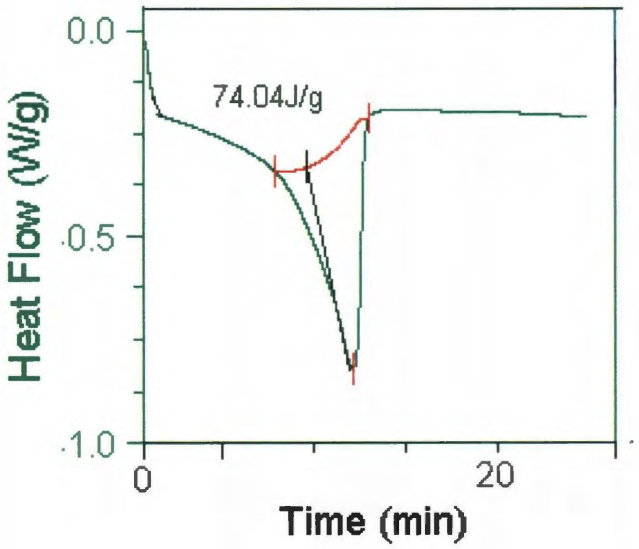

Figure 4.2. DSC curve of the porous MDPE for heat flow as a function of time.

DSC also measures the curve that heat flow as a function of time as shown in figure 4.2. The area of the exothermic peak indicates the energy released during the whole crystallization process. Then, crystallinity η can be calculated by the formula:

η = exothermic peak area/ crystallization energy *100%, where crystallization energy is the energy released when the polymer fully converts from the molten state into the 100 % crystal phase.

Crystallinity of the porous MDPE is calculated as 74.04 J/g / 293 (J/g) = 25.3 %. The remaining 74.7 % of MDPE is in an amorphous phase.

4.2 Experimental

4.2.1 Preparing the porous MDPE

The mixture of the raw MDPE powder (Sigma Aldrich Inc.) and toluene (the proportion of the raw MDPE to toluene was 1 gram to 20 ml) was placed in an autoclave and heated at 150°C for 1hour. This 1hour etching created pores on the powder surface. After the etching, the porous MDPE powder was separated from toluene by filtration.

4.2.2 Making the master batches

HiPco nanotubes (Unidym, Inc.) were purified before they were processed into master batches [44]. Three master batches, the raw MDPE/HiPco nanotube, the porous MDPE/HiPco nanotube and the porous MDPE/HiPco nanotube with the additional melt mixing (the porous MDPE/HiPco nanotube + MM) were prepared. To prepare the raw MDPE/HiPco nanotube master batch, the raw MDPE powder (19.6 g) was fed into the mixing bowl of the Haake polylab at 130°C. After one minute, the raw MDPE powder melted, and then the purified HiPco nanotubes (0.4 g) were added into the bowl. The raw MDPE and the purified HiPco nanotubes were mixed for 30 min at a rotation speed of 60 revolutions per minute. After cooling down, the resultant master batch of the raw MDPE/HiPco nanotube was in a bulk form. To prepare the master batch of the porous MDPE/HiPco nanotube, the mixture of the porous MDPE (19.6 g) and the purified HiPco nanotubes (0.4 g) in DMF (100 ml) was stirred by the sonic agitation (bath sonication at 40 kHz) for 5 min. Afterward, DMF was removed by filtration (Teflon filtration membrane, 200 nm pore size). The master batch of the porous MDPE/HiPco nanotube as-received after the filtration was in a powder form. The conditions for the additional

mixing were identical to that in preparing the raw MDPE/HiPco nanotube master batch. The porous MDPE/HiPco nanotube + MM master batch were in a bulk form too.

4.2.3 Characterization of the mechanical and electrical properties

Dog-bone specimens were prepared by injection molding (DACA Inc.) with a mold (ASTM D638 type V specifications). Five specimens were made from each type of the master batches. In addition, five specimens of the raw MDPE and the porous MDPE were fabricated. The tensile test was conducted using a screw driven INSTRON testing machine with a 5 kN load Cell. The crosshead speed was 2mm/min. Volume conductivity of the raw and the porous MDPE was measured by a Keithley electrometer (Model 6517A) equipped with an 8009 test fixture. The samples (diameter 60 mm and thickness 0.35 mm) were prepared by hot compression in a mold. For composites (volume conductivity larger than 10^{-6} $S.cm^{-1}$), samples (1 mm × 5 cm × 0.5 cm in thickness × length × width) were prepared by hot pressing and cutting. Keithley source meter (Model 2400) was applied in measuring the volume conductivity with a four-probe setup. A FEI scanning electron microscope (Model Quanta 400) was used to image the fracture surface of specimens, which were obtained by fracturing in liquid nitrogen. Prior to the imaging, the specimens were sputter-coated with a 5 nm gold layer.

4.3 Results and discussion

Figure 4.3 (a) and (b) show that the MDPE particles are approximately spherical and the average diameter of the particles is 100 microns. In the etching procedure, the pore structure depends on both etching time duration and temperature. At the relatively low temperature, the etching process is slow as opposed to high temperature where the

etching occurs fast and the porous structure collapses. The optimal etching condition was identified as150°C for 1 hrs, at which the surface of the MDPE particles were entrenched with deep pores. Diameter of the pores have an average of 1.6 microns and a small relative standard deviation as shown in figure 4.3 (c). The high resolution view of the pores as shown in figure 4.3 (d) indicates that the pores are not ideally circular (The pore size statistics is based on the approximation that diameter is the average of the long and short axis length for each pore). In the case of the etching time as short as 20 min, the shallow dents were created on the surface of the MDPE particles as shown in figure 4.3 (e) and (f). Etching for a longer time or at a higher temperature caused the porous structure collapse into fringy debris as shown in figure 4.3 (g) and (h). As a control experiment, the MDPE particles were etched in the ambient environment at 150°C for 1hr. the product was the fringy debris. This finding indicates that pressure is critical to maintain integrity of the porous structure during the etching process.

The diameter and length of the HiPco nanotubes varies from 0.8 nm to1.2 nm and from 300 nm to 1 micron respectively. With regard to the pore size, HiPco nanotubes readily fill into pores assisted by the sonic agitation in DMF. Larger pores would result in more nanotubes filled into the pores and cause the formation of aggregates. On the other hand, nanotubes could not penetrate into the pores if the pore size is too small. When the pore size has a good match with length of the nanotubes, the porous MDPE naturally functions as a size screen which prevents from formatin of the naontube aggregates larger than the pore size.

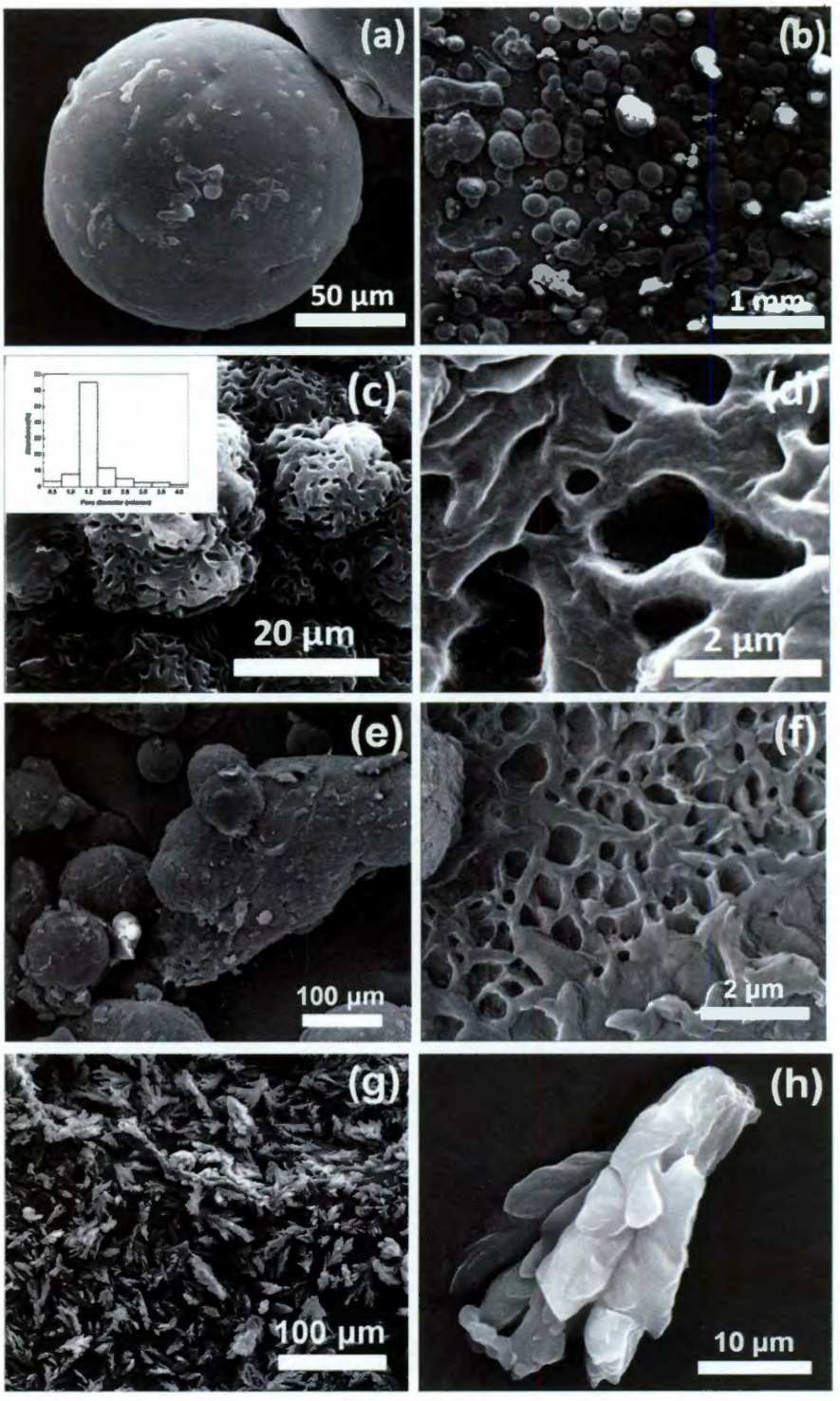

Figure 4.3. SEM images of the MDPE powder resulted from the etching at a variety of conditions: (a, b) are for the raw MDPE particle. The rest of the images are for the products as a result of the etching for different time duration. 1hr for (c,d), 20 min for (e,f) and 2hrs for (g,h). The inset of (c) is the corresponding statistics of the pore sizes.

Fabrication of the porous MDPE/HiPco nanotube master batch is comprised of two steps including sonication in DMF and filtration. Different from other solution-assisted dispersion methods [45][37][38], in which polymers are completely dissolved and removing the solvents has to rely on the time-consuming evaporation. Here the porous MDPE particles are in a solid form in DMF. The porous MDPE/HiPco nanotube master batch can be separated from the solvent simply by filtration. DMF can be collected for reuse. After mixed with the nanotubes, the white porous MDPE (figure 4.4 (a)) turns into the gray porous MDPE/HiPco nanotube master batch (figure 4.4 (b). The SEM image as shown in figure 4.4 (c) reveals that all nanotubes are absorbed by the porous MDPE because no pure nanotube aggregates can be observed separately from the porous MDPE. The image at a higher resolution (figure 4.4 (d)) shows that a part of the nanotubes covered on the surface of the porous MDPE as the other part penetrated into the pores. It is worth noting that the procedures in fabricating the porous MDPE and the porous MDPE/HiPco master batch can be readily scaled up. In addition, both toluene used for etching and DMF for dispersing the nanotubes can be recycled.

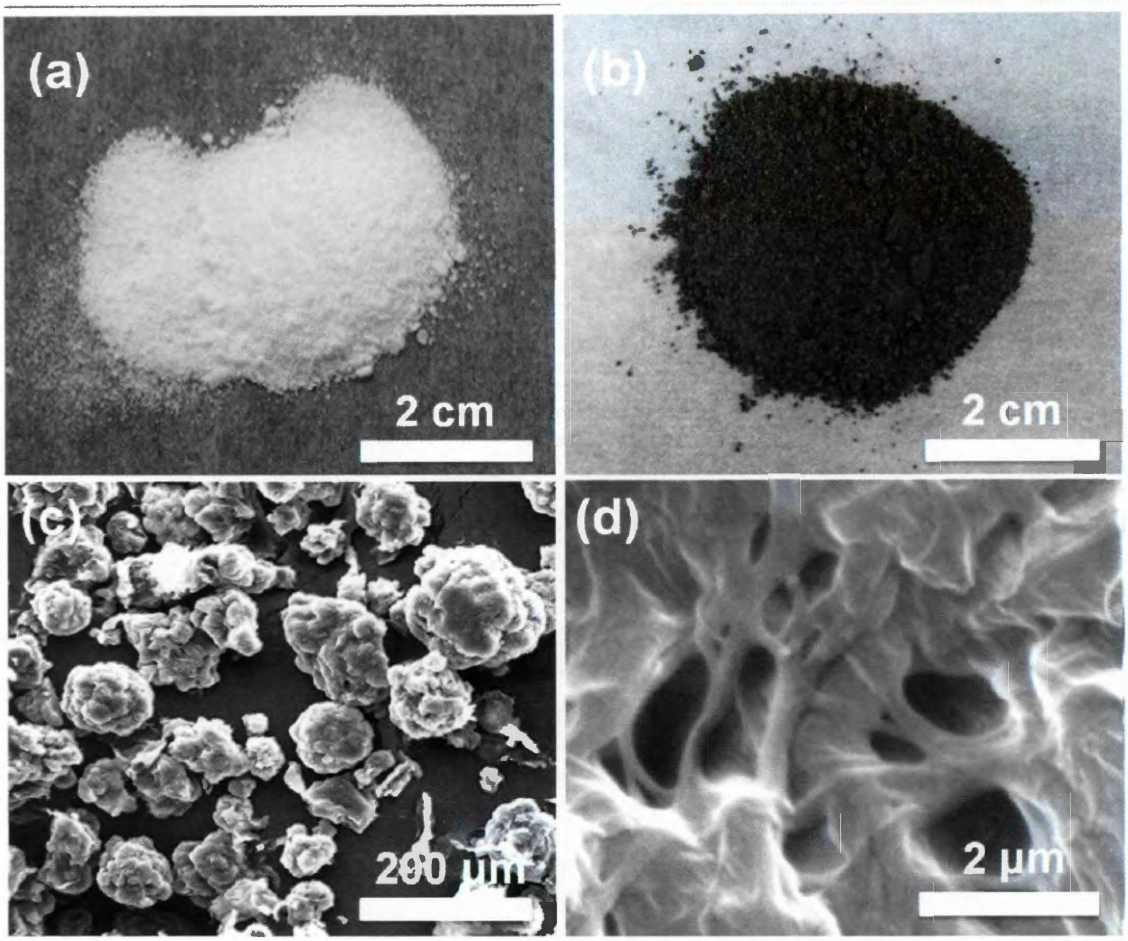

Figure 4.4. (a) Photos of the porous MDPE and (b) the porous MDPE/HiPco nanotube master batch. (c) SEM images of the porous MDPE/HiPco nanotube master batch, and (d) the corresponding image taken in zoom-in mode.

Tensile properties of the samples are shown in table 4.1. No significant difference in tensile strength and young's modulus between the raw MDPE and the porous MDPE samples indicates that the etching changes the morphology of the MDPE particles but does not influence their tensile strength. The raw MDPE/HiPco nanotube composite shows a 15.7 % increase in tensile strength along with a 36.0 % decrease in elongation with regard to the raw MDPE. With using the porous MDPE as the matrix, a more significant improvement in tensile strength is obtained. The composite prepared from the

porous MDPE/HiPco nanotube + MM master batch does not show much enhancement in tensile strength than the porous MDPE/HiPco nanotube composite. This indicates that the melt mixing is a redundant step when using the porous MDPE as the matrix. It is worth noting that the elongation of the porous MDPE/HiPco nanotube composite is 57 % larger than that of the raw MDPE/HiPco nanotube composite. This phenomenon can be explained by that the nanotubes are well dispersed within the porous MDPE matrix, whereas, nanotube aggregates still exist in the raw MDPE matrix. The fracture surface of the porous MDPE/HiPco nanotube composite is shown in figure 4.5. The nanotubes distribution over the fracture surface is homogeneous.

Table 4.1. Tensile properties of the composites and matrices

	Tensile Strength (MPa)	*Young's Modulus (MPa)*	*Elongation (%)*	*Toughness ($MJ.m^{-3}$)*
Raw MDPE	4.33 (0.28)	638 (16)	1.64 (0.19)	4.73 (0.31)
Porous MDPE	4.45 (0.26)	651 (15)	1.70 (0.17)	5.04 (0.28)
Raw MDPE/HiPco nanotube	5.01 (0.20)	709 (12)	1.05 (0.13)	3.51 (0.25)
Porous MDPE/HiPco nanotube	6.93 (0.25)	980 (23)	1.67 (0.20)	7.72 (0.28)
Porous MDPE/HiPco nanotube +MM	7.02 (0.21)	992 (14)	1.65 (0.17)	7.72 (0.24)

*The numbers in the parentheses indicate the standard deviations.

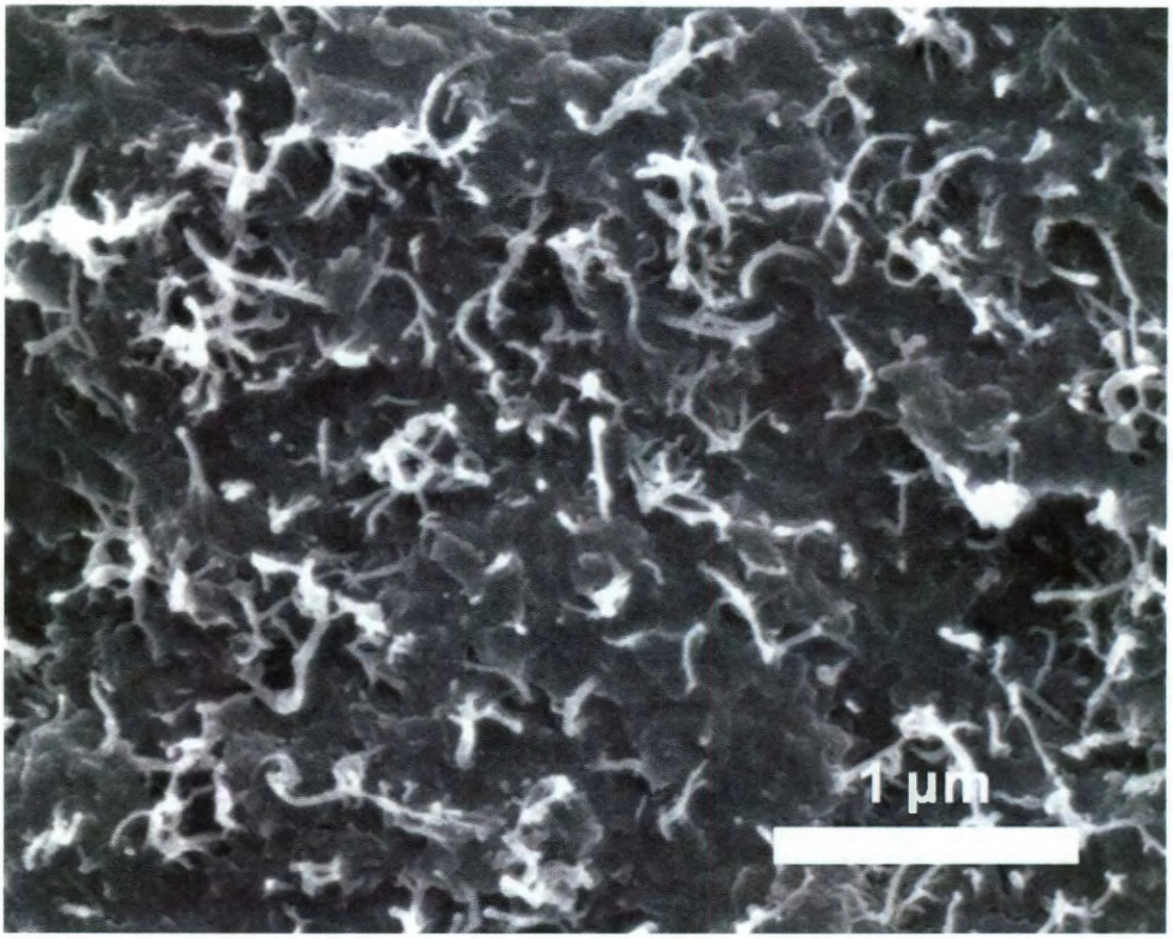

Figure 4.5. SEM image of the fracture surface of the porous MDPE/HiPco nanotube composite.

Volume conductivity of the three different types of composites as well as the porous MDPE and the raw MDPE as the baselines are listed in table 4.2. The matrices are insulating materials. After adding 2 wt% of the nanotubes, conductivity of the composites has been greatly improved. The composite using the porous MDPE as the matrix has higher volume conductivity than that using the raw MDPE. This could be ascribed to the better dispersion of the nanotubes in the porous MDPE. The better dispersion means that more effective conductive paths could be constructed. On the contrary, formation of the

aggregates can cause the conductive paths be discontinuous with the insulating polymers in between those aggregates [46].

Table 4.2. Volume conductivity of the composites and the matrices

	Volume Conductivity ($S.cm^{-1}$)
Raw MDPE	$1.39\ (0.08)*10^{-20}$
Porous MDPE	$1.47\ (0.07)*10^{-20}$
Raw MDPE/HiPco nanotube	$1.67\ (0.11)*10^{-2}$
Porous MDPE/HiPco nanotube	$1.33\ (0.06)*10^{-1}$
Porous MDPE/HiPco nanotube + MM	$1.22\ (0.05)*10^{-1}$

*The numbers in the parentheses indicate the standard deviations.

4.4 Conclusions

A method for scalable production of the porous MDPE particles was developed. The porous structure has larger surface area than the solid spherical structure of the raw MDPE. By carefully controlling the etching process, the size of the pores was maintained at an average of 1.6 microns, which is slightly larger than length of the HiPco nanotubes. Preparation of the porous MDPE/HiPco nanotube master batch was accomplished by the sonic agitation and filtration. The following melt mixing, proved as a redundant step, can be skipped. Dispersion of the nanotubes was achieved within the porous MDPE/HiPco nanotube composite. Enhancements in mechanical strength and electrical conductivity with regard to the raw MDPE were realized for the porous MDPE/HiPco nanotube composite at the loading ratio of 2 wt %. Moreover, the recyclability of solvents and the simplicity of the composite processing make the manufacturing cost efficient. The multifunctional porous MDPE/HiPco nanotube composite of light weight, improved conductivity and strength have a variety of applications such as sporting goods and parts in the space shuttle.

Chapter 5: Continuous nanotube/HDPE composite cables with high nanotube loading ratio

5.1 Introduction

5.1.1 Melt spinning

Melt spinning is a technique for producing wires or fibers by spinning the molten materials out of a nozzle. When the melt spinning instrument is attached with a feeding setup, the wires/fibers can be continuously prepared. This scalable method is applied in our research for producing conductive composite wires. Many groups have studied nanotube-filled composites [46]. Most nanotube-filled composites have a percolation ratio below 5 wt %, at which a sharp drop in resistance occurs. However, resistivity of the samples with the loading ratio at the percolation ratio is still too high to enable samples be suitable for conductor applications. In this research, a particular attention was paid on the samples with loading ratio higher than 5 wt %.

5.1.2 Nanotube conducting networks in HDPE

In a composite with an insulating polymer as the matrix, charge carriers were conducted through nanotube networks primarily based on two mechanisms: tunneling between two touching nanotubes and hopping between two separated nanotubes. The tunneling mode is dominant when the concentration of nanotubes in the composite is high, whereas, the hopping mode is dominant when concentration of nanotubes is low. When two nanotubes are touched with each other, several factors determine the tunneling efficiency such as

chirality of the nanotubes, the crossing angle between two tubes, and the overlapping length [47]. The following three paragraphs elaborate these three factors individually.

Fuhrer, M. S. et al. reported that the tube-to-tube resistance between the semiconducting nanotube (sc-CNT) and the metallic nanotube (m-CNT) is three orders of magnititude higher than the met-met junction and two orders of magnitude higher than the sc-sc junction [17]. To maximize conductivity in a nanocomposite cable, the ideal senario is that the conducting networks are exclusively assembled by metallic nanotubes. However, in reality, mass production of pure metallic nanotubes is still challenging. The nanotubes used in this research are all mixtures of sc-CNTs and m-CNTs. Based on the available nanotubes, a practical solution to reach high conductivity is increasing concentration of nanotubes. Because higher concentration means that more direct tube-to-tube contacts are constructed, and hence more met-met junctions are created as well.

Buldum, A. and Lu, J.P. calculated the contact resistance between two (10, 10) nanotubes as a function of their crossing angle (figure 5.1) [47]. The resistance reaches minimum when two nanotubes are parallel to each other. This result indicates improving alignment of nanotubes would be an efficient method for increasing conductivity of the composite.

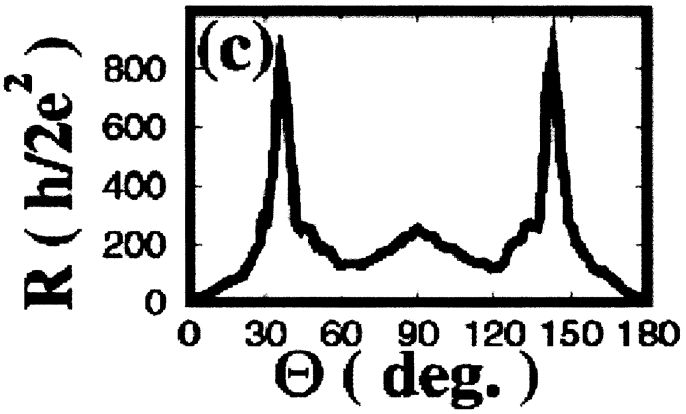

Figure 5.1. The contact resistance between two (10,10) tubes as a function of the crossing angle between them. The two nanotubes are in-registry at 0°, 60°, 120° and 180° [47].

Buldum, A. and Lu, J.P. also calculated the conductance between two (18, 0) nanotubes as a function of their overlapping length (figure 5.2) [47]. The conductance oscillates in a fashion that it reaches a local maximum as the overlapping length increases by every unit-cell length of the nanotube. In general, the peak conductance value increases as the overlapping length increases. This result led to the use of longer nanotubes as the fillers in the composite in order to achieve higher conductivity because long overlapping length is beneficial for tunneling.

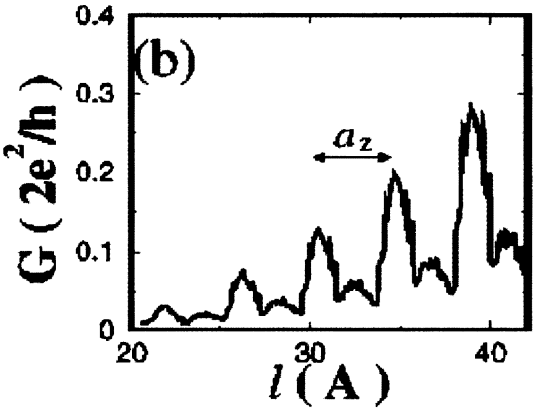

Figure 5.2. Variation of conductance with l for the (18, 0)-(18, 0) junction. The period is the unit cell length (a_z = 4.26 Å) for zigzag tubes [47].

Other than the direct touching mode, another mode is that two nanotubes are separated from each other, in between intercalated with the insulating layer. Charge carriers can hop over the insulating layer and transfer from one to the other nanotube. The hopping efficiency is determined by the thickness of the insulating layer. Figure 5.3 clearly shows that the tunneling resistance increases exponentially as the thickness of the insulating

layer increases [155]. For tubes separated by an insulating layer of the same thickness, the larger diameter as the tubes have, the smaller tunneling resistance between tubes occurs. To optimize conductivity, the inter-tube distance needs to be controlled under a certain value, at which the corresponding tunneling resistance is comparable to the intrinsic resistance of a nanotube itself. Otherwise, the insulating matrix would play a dominant role in determining resistivity of the composite. The information from the figure 5.3 provides a guideline for processing the conducting composites. From the resistance of the nanotube, the maximum inter-tube distance (at which tunneling resistance is equal to the intrinsic resistance of the tube) can be estimated; furthermore, concentration of the nanotubes can be calculated.

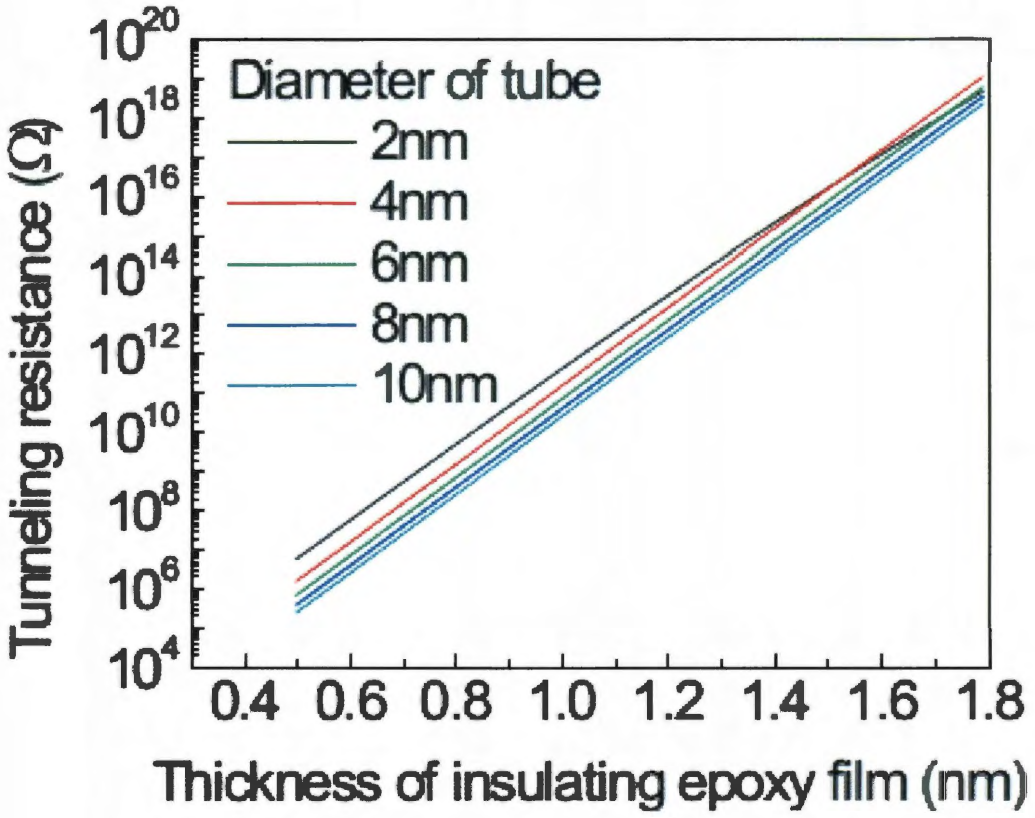

Figure 5.3. The tunneling resistance as a function of the thickness of epoxy in-between nanotubes [155].

Many factors could contribute to resistivity of the nanotube-filled composite such as structural defects on nanotubes, impurities as well as inter-tube barriers. A real sample normally contains all these resistivity contributors so that a combination of different mechanisms is needed to explain its conduction behavior.

If nanotubes were aligned and inter-tube distances were optimized within a nanotube fiber, the fiber would behave like a metal [156]. In this case, the metallic conduction mechanism is applicable for modeling the electrical properties of the nanotube fiber. Resistance, R as a function of temperature, T for the fiber can be formulated as

$$R = \alpha T, \text{ where } \alpha \text{ is temperature coefficient of resistance}$$

In 1997, Fischer et al. found that nanotube ropes and mats have a negative temperature coefficient of resistance ($dR/dT < 0$) at the low temperature region [157]. Metallic conduction model cannot fit the R-T curve at the low temperature region. Kaiser et al. observed the similar phenomenon in 1998 and proposed heterogenous conduction model to explain the crossover from the positive to negative sign of the temperature dependence of the resistance as temperature decreases [158]. At the high temperature region, the metallic conduction model is still valid, but at the low temperature region, fluctuation-induced tunneling was used to fit the resistance dependence of temperature [159]. The relation between resistance and temperature can be described by the formula:

$$R = R_t \exp (T_c/T+T_s),$$

Where parameters T_c and T_s are defined by the following equations:

$$T_s = 16\varepsilon_0 \hbar A V_0^{3/2}/(\pi e^2 k_B (2m_e)^{1/2} w^2),$$

$$T_c = 8\varepsilon_0 A V_0^2/(e^2 k_B w^2),$$

Where w is the width of the tunneling junction, A labels its area, and V_0 is the height of the contact potential; k_B stands for Boltzmann constant, $\hbar$ is planck constant, e is electronic charge, m_e is electron's effective mass, and ε_0 is the vacuum permittivity [160].

Other than fluctuation-induced tunneling model, variable range hoping (VRH) model can also be applied to explain the low temperature conduction behavior of the nanotube ropes [161].

Variable range hopping model defines the resistance dependence of temperature as

$$R = R_0 \exp (T_0/T)^{1/n}, \text{ where}$$

$$T_0 = \beta/k_B \xi^3 g,$$

where β is a constant, k_B is Boltzmann constant, ξ denotes the localization length, and g is the density of states.

The nanotube-assembled macroscopic systems (nanotube fibers, ropes or matts) consist of large conductive segments (where electrons are delocalized and free to move over large distances as compared to the atomic dimensions) separated by small insulating gaps. Due to small size of tunnel junctions, thermal voltage fluctuation resulting from the thermal motion of electrons in the conduction region in the vicinity of the tunnel barrier can drastically change the electron tunneling probability through the barrier. The tunneling through inter-tube barriers is well explained by fluctuation-induced tunneling model. The conduction within the tubes can be well described by metallic conduction

model. Figure 5.4 shows the fitting of R-T curve of a DWNT cable (More detailed research on the DWNT cable will be covered in chapter 6.). The low tempreture and high temperature sections of this curve are individually fitted by fluctuation-induced model and metallic conduction model. Based on a converted form of fluctuation-induced model, InR is proportional to 1/T. The experimental data (as shown in the inset of figure 5.4) shows a good fitting to the theoretically predicted linear relationship. In the high temperature region, metallic conduction model gives a good fitting with the experimental data.

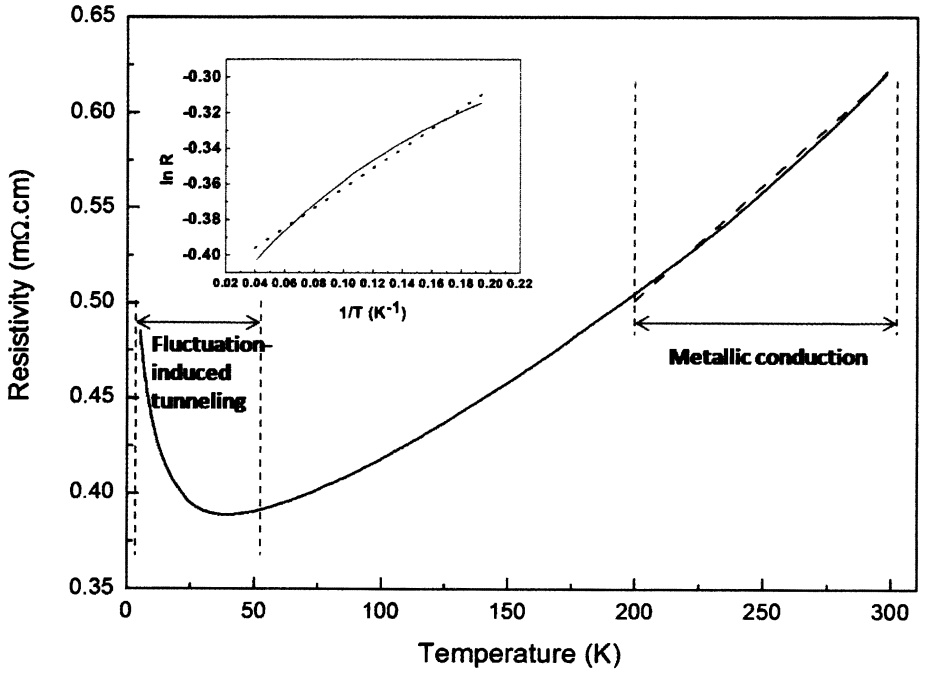

Figure 5.4. R-T curve for a DWNT cable. The fittings are applied in high temperature and low temperature regions individually. The solid line is drawn from the experimental data. The dotted lines are generated by the fittings based on fluctuation-induced model and metallic conduction model individually.

For the composites, within which 3-D nanotube networks randomly distribute and the inter-tube distances are relatively large (compared to the pure nanotube fiber system), metallic conduction model is no longer valid. To model the conduction behavior of the composites, the percolation theory is normally applied [154, 162-165]. It basically describe a phenomenon that when nanotube concentration is very low, resistivity of the composite is as large as that of the insulating matrix, but as the nanotube concentration reaches a certain value (defined as percolation ratio), a sharp drop occurs in resistivity. The resistivity as a function of nanotube concentration above the percolation ratio can be decribed by the formula:

$$\rho \quad (\Phi - \Phi_c)^t \text{, where}$$

ρ is resistivity, Φ_c is the critical concentration of the nanotubes. t is a exponential coefficient, which varies by different samples.

5.2 Experimental

5.2.1 Nanotube purification

Purification was conducted on nanotubes before they were added into the composite. For the project, study of the composite wires at high loading ratios, three types of nanotubes were used. They were HiPco nanotubes (Unidym Inc.), CG nanotubes (Southwest Inc.) and Multi-walled Nanotubes (Bayer Inc.). Impurities of different components and quantities required different methods to remove. Two questions needed to be addressed for designing effective purification protocol for different nanotubes. What is the composition of the impurities, and how much impurities are there in the raw nanotubes? Extensive characterizations revealed the detailed information. First, TEM was used to identify the existence of impurities for three types of nanotubes. Then, XPS and EDX were applied to characterize the composition of the impurities. Finally, TGA was utilized to measure the weight ratio of the impurities.

Figure 5.5 showed that black dots were scatteredly distributed all over the HiPco nanotubes. Nanotube diameter was homogeneous and the average diameter was 1.2 nanometers. HiPco nanotubes were majorly comprised of single-walled nanotubes. They were bundled by van der Waals interactions. XPS of the raw HiPco nanotubes (figure 5.6) showed a significant peak at 707 eV, which was caused by the iron catalysts. Furthermore, TGA (figure 5.7) revealed that weight ratio of iron is about 15% (this value varies from batch to batch). To remove iron in the HiPco nanotubes, we washed the raw nanotubes in the solution of 30 % hydrogen peroxide and 1M hydrogen chloride (4:1 by volume) at 60°C for 4 hrs. In this purification process, 30 % hydrogen peroxide was used to remove

the amorphous carbon covered over the iron particles and so that hydrogen chloride could directly react with the iron particles. After 4 hours purification treatment, most iron particles were removed. Normally, after one cycle of the purification, impurity ratio decreased from 15 wt % to less than 5 wt %. The second cycle of the purification could further decrease impurity ratio down to less than 2 wt %. Figure 5.8 showed the HiPco nanotubes after one cycle of the purification treatment. It was observed that number of black dots decreased significantly compared to the raw HiPco nanotubes.

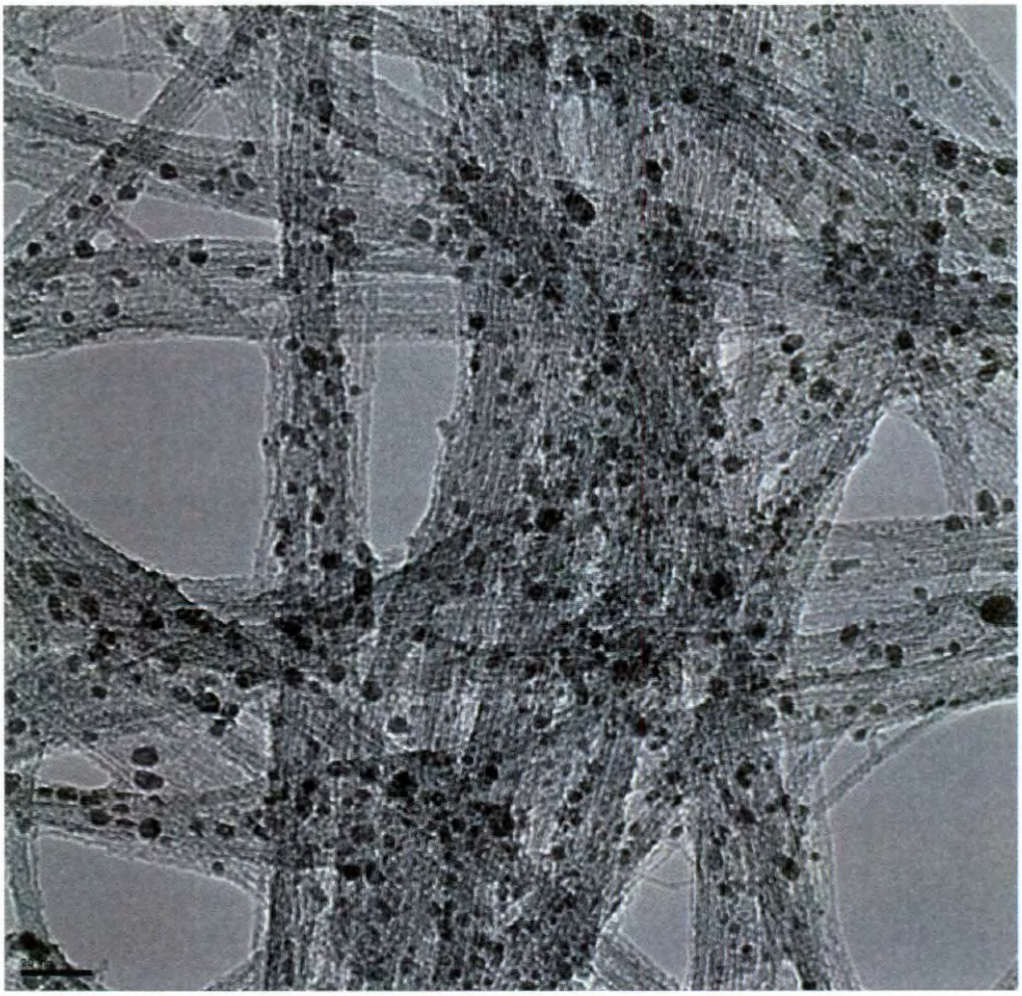

Figure 5.5. TEM image of the raw Hipco nanotubes.

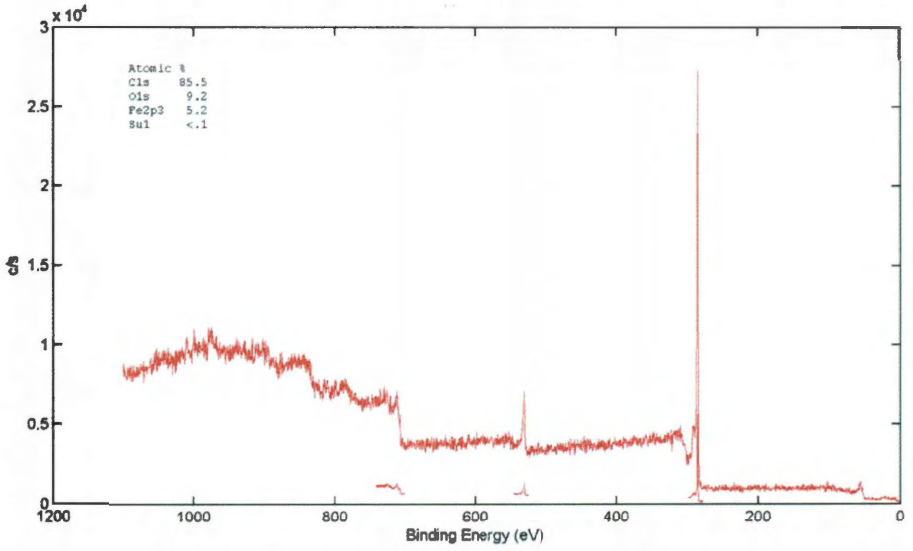

Figure 5.6. XPS spectrum of the raw HiPco nantoubes.

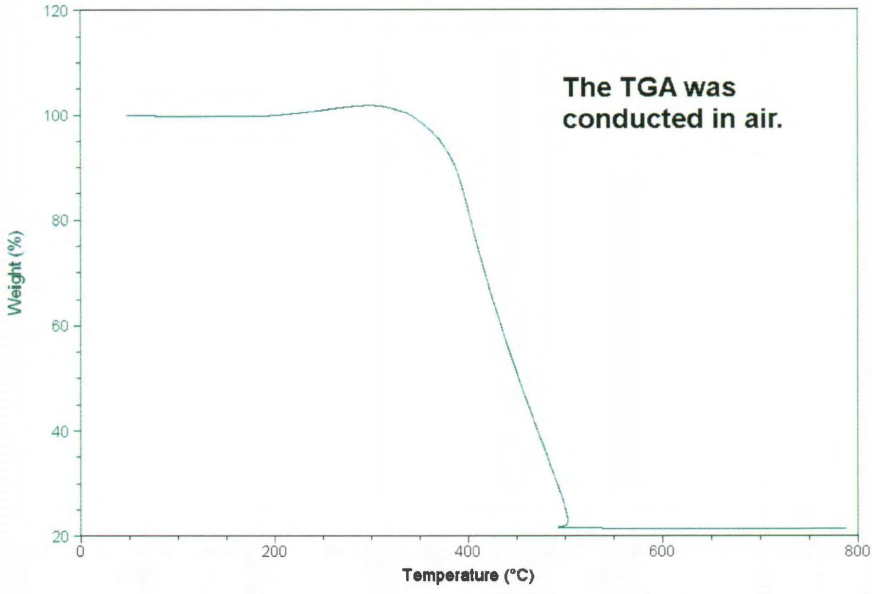

Figure 5.7. TGA curve of the raw HiPco nanotubes.

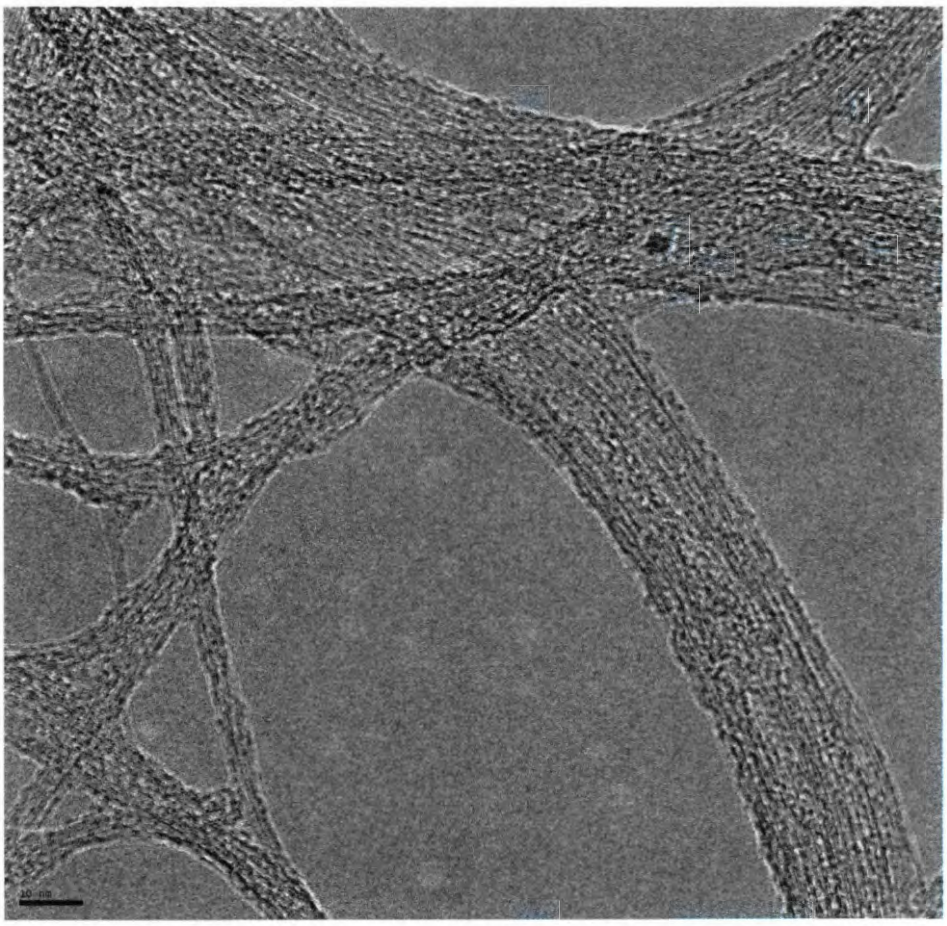

Figure 5.8. TEM image of the Hipco nanotubes after one cycle of the purification.

Figure 5.9 showed the CG nanotubes as-received from the vendor. They were single-walled nanotubes too. Compared to HiPco nanotubes, CG tubes did not contain much metal catalysts. However, their surface was rough and wrapped by some irregular-shaped amorphous carbon. In order to remove amorphous carbon, we boiled raw CG tubes in the 30 % hydrogen peroxide at 60°C for 4 hrs. This method proved to be effective for removing amorphous carbon in purifying the HiPco nanotubes. After the amorphous carbon was washed away, nanotubes were annealed at 1500 °C for 4 hrs. Figure 5.10 showed that the CG nanotubes were almost free of metal catalysts after the purification.

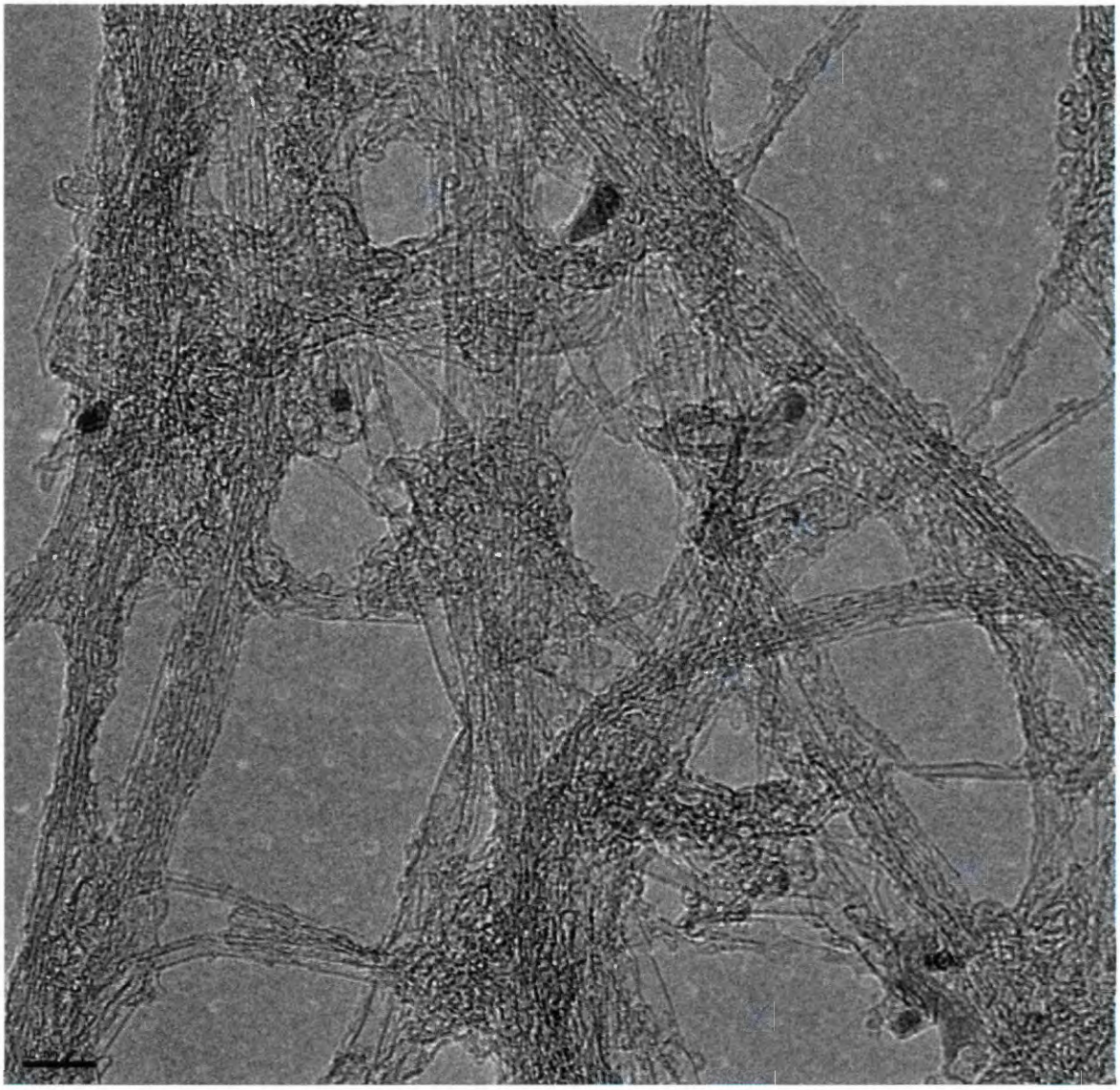

Figure 5.9. TEM image of the raw CG tubes.

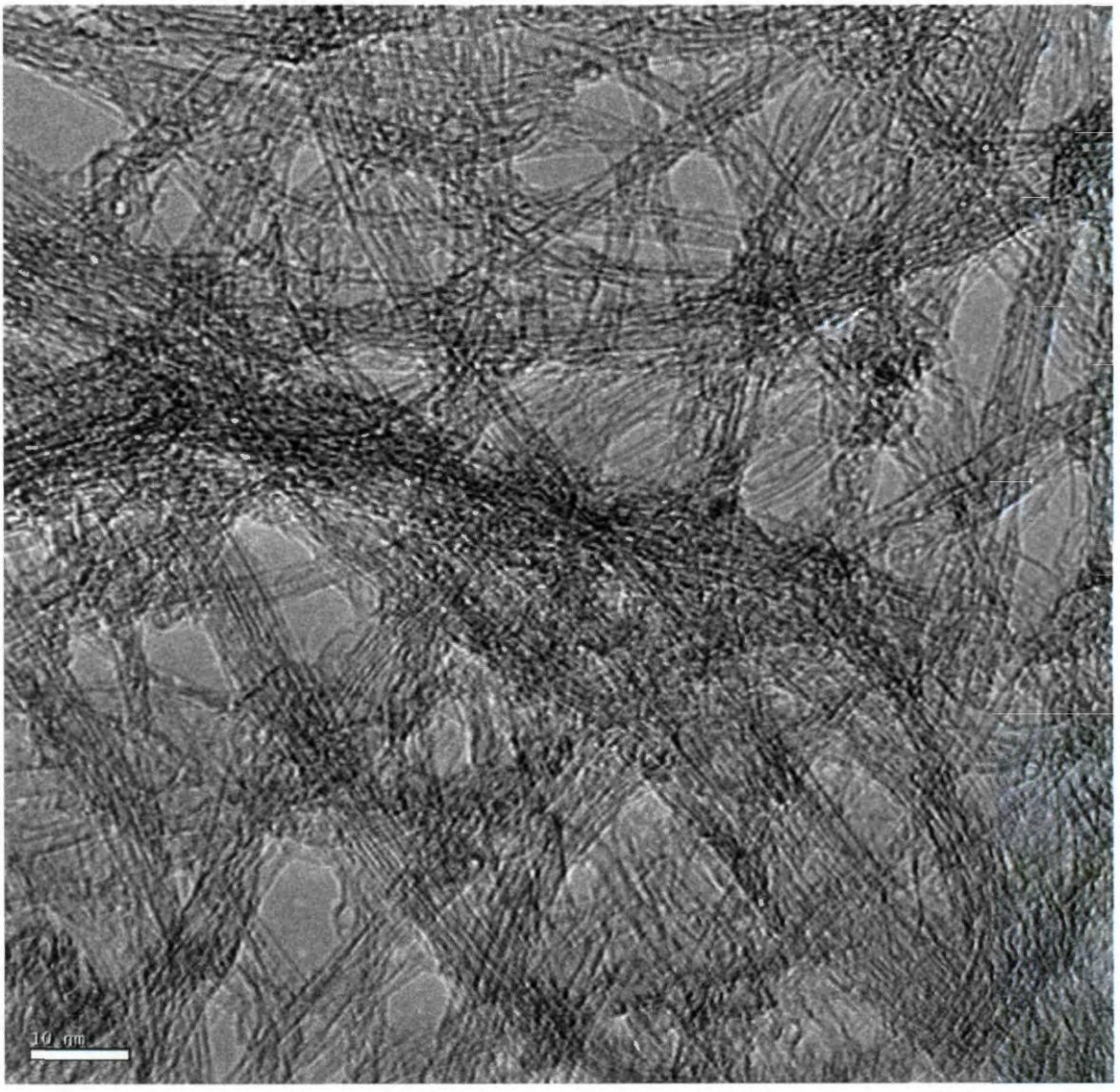

Figure 5.10. TEM images of the purified CG tubes.

Figure 5.11 illustrated the Bayer nanotubes. These nanotubes primarily were multi-walled with diameters varying from few nanometers to tens of nanometers. From Figure 5.11, we could tell that Bayer nanotubes were pure and their surfaces were smooth. In the following experiments, Bayer nanotubes were used in their as-received form.

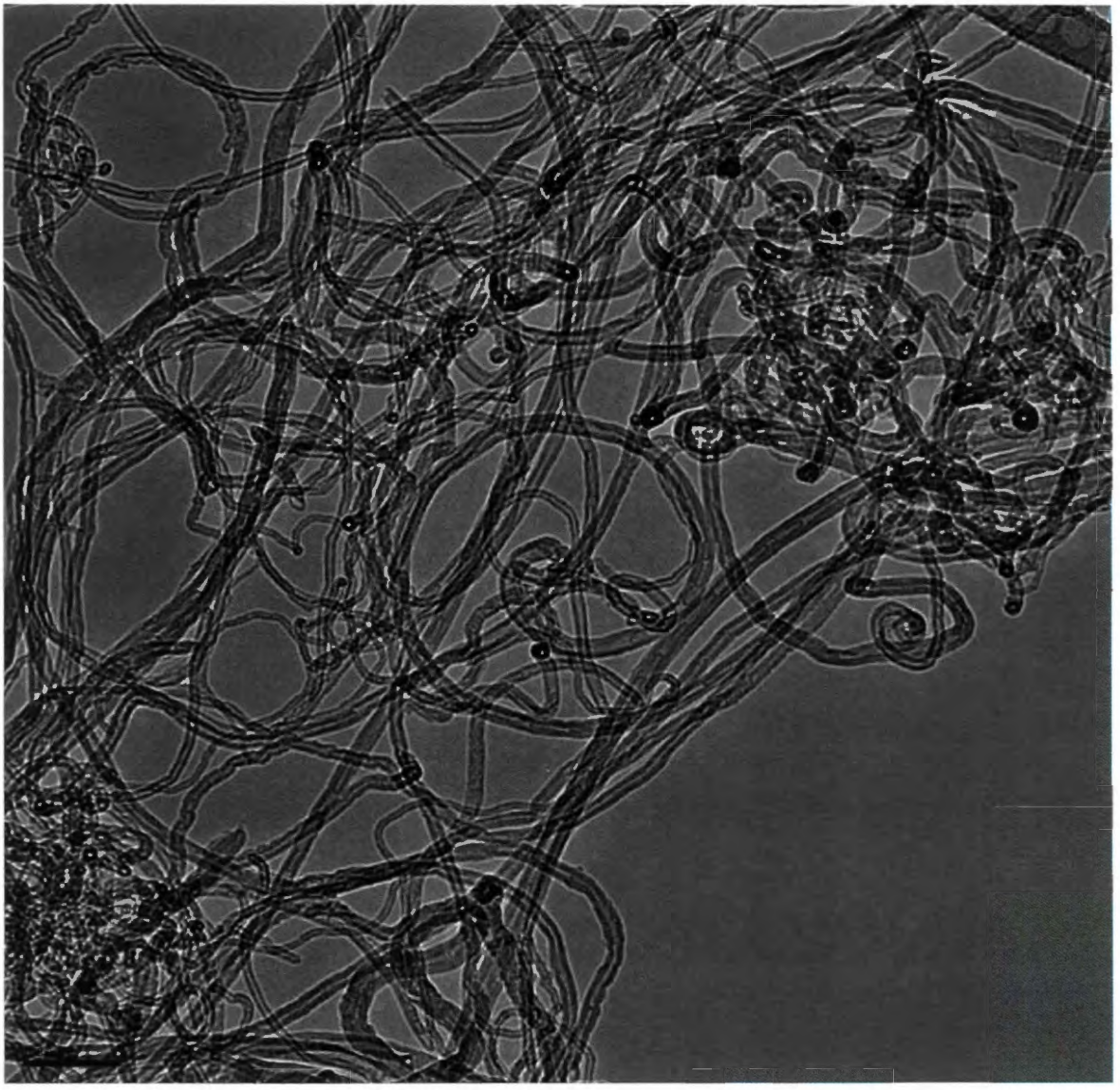

Figure 5.11. TEM image of the Bayer nanotubes.

5.2.2 Fabrication of nanotube-filled composite wires

Incipient wetting is a precursor step before melt mixing. The solvent used in the incipient wetting has to be carefully selected based on its ability for dissolving the polymer matrix and dispersing nanotubes. It is not only required to be able to soften the polymer matrix but also to disperse nanotubes efficiently. After mixing nanotubes with the polymer powder in the solvent and subsequently removing the solvent, the nanotubes are homogeneously stuck onto the surface of the polymer powder as shown in figure 5.12. The detailed procedures for the incipient wetting are described as the follows:

Bayer nanotubes and HDPE powder were mixed in chloroform along with intense sonication (100 ml chloroform was used to disperse 20g mixture of the nanotubes and HDPE powder). Followed by the mixing step, chloroform solvent was removed under 60°C heating in a vacuum oven.

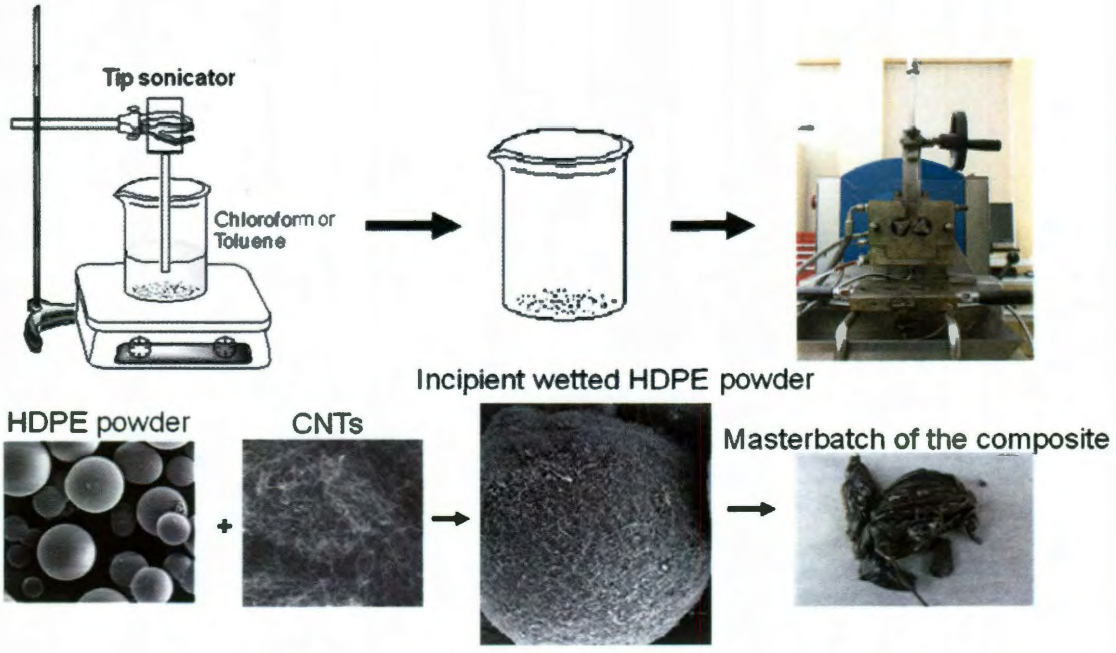

Figure 5.12. Schematics of the procedures for making Bayer CNTs/HDPE masterbatch.

As the HDPE powder was well wetted with the nanotubes, the incipient Bayer CNTs/HDPE powders were fed into a mixer. The melt mixing was conducted at 150°C for 30 mins. The rotation speed of the rollers was set at 80 rev/min. After the melt mixing, the resultant bulk Bayer CNTs/HDPE masterbatch was pelletized into small pieces and fed into an extruder. The extruder had three heating zones-the feeding zone, the mixing zone and the extruding zone which individually operated at 145°C, 150°C and 155°C. The screw rotation speed was set at 60 rev/min. As the materials were delievered to the end zone by the screw and run through the nozzle, the composite wires were formed. Figure 5.13 showed the schematics of the fabrication process.

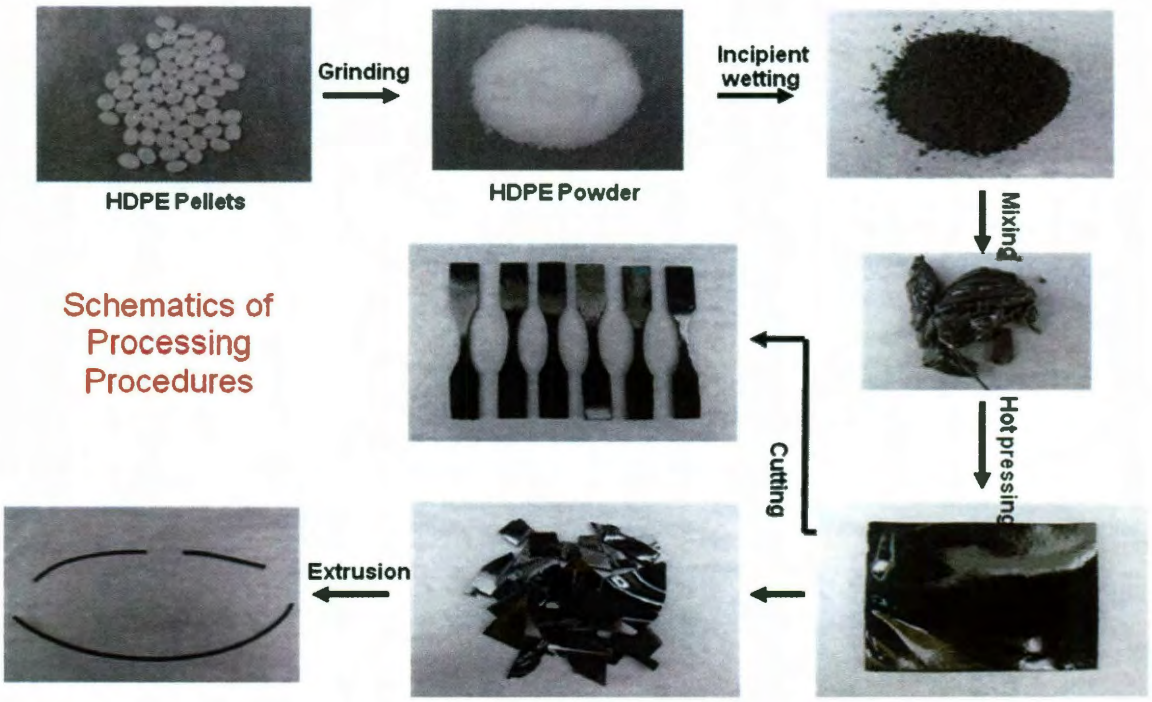

Figure 5.13. Schematics of the procedures for making Bayer CNTs/HDPE composite wires.

Injector, miniextruder, Haake extruder and M-scientific extruder (as shown in figure 5.14) were used to carry out melt spinning. These four instruments can satisfy a wide spectrum

of production demands from the experimental scale to the industrial scale. The injection molding is applicable for processing a small amount of materials (the minimum amount is 3 grams). Whereas, for miniextruder, Haake extruder and M-Scientific extruder, the minimum amounts for consistently making composite wires are 10 grams, 100 grams and 200 grams individually. The major difference the injector from extruders is that injector does not have lead screws, which give the additional shear forces to materials.

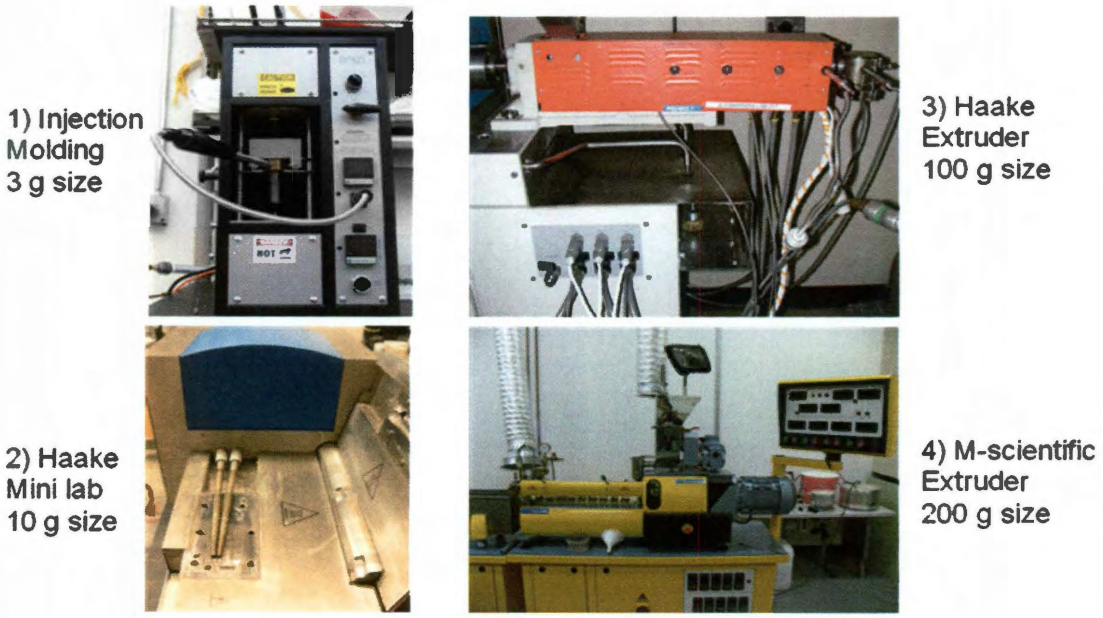

Figure 5.14. Photos of the four instruments applied for producing the Bayer CNTs/HDPE composite wires.

5.3 Results and discussion

5.3.1 Electrical conductivity of the composite wires at high loading ratios

Composite wires individually filled with 10 wt% HiPco, Bayer or CG nantoubes were prepared. Average resistivity of HiPco nanotubes/HDPE and Bayer nanotubes/HDPE composite wires respectively were 110 and 114 ohm.cm. But average resistivity of CG nanotubes/HDPE composite wires was 1250 ohm.cm. This indicated that HiPco nanotubes and Bayer nanotubes were more desired as fillers in improving the conductivity than CG tubes. This might be attributed to the fact that HiPco and Bayer nanotubes had fewer defects than CG tubes. Since there was no significant difference in resistivity between HiPco nanotubes and Bayer nanotubes filled composites, but the HiPco nanotubes were much more costly than Bayer nanotubes, therefore in this research solely Bayer nanotubes were used in studying the electrical properties of the composites at high loading ratios.

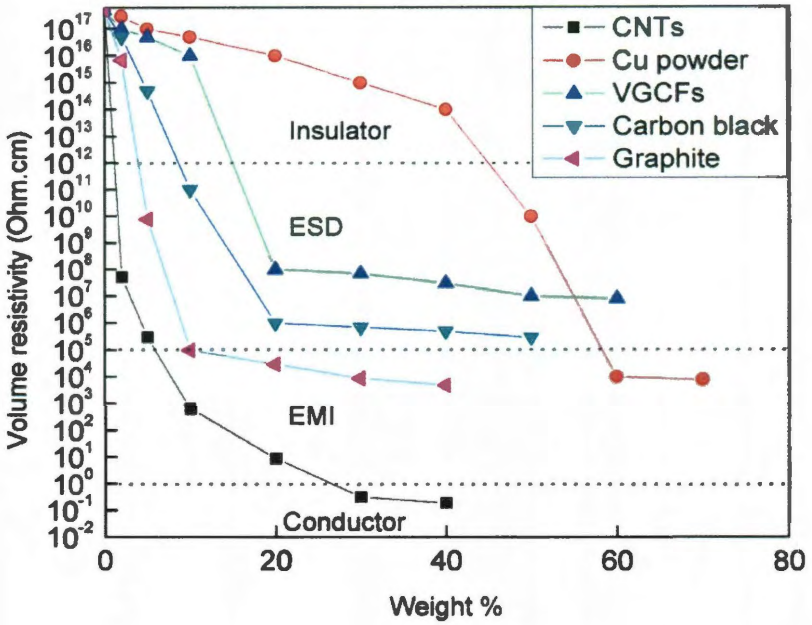

Figure 5.15. Resistivity as a function of loading ratio for 5 different composite systems. The matrix of all the composites is HDPE. The fillers are varied including Bayer CNTs, Cu powder, VGCFs, Carbon black and graphite.

Bayer nanotubes at loading ratios from 2 wt% up to 40 wt% were added into HDPE to make composite wires. 40 wt% is the uplimit of loading ratio, beyond which the HDPE as the binding material is too few to maintain the mechanical integrity of the composite wires. Figure 5.15 shows that a sharp drop in resistivity occurs at a loading ratio of 2 wt%. This indicates that the critical percolation ratio (at which, the conducting nanotube networks start to form) of the nanotubes-filled composite wires is around 2 wt%. Resistivity of the composite wires at the critical percolation ratio is ~10^5 ohm.cm. As resistivity is at this level, the composite wires are suitable for electrostatic discharge (ESD) applications but not for conducting wires (The ranges of resistivity for ESD, EMI and conductor applications are labeled in figure 5.15). Adding more nanotubes is needed

to further enhance conductivity of the composite wires. As loading ratio increases to 40 wt%, resistivity of the composite wires reaches the minimum, 0.14 ohm.cm. Within the composite wires of 40 wt% nanotubes, the direct tube-to-tube contacts are more prevailing than what happened for the composite wires of a smaller loading ratio. In the as-prepared composite wires, the nanotube networks are 3-D randomly arranged and the insulating polymers are inevitably existing in-between nanotubes.

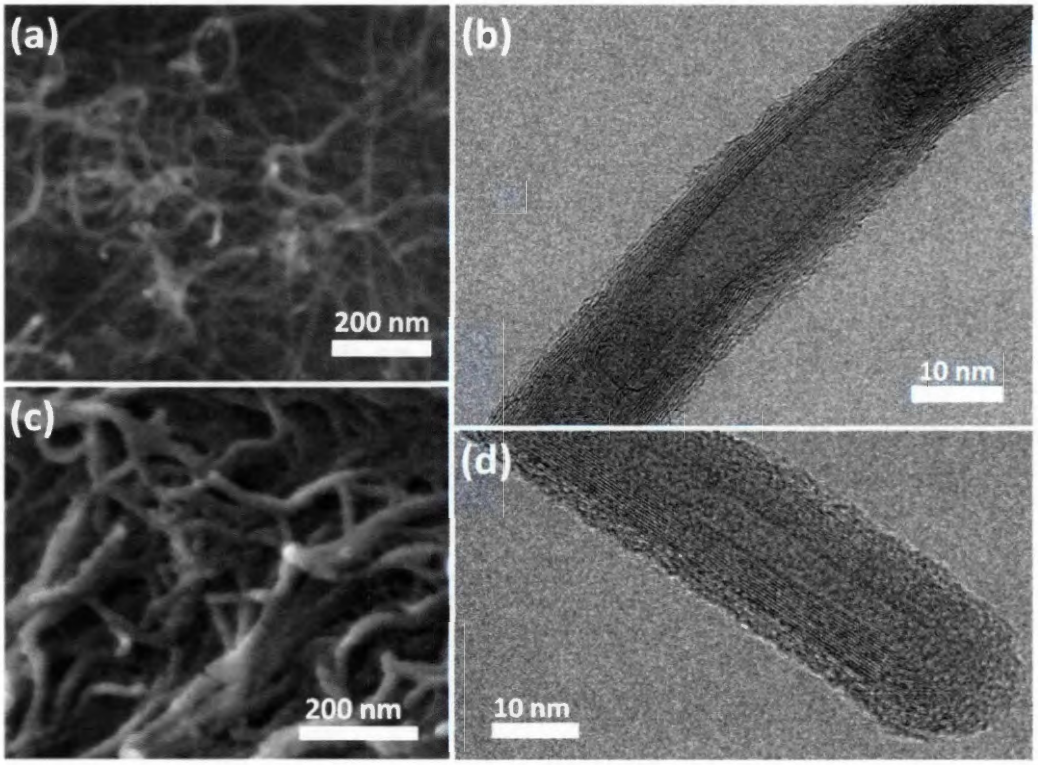

Figure 5.16. Morphology analysis on pure Bayer nanotubes and the nantubes within a MWNTs/ HDPE composite: (a) SEM image of the pure Bayer MWNTs. (b) TEM image of a single Bayer MWNT. (c) SEM image of the fracture surface of the MWNTs/HDPE composite. (d) TEM image of a fractured piece from the MWNTs/HDPE composite.

Comparing the image of pure Bayer nantoubes to that of the nanotubes in the HDPE matrix, we can clearly see the nanotubes were coated with a layer of HDPE polymer. The high resolution TEM image (figure 5.16 (d)) reveals that the thickness of the polymer

coating layer is about 1 nm. This finding provides us thoughts about how to improve conductivity of the composite wires. It is critical to prevent the polymer from wrapping around nanotubes and increase the number of the direct tube-tube contacts.

To further improve conductivity of the composite wires of 40 wt% loading ratio, two strategies can be applied. One is to improve the alignment of the nanotubes. The other is to optimize the tube-to-tube contacts.

5.3.2 Strategies for enhancing electrical conductivity

Either diminishing the nozzle size or increasing the take-up speed was found to be effective to improve the alignment of nanotubes [166-168]. As a result, conductivity of the composite wires can be enhanced. For the Bayer nanotubes/HDPE system, the conductivity was increased by 3 fold by narrowing the diameter of the nozzle from 3 mm to 1 mm. Via increasing the take-up speed from 20 m/min to 100 m/min, conductivity of the composite wires was enhanced by 2 times.

Annealing was another effective method for improving conductivity of the composite wires [169-171]. The enhancement effect was more pronounced for the samples of low loading ratio than that of high loading ratio. Figure 5.17 showed that annealing caused conductivity of the composite wires of 10 wt % nanotubes increased by two orders of magnitude. For the sample of 40 wt %, the enhancement effect greatly weakened at the same annealing condition. Figure 5.18 illustrated the annealing time effect on the conductivity. The enhancement effect became saturated upon 2 hrs annealing. Longer annealing time did not improve conductivity. Figure 5.19 showed resistivity decreased

slightly as the temperature increased from 210°C to 300°C. The conductivity enhancement might be due to that annealing caused the intercalated polymer between the nanotubes melt and hence, the contacts between the nanotubes were improved.

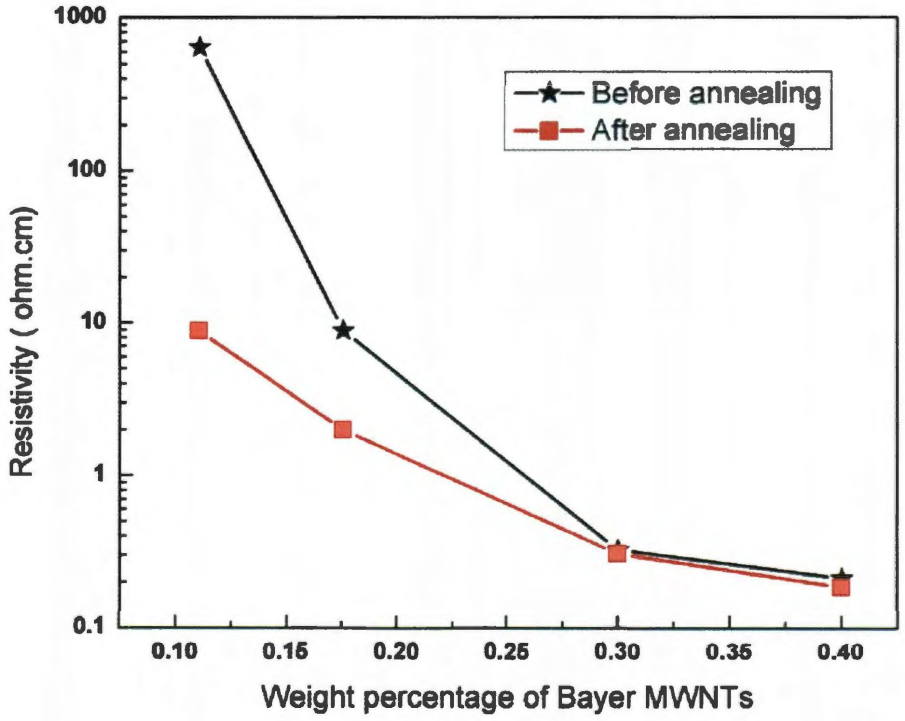

Figure 5.17. Resistivity of the composite wires with various loading ratios before and after the annealing at 210°C for 2 hrs in Argon.

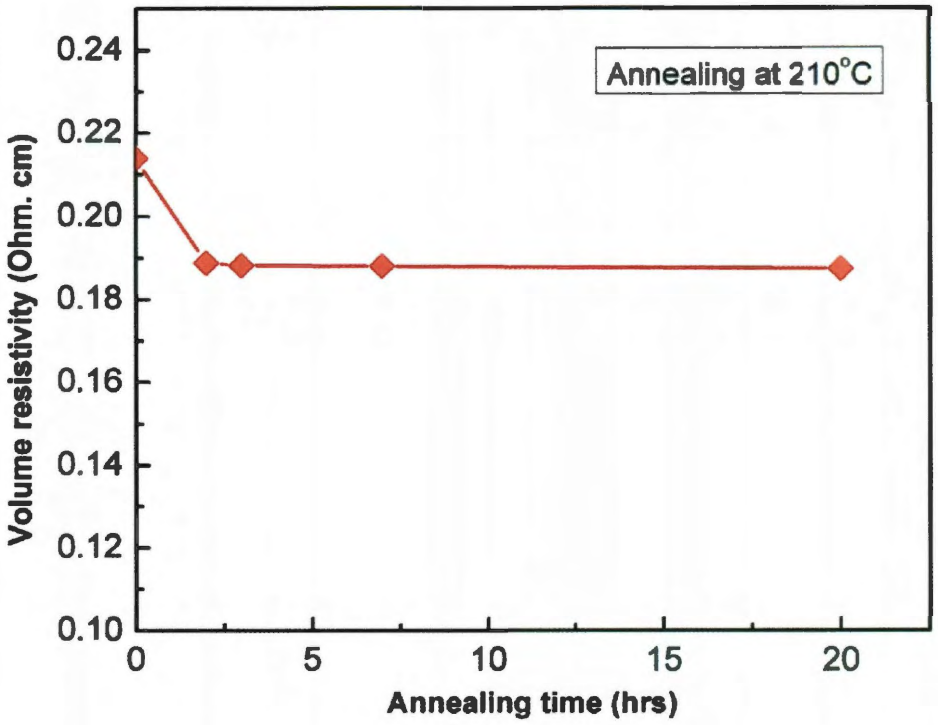

Figure 5.18. Resistivity of the composite wire loaded with 30 wt% Bayer nantoubes as a function of annealing time.

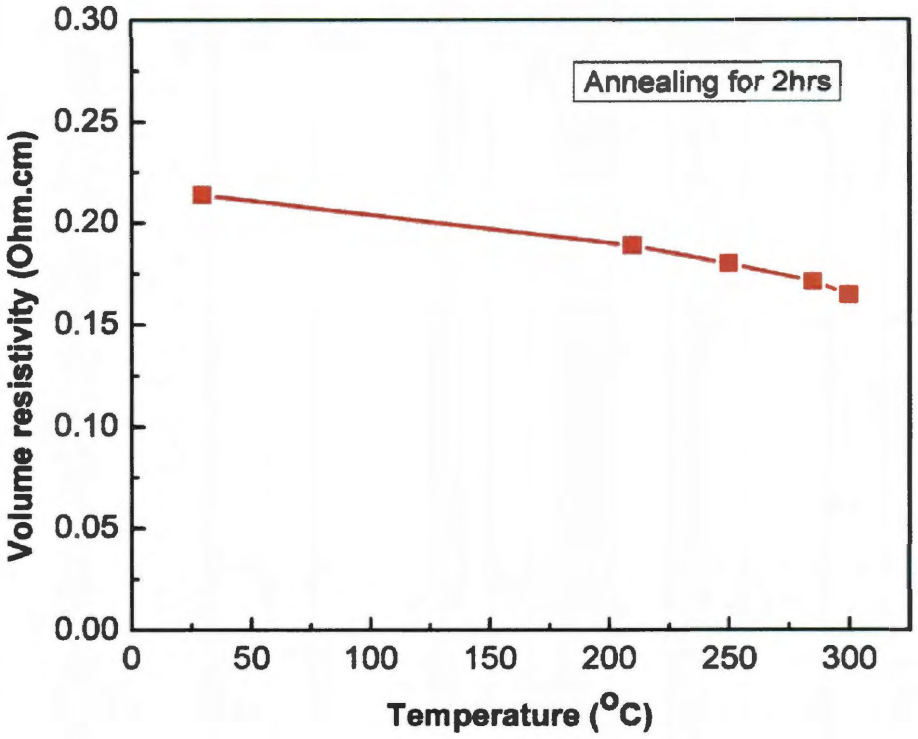

Figure 5.19. Resistivity of the composite wire loaded with 30 wt% Bayer nanotubes as a function of annealing temperature.

Other than the forementioned methods for improving conductivity, doping was another method applied in this research. Doping not only could be employed on the nanotubes before adding them into the polymer matrix but also on the composite wires after the CNTs/HDPE wires coming out from the extruder. Before filling the nanotubes into the HDPE matrix, they were doped by $SOCl_2$ [172-175]. The doping made the nanotubes more conductive and facilitated their dispersion within the polymer matrix. The composite wires loaded with the $SOCl_2$ doped CNTs showsed 50 % increase in conductivity than their counterpart loaded with pristine CNTs at the same loading ratio. Post-treatment also could enhance conductivity of the composite wires. The as-produced

composite wires were placed in iodine steam environment for 8hrs at 120°C. After the iodine doping, resistivity of the composite wires reduced by a factor of 3.

5.4 Conclusions

A variety of strategies have been attempted to improve conductivity of the composite wires. However, resistivity reached the bottleneck at the level of 10^{-2} ohm.cm in the nanotubes/HDPE composite system. It was still far behind the goal to make a macroscopic wire of competitive conductivity to metals. Through study the microstructure of the composite (as shown in figure 5.16), the polymer wrapped around the nanotubes was identified as the major block for improving the conductivity. To meet the goal, I started the study of pure nanotube wires. The detailed work was introduced in chapter 6.

Chapter 6: Iodine doped nanotube cables exceeding specific conductivity of metals Model

6.1 Introduction

Since its discovery [31], researchers have tried to translate the excellent properties of individual carbon nanotubes (CNTs) to larger assembled components. Among these, a macroscopic cable that would replace metals as a universal conductive wire would have large applicability [24], such as electricity transmission, aerospace and automobile industry. Several methods have been developed for creating multi-walled, double-walled and single-walled carbon nanotube based fibers based on wet and dry spinning methods, over the years [24-30, 103-109, 176-179]. The main premise for these works has been to generate nanotube fibers with good mechanical properties. The electrical properties have also been reported with resistivities over a large range between $7.1*10^{-3}$ Ω.m to $2*10^{-6}$ Ω.m. In the table 6.1, we have listed and compared the resistivities of various nanotube fibers and metals prepared by a variety of techniques. For these fibers, up to now, their resistivity values is 2 to 3 orders higher than that for oxygen free Cu, ($1.68*10^{-8}$ Ω.m), one of the most conducting metals widely used in current carrying applications. Here we report fabrication and doping of carbon nanotube cables (we have chosen to use the terminology "cable" rather than fiber, as the main application pursued here is electrical transport), with resistivity one order of magnitude closer to the resistivity of Cu than predecessors. We believe that the superior conductivity is achieved by a synergistic effect of the unique structure of the CNTs, the rational design of processing and doping.

Table 6.1: The resistivity of carbon nanotube fibers published in major articles up to date and in this work, as well as copper and aluminum.

Ref.	CNT characteristics			Comments	Electrical resistivity (Ω.m)
	Type	Length (Microns)	Diameter (nm)		
1	SWNT	<1	~1	annealed	$1*10^{-4}$
2				as-spun	$1.5*10^{-3}$
3				annealed	$7.1*10^{-3}$
4				annealed	$2*10^{-6}$
5	SWNT grown by arc discharge	-	-	as-withdraw	$3.3*10^{-6}$
6	DWNT	-	8-10	as-spun	$2*10^{-6}$
7	MWNT	100	10	twisted	$3.3*10^{-5}$
8	MWNT	650	10	un-twisted	$5.9*10^{-5}$
				twisted	$2.4*10^{-5}$
9	MWNT	-	-	twisted	$2.4*10^{-5}$
				coated with 5 wt% PVA	$1.1*10^{-5}$
This work	DWNT	>10	2-3	Raw	$5*10^{-7}$
This work	DWNT	>10	2-3	Iodine doped	$1.5*10^{-7}$
Ref.	Elements			Comments	
10	Copper			Oxygen free at 20°C	$1.68*10^{-8}$
11	Aluminum			Oxygen free at 20°C	$2.82*10^{-8}$

6.2 Experimental

6.2.1 Preparation of nanotubes by flow catalytic CVD

Double-walled carbon nanotubes (DWNTs) are grown by flow catalytic chemical vapor deposition (CVD) method, in which catalysts are introduced in the reaction chamber by the carrier gas flow in a vapor form [180-182]. Figure 6.1 shows that DWNTs are flowing out from the high temperature reaction region to the downstream end of the tube. The DWNT networks macroscopically have an open-ended cylindrical shape, appeared like a "stocking". The "stocking" wall is marked by the arrow in figure 6.1.

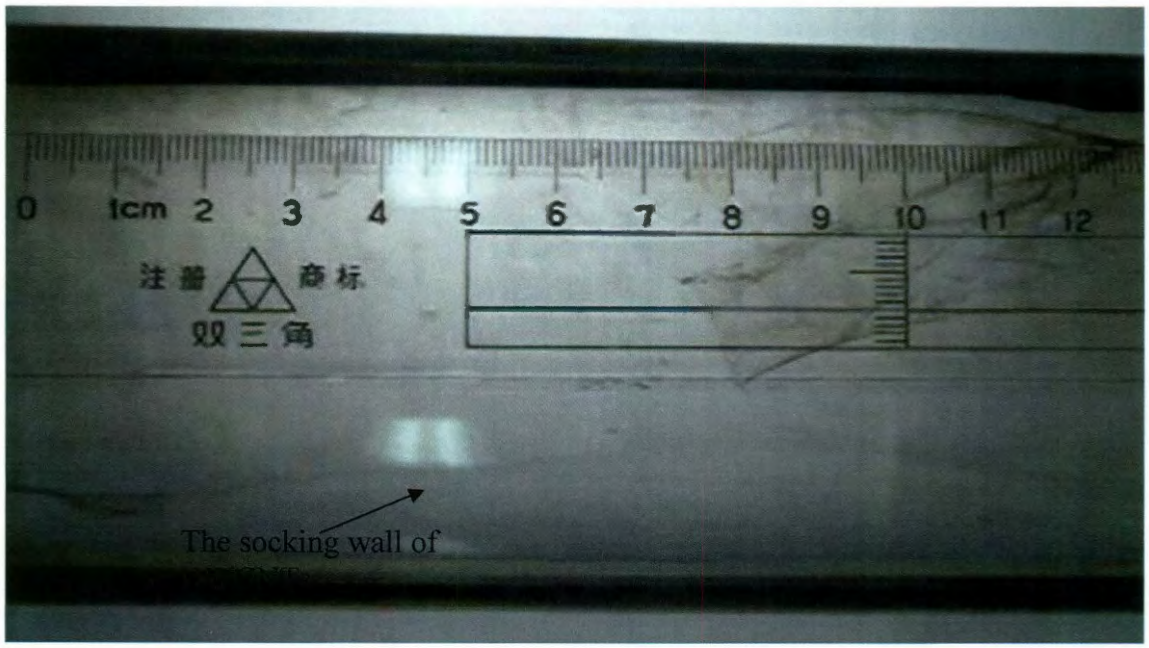

Figure 6.1. The downstream end of the CVD tube. Within the tube, DWNTs flow out like a thin-walled "stocking" continuously.

As the growth continues, DWNTs accumulates at the downstream end as shown in figure 6.2. The cone structure is composed of several layers of DWNTs film converged at the

left hand side. If a take-up system is attached at the downstream end, the DWNTs can be continuously pulled out from the furnace and the fibers could be continuously prepared.

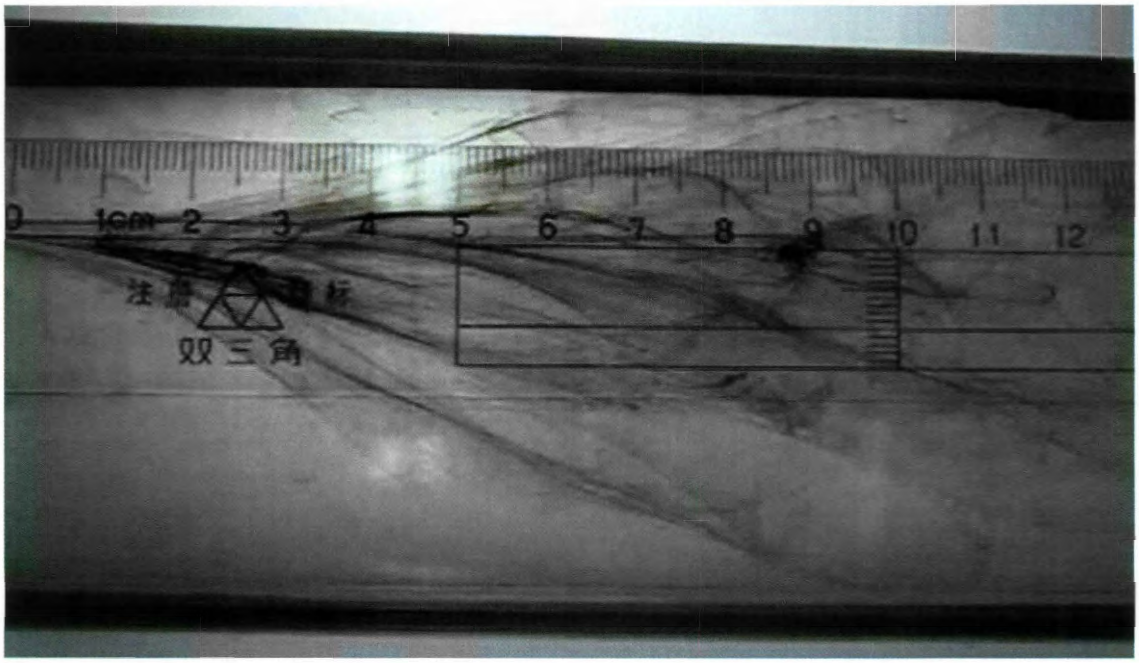

Figure 6.2. As the reaction proceeds, DWNTs accumulates at the downstream end and forms a cone structure. This cone is composed of several layers of DWNT "stocking" converged at the left hand side.

After the furnace cools down, the fluffy multilayered cone shrinks into a relatively more dense form as shown in figure 6.3. As collected from the furnace, the DWNT bundle contains catalysts.

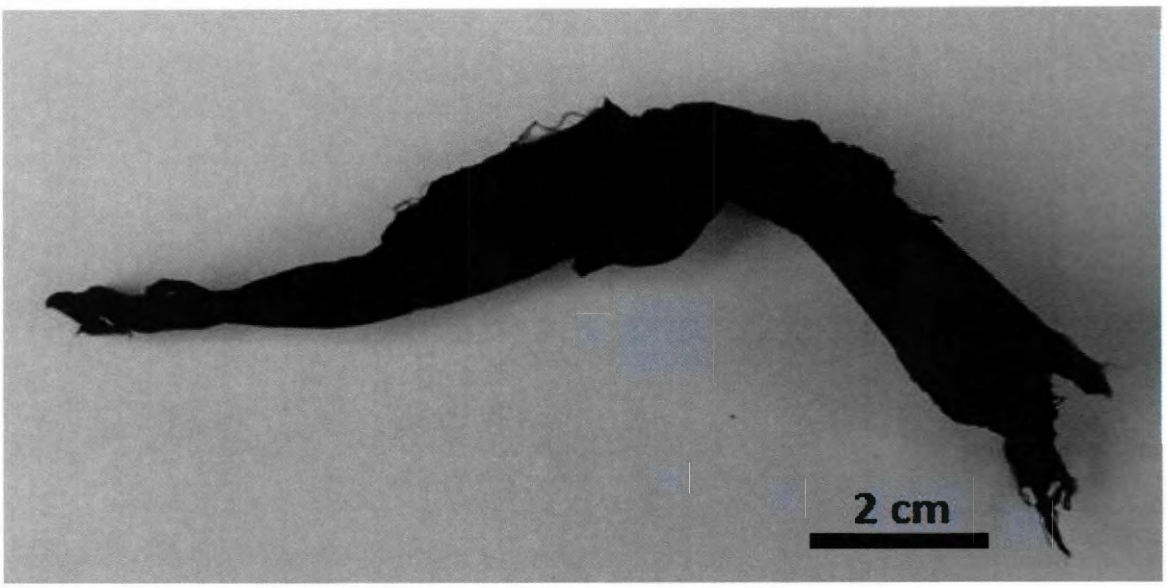

Figure 6.3. The DWNTs produced in one batch as they are collected from the cool-downed furnace.

6.2.2 Making nanotube fibers and improving their conductivity by iodine doping

Nanotube purification

The DWNTs as-grown contain catalysts. It was found that impurities cause degradation in conductivity. Therefore, we purified DWNTs before making them into cables. The DWNTs were first oxidized by heating the raw macroscopic DWNT bundle in air at 400°C for 1 hour. The oxidization treatment can attach oxidized functional groups to nanotubes and make DWNTs be of a better wettability with water. Then the oxidized DWNTs were soaked into a 30 % hydrogen peroxide solution for 72 hours. This soaking process can crack the amorphous carbon and make the catalysts dissociate from the carbon nanotubes. Afterward, the DWNTs were transferred into a 37% hydrogen chloride solution and soaked for another 24 hours. Then, the DWNTs as received from the

previous procedure were washed by DI water until they reach a neutral pH [44]. After the purification, the catalyst weight percentage is below 1 %.

Soaking in sulfuric acid

The diameter of cables is determined by how much DWNTs would be used to make the cable. The purified DWNTs in water are in a bundled form because of van der Waals interaction between tubes. The big bundle would result in making a cable of diameter larger than 20 μm. To peel off a small amount of DWNTs from the bundle to make a cable of diameter sub-10 μm, the bundle needs to be spread. The DWNT bundle was loosened up and spread into thin films by soaking in 98% sulfuric acid for 24 hours. After the soaking treatment, the DWNTs have a form as shown in Figure 6.4. From the thin film, a small amount of DWNTs in a ribbon form can be peeled off.

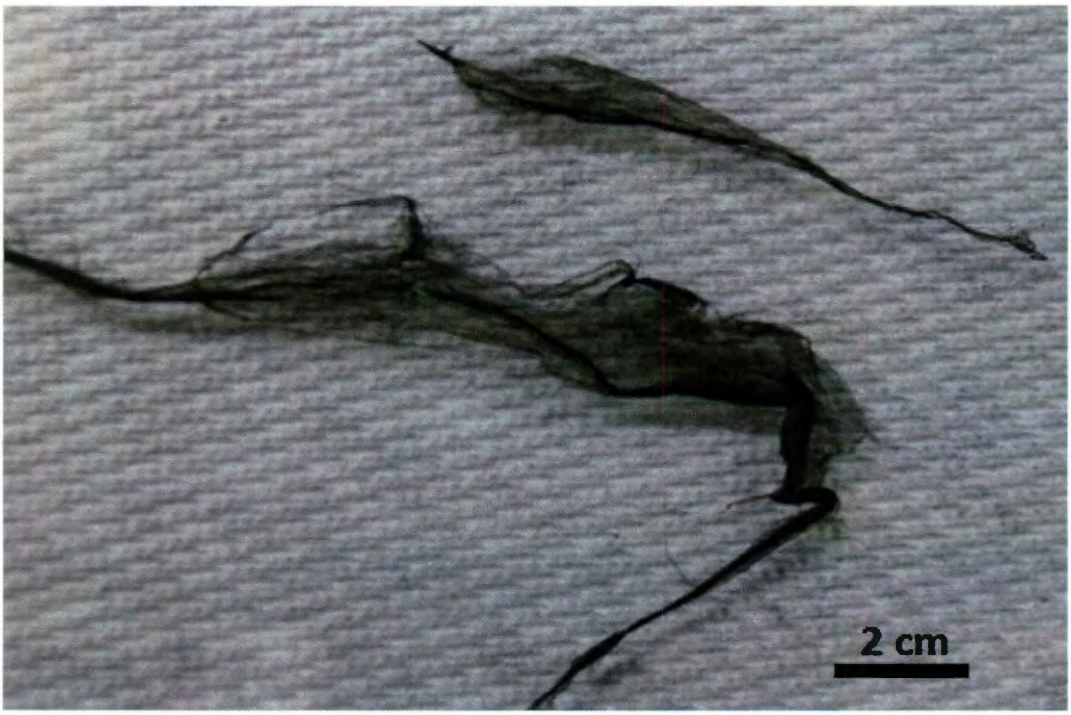

Figure 6.4. The DWNT bundle loosens up after soaking in 98% sulfuric acid. As shown is two pieces of thin film peeled off from the macroscopic bundle. The fibers of sub-10 μm diameter were produced from the even smaller ribbons, which were separated out from the thin films.

Shrinking

When the DWNT ribbon was taken out from the sulfuric acid solution, it would agglomerate into a spherical particle because the surface tension caused by the residual sulfuric acid is isotropic. To retain the length in the long axis direction of the ribbon, we applied the pulling force on the two ends of the ribbon to counteract the tension force from the sulfuric acid when the ribbon was taken out of the sulfuric acid solution. Then, the ribbon was dipped into the DI water to wash out the residual acid. Afterward, the ribbon was taken out of the water. Along with the water evaporation process, the ribbon shrunk into the cables as shown in Figure 6.5. The shrinking was a synergistic effect of the van der Waals force between tubes and the surface tension force from the water. At the last step of shrinking, other solutions such as ethanol, acetone and chloroform can be the substitutions for water. Microscopically, the original loose DWNT networks shrunk into a dense form.

After the raw cables were prepared, the iodine doping was conducted by placing the raw DWNT cables in the iodine vapor (the iodine vapor concentration is 0.2 mol/l) at 200°C for 12 hrs.

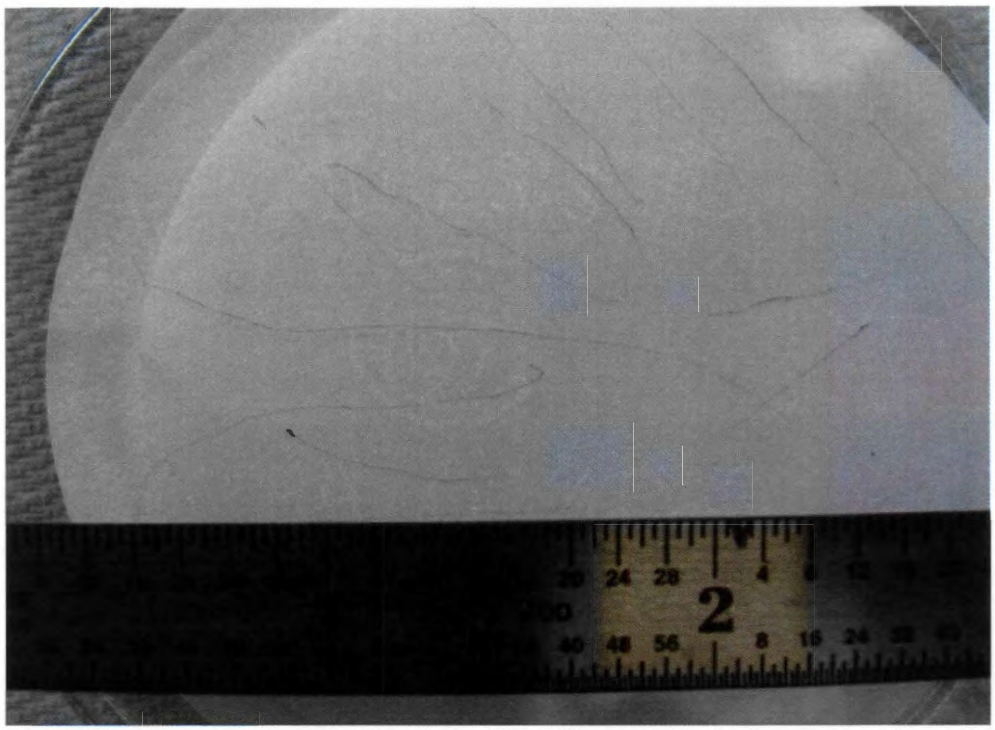

Figure 6.5. Fibers have a variety of lengths. The fiber length is determined by the length of DWCNT ribbon peeled off from the macroscopic bundle. The growth can be adjusted into a continuous process. Then, the DWCNT big bundle and fiber of an arbitrary length can be prepared.

6.2.3 Miscroscopy and elemental analysis on the nanotubes and the nanotube fibers

Transmission electron microscopy (TEM) was applied to observe nanostructures of DWNTs and iodine doped DWNTs. Scanning electron microscopy (SEM) was used to measure the diameter of cables and to observe the structure as well as the morphology of DWNTs before and after each step of the processing. The elemental composition of the iodine doped cables was characterized by x-ray photoelectron spectroscopy (XPS). To understand the distribution of iodine atoms, the elemental mapping for the iodine doped DWNTs was obtained via a Gatan imaging filter (GIF) attached with the TEM. In addition, Polarized Raman spectra of the raw and iodine doped cables were collected for

both the parallel and perpendicular directions to the long axis of the cables. For this study, a 632 nm laser associated with an 1800/m grating were used. X-ray diffraction spectra were collected for both the raw and iodine doped DWNTs. The X-ray source was generated from a Mo target.

6.2.4 Characterization of the eletrical and mechanical properties of the nanotube fibers

Electrical property measurements

Resistivity was calculated based on the length L, diameter D and resistance R of the cables using the formula, resistivity = $R*D^2*\pi/4/L$. The calculation is based on the assumption that cables are in a cylindrical shape. In fact, the cross section of some cables is not an ideal circle but an ellipse. In the calculation, we used long axis length as the diameter. By this approximation, the real resistivity of the cable is lower than the calculated value. Diameter, D of each cable plugged into the formula was an average based on the measurements at three different locations along the cable's long axis direction. The data reported in this study was based on the cables with a diameter variation smaller than 10% along the cable's long axis direction. The resistance was characterized by a Keithley 2400 in a four-probe configuration. The representative I-V curve for reading the resistance of the cable was shown in Figure 6.6.

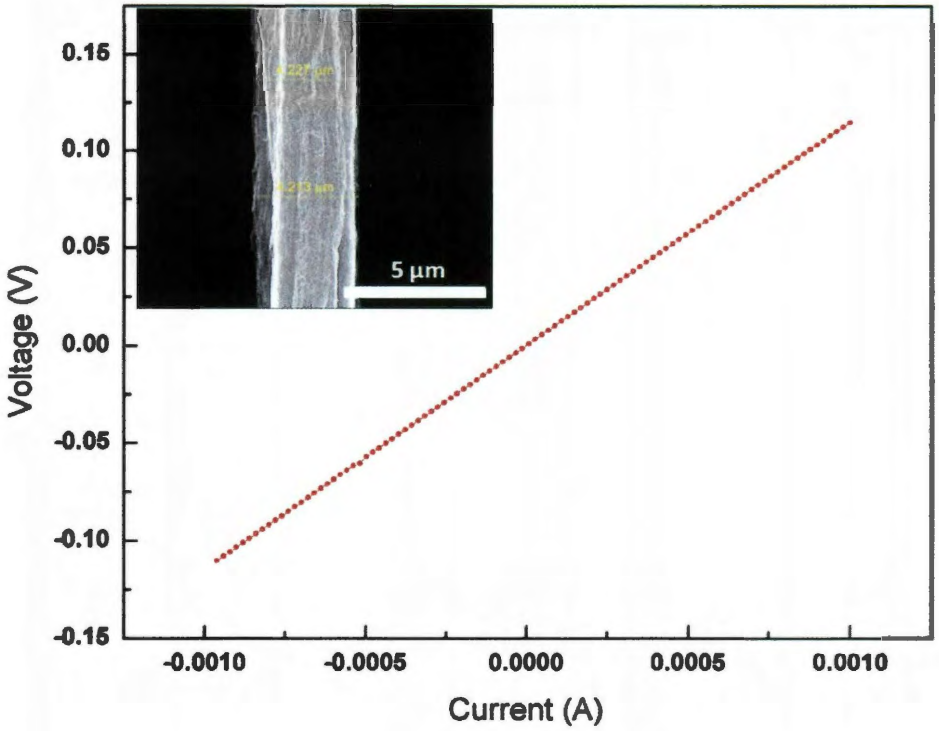

Figure 6.6. I-V curve for the iodine doped fiber. I-V curve is linear when the passing current is smaller than 1 mA. The linear feature is common for both the doped and the raw fibers. The slope of the I-V curve indicates the resistance of the iodine doped fiber as 114 Ω. The distance between two inner electrodes is 0.65cm. The average diameter of the iodine doped fiber is 4.22 µm as shown in the inset image. Plugging in the values of resistance, length and diameter into the formula, resistivity = $R*D^2*\pi/4/L$, the resistivity is calculated to be $2.43*10^{-5}$ Ω.cm.

Current carrying capacity was defined by the ratio of the critical current to the cross sectional area. The cable was connected with a Keithley 2400, which was the current source by two electrodes. The current passing the cable was stepwise increased. The critical current was recorded at the moment that the cable was burned. The representative current versus time curve for recording the critical current was shown in Figure 6.7.

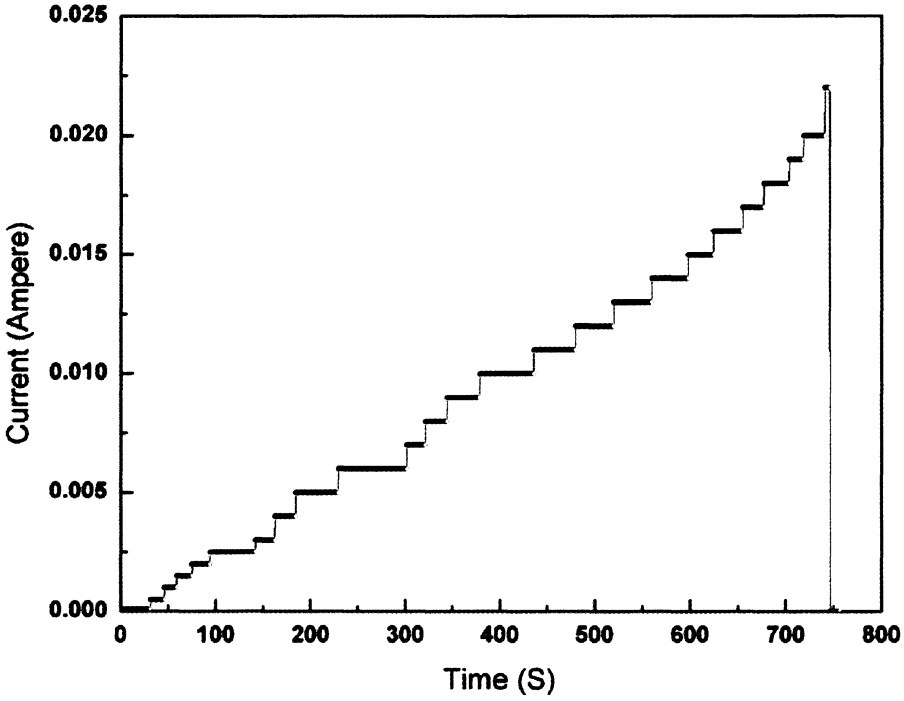

Figure 6.7. Curve showing current as a function of time used to determine the critical current. Critical current is the current at which the fiber breaks. The current was increased in a stepwise manner until the iodine doped fiber with a diameter of 4.2 microns broke at 22.5 mA. The current carrying capacity of this fiber is $1.62*10^5$ A/cm^2. The formula for calculating the current carrying capacity is shown as below:

$$\text{Current carrying capacity} = \frac{\text{Critical current}}{\text{Cross section}} = \frac{I}{(\pi D^2/4)}$$

Mechanical property measurements

Tensile testing was conducted on five undoped and five doped cables using an electrodynamic test system (Electroplus 3000, Instron). The strain rate was set at 0.2%/s.

6.3 Results and discussion

6.3.1 Microstructure of the nanotubes and the nanotube fibers

Figure 6.8 shows the nanotubes aligned in one direction. Figure 6.9 (a) shows the nanotube bundles interconnected and formed into a continuous network. The small bundles and the nanotubes by themselves are several microns long. After the nanotubes were fabricated into the cable as shown in Figure 6.9 (b), the natural alignment of the nanotube stock was retained which turns out to be beneficial for the conductivity of the cable. The nanotubes we have used here (Inset of figure 6.10) are double-walled (DWNT), the diameters are in the range of 2-3 nm and uniform (figure 6.10).

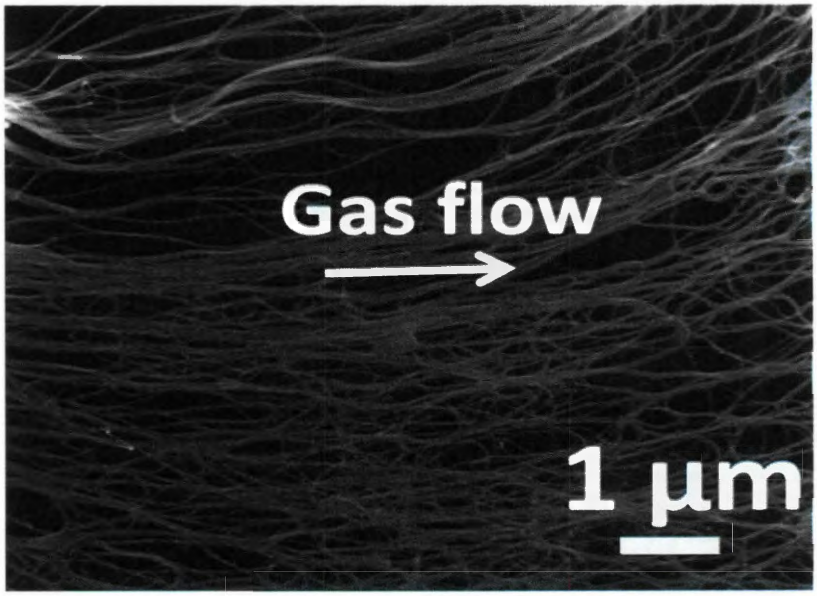

Figure 6.8. SEM image of a small piece of the carbon nanotube film peeled off from the "stocking". Carbon nanotubes are aligned in the gas flow direction as marked by the white arrow.

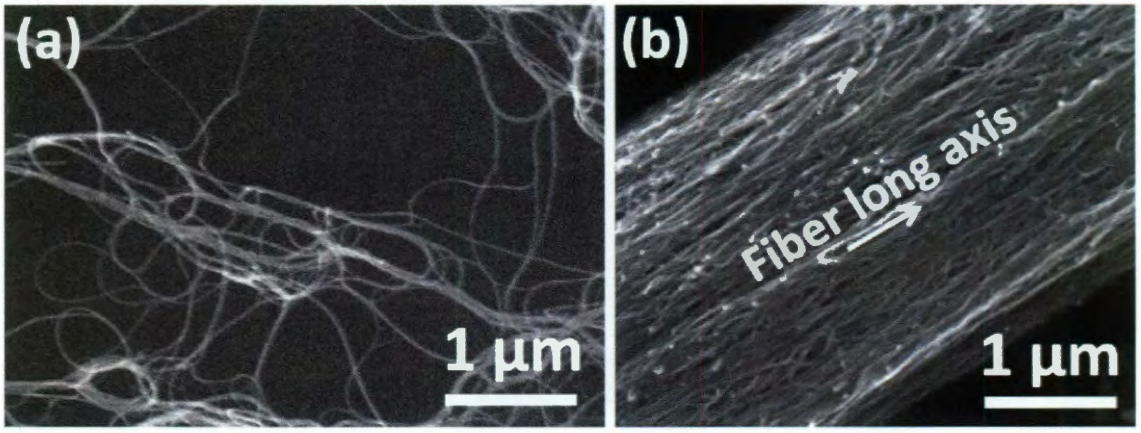

Figure 6.9. Morphology of the raw DWNTs and DWNT cable. (a) SEM image of the "stocking" wall. It shows the carbon nanotube bundles are interconnected. (c) SEM image of the raw carbon nanotube cable.

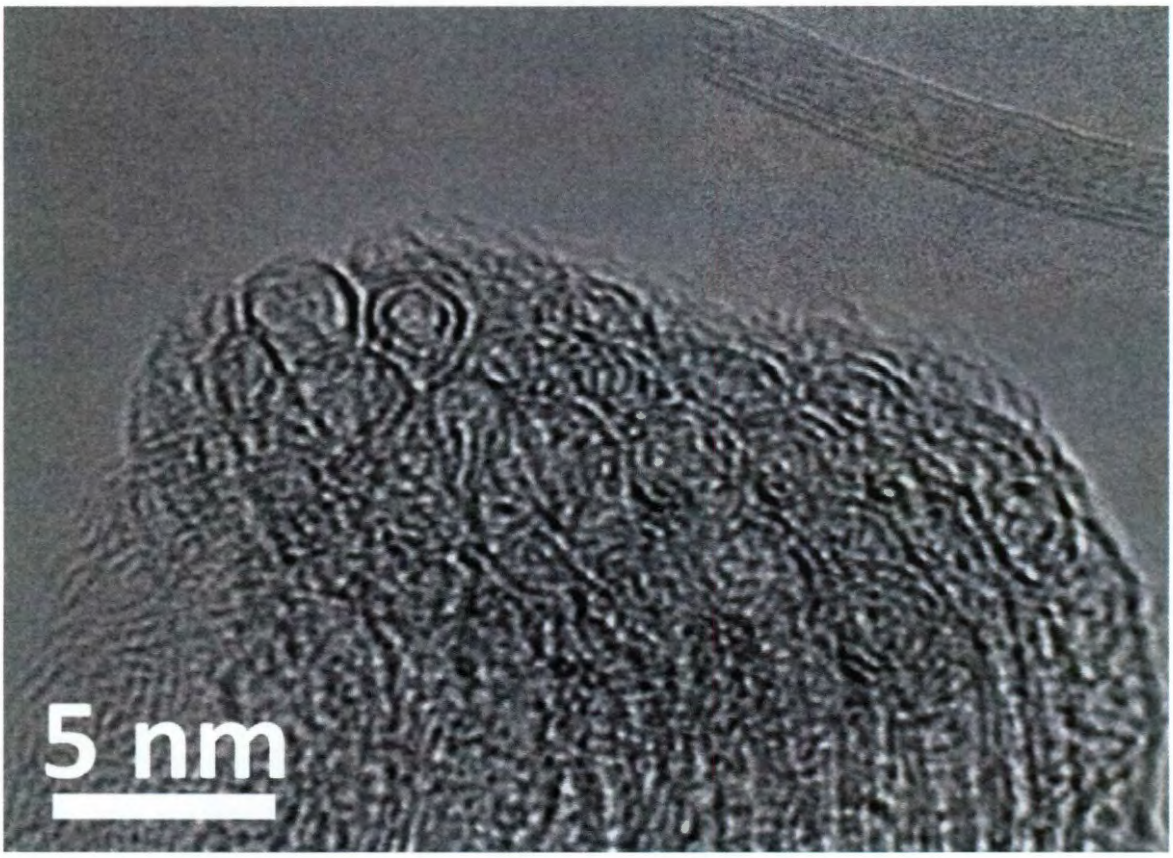

Figure 6.10. TEM image of a DWNT bundle tip.

6.3.2 Microstructure and elemental composition of the iodine doped nanotubes and nanotube fibers

To improve the conductivity of the raw DWNT cable, the nanotubes were doped with iodine [184-194]. The raw DWNT cables were placed in the iodine vapor at 200°C for 12 hrs. Figure 6.11 shows that the surface morphology of the iodine doped cable is similar to the raw cable. By SEM, we could not observe change in diameter or other morphology change caused by the iodine doping. Figure 6.12 (b) shows high contrast dark spots distributed over the surface of DWNTs, which could correspond to iodine clusters and atoms. The GIF elemental mappings for carbon and iodine as shown in figure 6.13 (a) and figure 6.13 (b) indicate that the location of carbon and iodine overlap, suggesting that iodine is uniformly present within the cable. Figure 6.14 is a schematic for the proposed model, where the Iodine atoms are homogeneously adsorbed on the surface of DWNTs. The molecular simulation shows that iodine atoms are less likely to penetrate into the inter-layer spacing or inside of the tubes, especially when they are well capped. For the DWNT bundles, the iodine atoms can penetrate into interstitial spaces between tubes and form an intercalated structure. To reveal the bonding of iodine atoms with the DWNTs we observed their x-ray photoelectron spectra (XPS). The doped cable without any further treatment has an iodine atomic percentage of 3.3%. After washing and sonicating in ethanol, the iodine concentration drops to 2.1%. In an independent experiment, heating (150°C for 72hrs) in vacuum of the doped cable brought the iodine level to 2.3% (Figure 6.15 (a)). These experiments show that the physically bonded iodine can be removed and the iodine that remained on the surface of the DWNTs has a relatively strong chemical bonding. In comparison to the carbon XPS spectra before and after the doping (inset of

figure 6.16 (b) and figure 6.16 (b), respectively), we can see the peak appearing at 285.2 eV after the doping, which corresponds to the energy of the C-I bonds. The peaks at 284.5 eV and 288.7 eV are assigned to C-C and C-O bonds, respectively. The C-O bonds are introduced during the purification procedure.

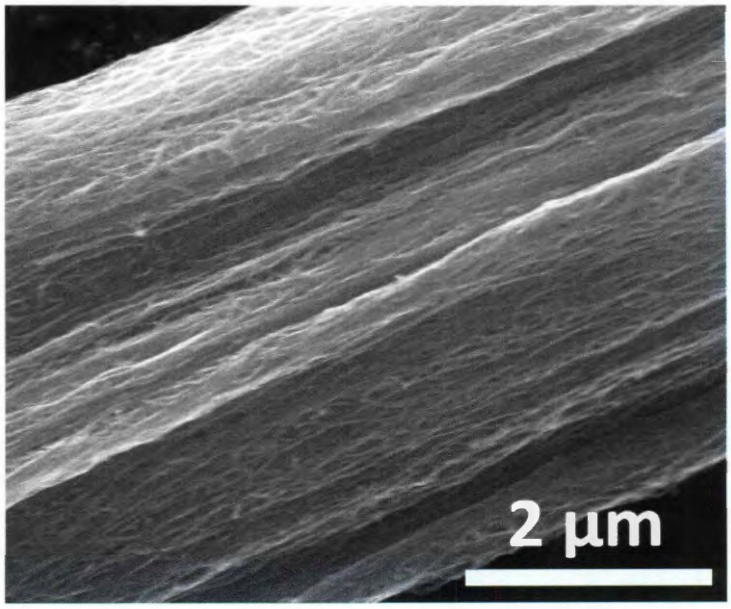

Figure 6.11. SEM image of the iodine doped cable. The nanotubes are aligned in the long axis direction of the cable.

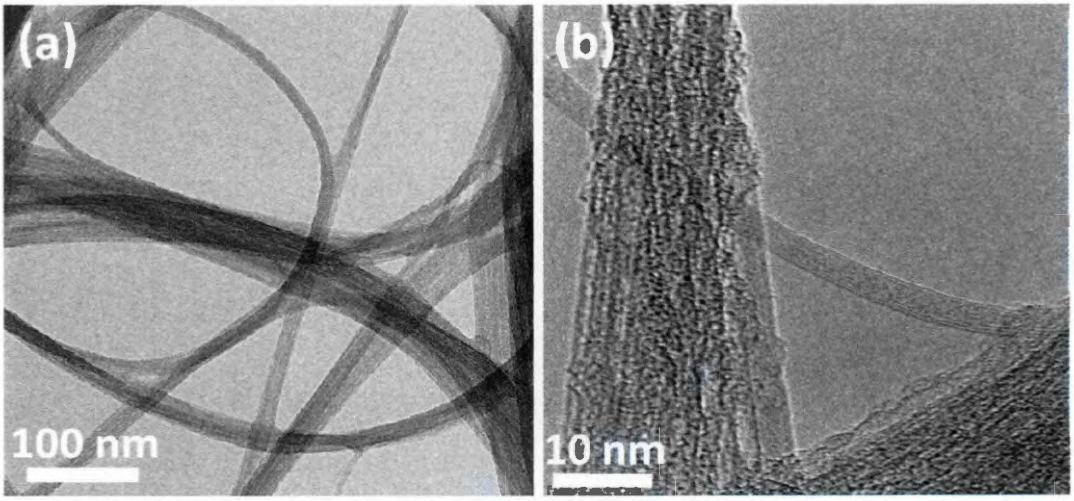

Figure 6.12. TEM images of the iodine doped DWNTs. (a) TEM image of iodine doped nanotube bundles corresponding to the elemental mappings in figure (1). (b) TEM image of the iodine doped carbon nanotubes. The black dots wrapped around the cable are appearing after the iodine doping.

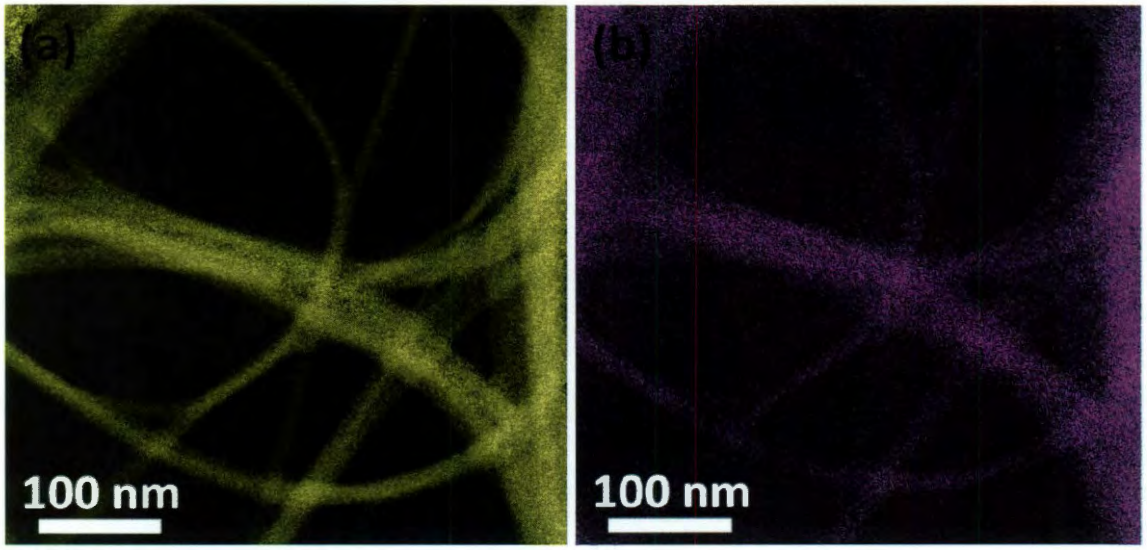

Figure 6.13. (a) Elemental mapping of carbon by Gatan image filter (GIF). (b) Elemental mapping of iodine.

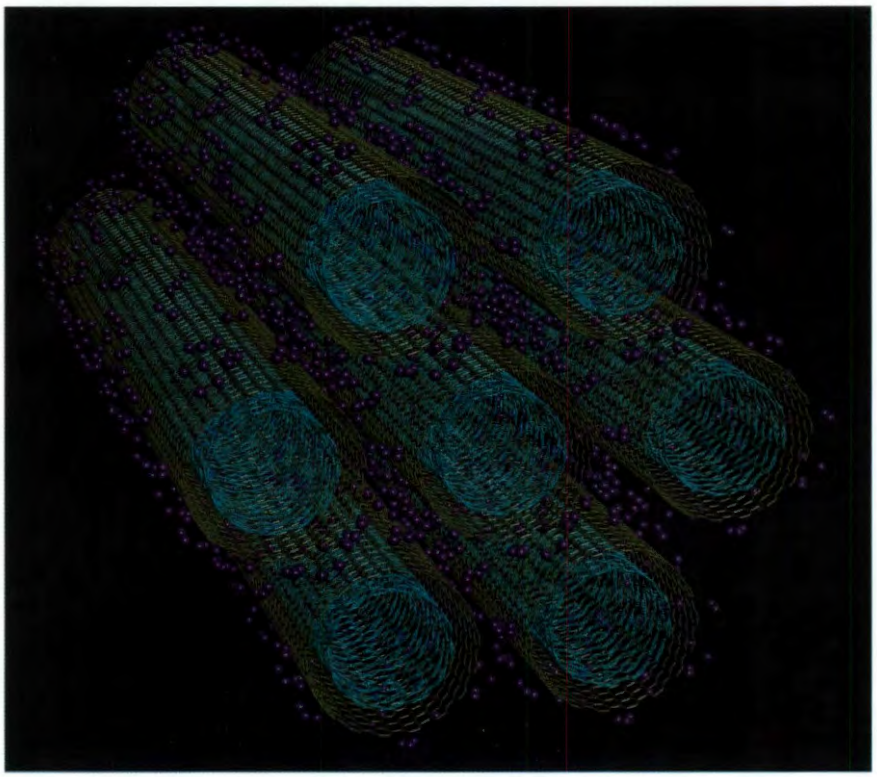

Figure 6.14. A schematic illustrating the speculated model for iodine doped nanotube bundle. The iodine atoms are decorating the surface of the nanotubes.

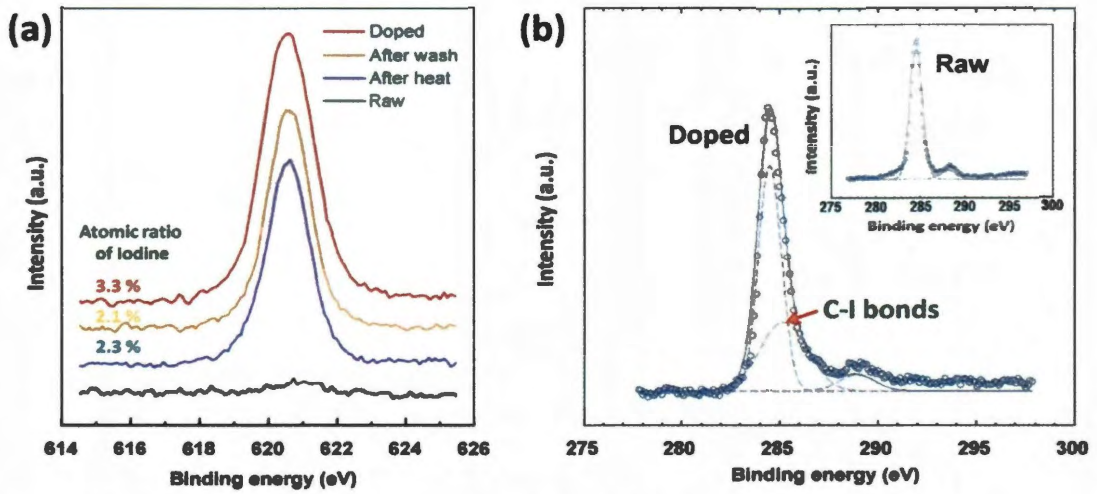

Figure 6.15. XPS spectra of the I-doped cable. (a) Iodine spectra at different treatments. The black and red lines are the spectra for the cable before and after the iodine doping, respectively. The yellow line is collected from the doped cable after it was washed by ethanol. The blue line is collected from the doped cable after it was heated in the vacuum oven at 150°C for 72hrs. Inset of (b) and (b) are the XPS spectra for the cable before and after the iodine doping. The spectra curves (blue circles) are de-convoluted (dashed lines) by Gaussian fitting (solid lines), indicating multiple bonding energies.

In addition, Raman spectra of the doped and undoped cables were collected at the parallel and perpendicular directions as shown in figure 6.16 (fiber long axis direction with respect to the laser polarized direction).

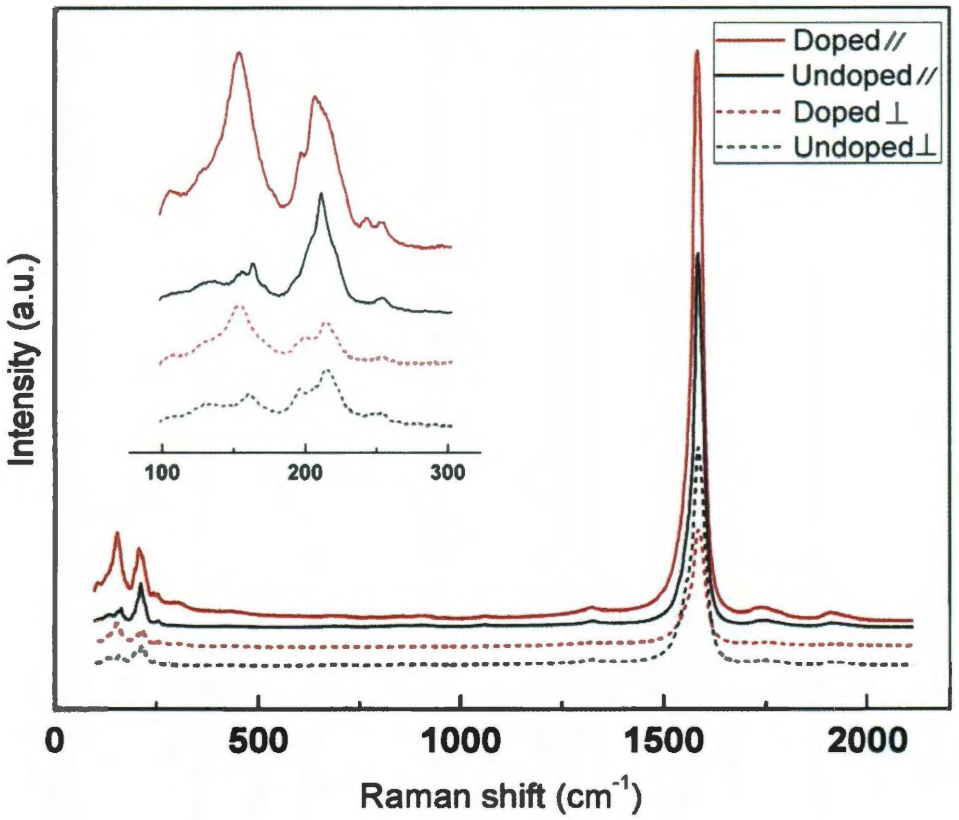

Figure 6.16. Raman spectra of the undoped and the doped cables for both the parallel and perpendicular directions to the long axis of the cables. After the doping, a peak appeared at 154 cm^{-1}. This peak might be caused by the C-I chemical bonding. The fact that the peak intensity in parallel direction is larger than that in perpendicular direction indicates the DWNTs are aligned in the long axis direction of the cables.

6.3.3 Electrical and mechanical properties of the nanotube fibers

Resistivity of 34 raw DWNT cables with a diameter varying from 4.1 μm up to 44.7 μm was measured. Figure 6.17 shows that statistically the cables of diameter >10 μm have larger resistivity compared to cables of diameter <10 μm. The size effect could be due to the fact that defects such as voids are invariably introduced into the larger cables during the fabrication process. The lowest resistivity found for the raw cables is ~$5*10^{-7}$ Ω.m.

After doping with iodine, the cables further decreased in resistivity. The chemically bonded iodine as acceptors form $(I_3)^-$ and $(I_5)^-$ polyiodide chains in the intercalated sites while mobile holes are created in the DWNTs. Due to the increasing density of mobile holes, the electrical conductivity of the cables was improved by the iodine doping [185, 186]. X-ray diffraction spectra (Figure 6.18) shows that the (002) peak at $2\theta \sim 10.86^{o}$ corresponding to the inter-layer spacing between the outer and inner wall of the DWNTs shifts to the higher angle after the iodine doping [195, 196]. The shift is due to the suppression of the inter-layer spacing from 3.76 Å to 3.63 Å. The X-ray spectra could be a direct indication of charge transfer and covalent bond formation (A more detailed discussion about the XRD pattern is included in Appendix A). The lowest resistivity observed in our cables corresponds to $\sim 1.5*10^{-7}$ Ω.m for the doped cables. Although the raw DWNT cables are not as conductive as metals, their specific conductivity (conductivity/weight) value is very high as the density of the nanotube cable is much lower than the density of metals. The raw DWNT cables have an average density of 0.28 g/cm^3 and the iodine doped cables have an average density of 0.33 g/cm^3. In terms of specific conductivity, the raw and doped cables are comparable with metals. For the iodine doped cables, the highest specific conductivity of $1.96*10^4$ $S.m^2/kg$ was observed, which is higher than that of Al and Cu, but slightly lower than that of sodium, which has the highest specific conductivity among metals of $2.16*10^4$ $S.m^2/kg$. A comparison in specific conductivity among raw, doped DWNT cables and a variety of metals is shown in Figure 6.19 (Mean free path of the DWNT cable is calculated in Appendix B).

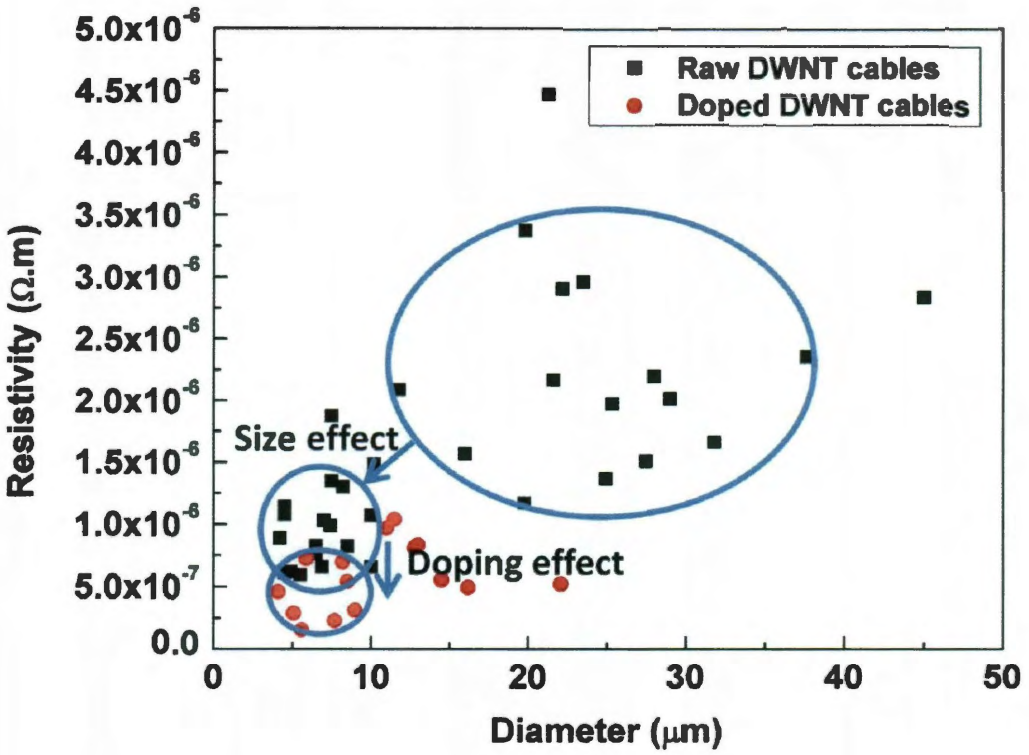

Figure 6.17. The resistivity as a function of diameter for 34 raw DWNT cables and 15 iodine doped cables.

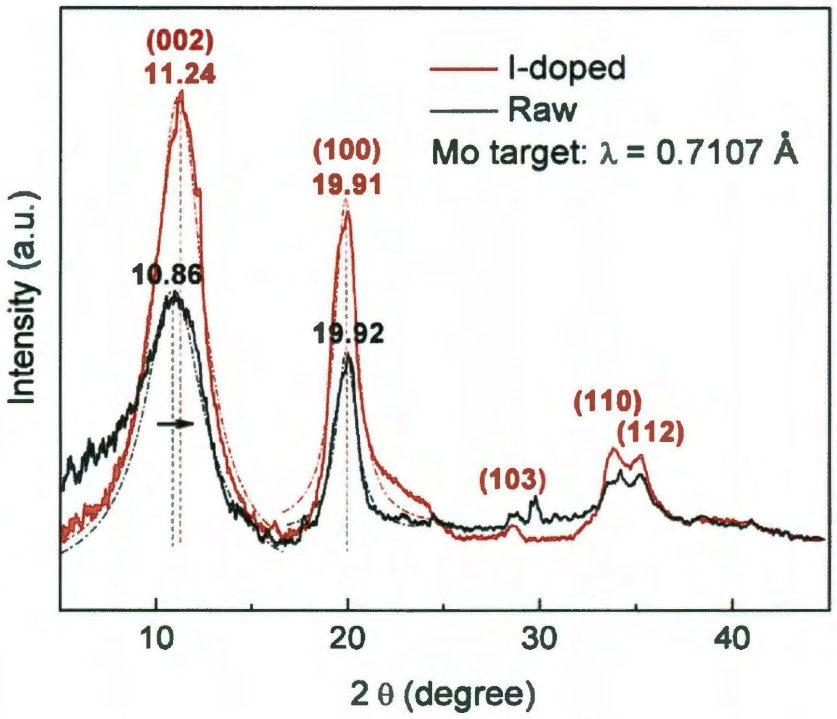

Figure 6.18. X-ray diffraction spectra for the raw and iodine doped cables. The (002) peak at $2\theta \sim 10.86^{\circ}$ corresponding to the inter-layer spacing between the outer and inner walls of the DWNTs shifts to $2\theta \sim 11.24^{\circ}$ after the iodine doping. The (100) peak at $2\theta \sim 19.92^{\circ}$ corresponding to the honeycomb lattice (The lattice spacing, d = 2.05 Å) on the nanotube wall almost does not shift. The dotted curves are the peaks generated by Gaussian fitting.

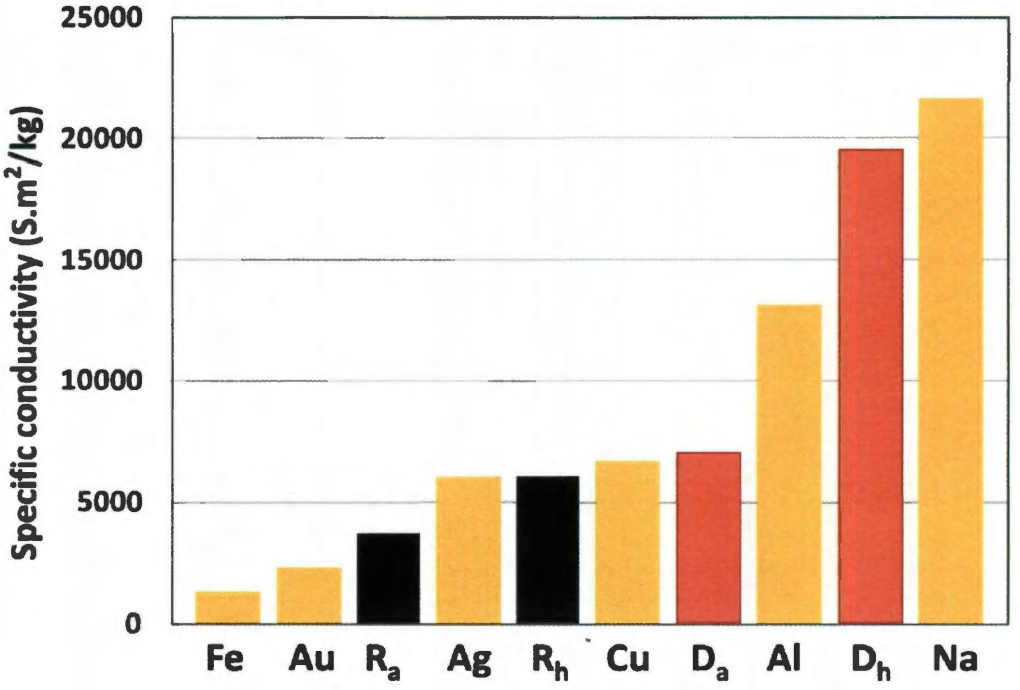

Figure 6.19. A comparison in specific conductivity among raw, doped cables and several metals. R_a and R_h represent for the average and the highest one for the raw cables. D_a and D_h are the values for the doped cables.

Copper is the most commonly used raw material for conducting wires. In this study, we compared the relative resistance (the ratio of the measured resistance, R_T to the resistance at 300 K, $R_{300\,K}$) of our cables with that of copper in the temperature range from 200 K to 400 K (normal operating temperature range for conducting wires). As shown in figure 6.20, the reduced resistance versus temperature curves for copper and the DWNT cables are both linear from 200 K to 400 K. For the iodine doped cable, the resistance at 200 K to 400 K varies by -9% and 9% with respect to the resistance at 300K. By contrast, the corresponding variations in copper are -43% and 43% [197]. We also studied the stability of the electrical properties for the iodine doped cables. At room temperature, the doped cables kept the resistance value at a constant level for the whole testing period of a

minimum seven days. Figure 6.21 shows the resistance as a function of temperature measured on two of the doped cables. In the first experiment, a 10.2 μm cable was continuously cooled down from room temperature to 20 K, heated up to 420 K, and cooled down to 20 K again. The heating/cooling ratio was 1K/min. The resistance vs temperature plots show no hysteresis. This indicates that the iodine doping is stable upon the thermal cycling in this time scale.

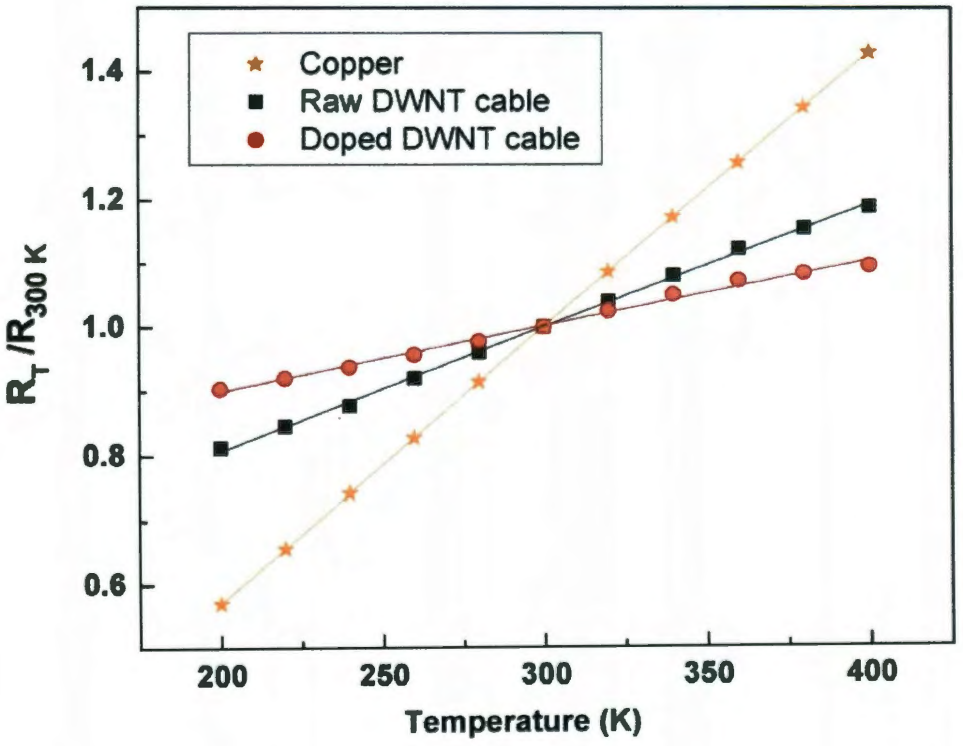

Figure 6.20. The relative resistance as a function of temperature.

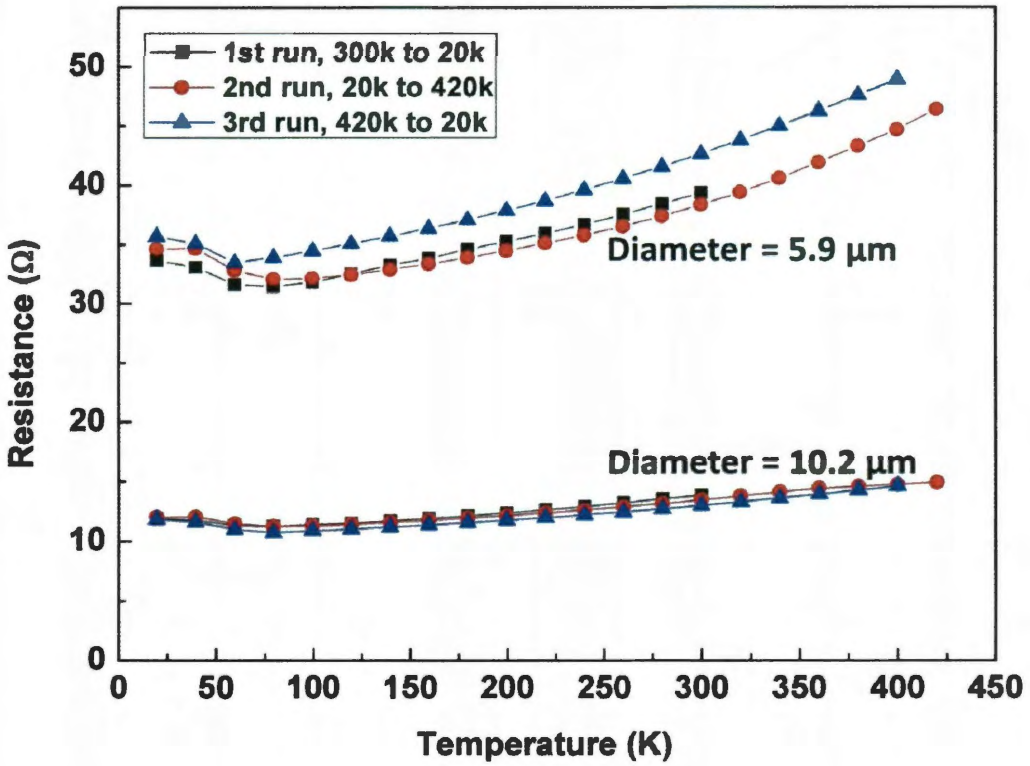

Figure 6.21. The resistance as a function of temperature for two doped cables. The thermal treatment for the cable of 10.2 μm in diameter is continuous, but for the cable of 5.9 μm in diameter, after the 2nd run of the heating process, the temperature was held at 420 k for 4hrs, and then continued with the 3rd run.

Current carrying capacity is a property which measures the maximum current that can be passed through the unit cross sectional area of a conducting medium before it fails. An individual MWNT has extremely high current carrying capacity of 10^9-10^{10} A/cm^2 [198, 199]. This compares with nanoscale copper having a capacity of 10^6 A/cm^2 [200]. However, the current carrying capacity for the macroscopic nanotube cables as reported in literature is much lower than that for individual single-walled nanotubes, 10^5 A/cm^2 [199]. That finding is consistent with our results based on seven raw and seven iodine doped DWNT cables, which have current carrying capacities ranging from 10^4 to 10^5

A/cm^2. Although the macroscopic cables do not have the extremely high current carrying capacity of individual nanotubes, they still have a sufficiently high capacity to be capable of loading utilities even for small diameter cables. From W. H. Preece's formula, we calculated the current carrying capacity of the copper wires, in open air, to be $3.2*10^5$ to $3.2*10^4$ A/cm^2 with their corresponding diameters varying from 1 μm to 100 μm [201]. DWNT cables' current carrying capacity is in the same range as that of copper wires (A direct comparison is included in the Appendix C).

The nanotube cables also have the ability to be joined and assembled into larger structures. For example, two parallel DWNT cables were twisted and braided into one as shown in figure 6.21 (a). Before twisting, the two cables had resistances of 24 Ω and 20 Ω individually. Theoretically, the twisted thick cable from these two cables in a parallel configuration should have a resistance of 10.9 Ω ($R_{theoretical}$ = 24 Ω *20 Ω/ (24 Ω +20 Ω). From the measurement, we found that the assembled thick cable has a resistance of 10.5 Ω. This difference might be due to fact that the twisting renders better packing of the nanotubes in the cables and hence decreases the electrical resistivity of the individual cables themselves. This is a good indication suggesting that larger cable/wire structures of any arbitrary sizes can be built from the individual cables without sacrificing their electrical properties. Two individual cables (cable 1, diameter = 13 μm; cable 2, diameter = 11.5 μm) were also serially connected by a tie as shown in Figure 6.22 (e). The two cables were knotted by a micromanipulator. Traditional weaving techniques used in the textile industry should also be applicable for making such connections between cables. The resistivity of cable 1 and 2 individually are $9.6*10^{-5}$ Ω.cm and $9.35*10^{-5}$ Ω.cm, respectively. Based on the resistivity, diameter and length of each cable (length is for the

segment between the tie and its adjacent electrode), we can calculate the resistance of cable 1 and 2 as 15.33 Ω and 16.34 Ω. The assembled structure of cable 1, cable 2 and the tie has a resistance of 31.9 Ω. The resistance from the tie would then be ~0.23 Ω suggesting that no significant resistance is introduced by the knot and indeed several short cables could be easily assembled to longer ones. The cable as the conducting wire is demonstrated in a circuit as shown in figure 6.22 (b) and (d). A household bulb (9 watts, 0.15A, 120V) was connected with the public power supply through the twisted wire. The light bulb was powered up. The circuit was turned on for 3 days. The nanotube cable functioned well for the whole testing period. In the circuit, the cable replaced a section of copper wire as shown in figure 6.22 (c). Here the nanotube cable is much smaller in diameter than copper wires. It is also found that the cables are mechanically quite robust. The average ultimate tensile strength for the undoped and doped cables are obtained are 320 MPa and 640 MPa, respectively, comparable to metals. Figure 6.23 shows the stress-strain curves for the two samples; after doping, the cable's strength increased but the strain to failure became smaller.

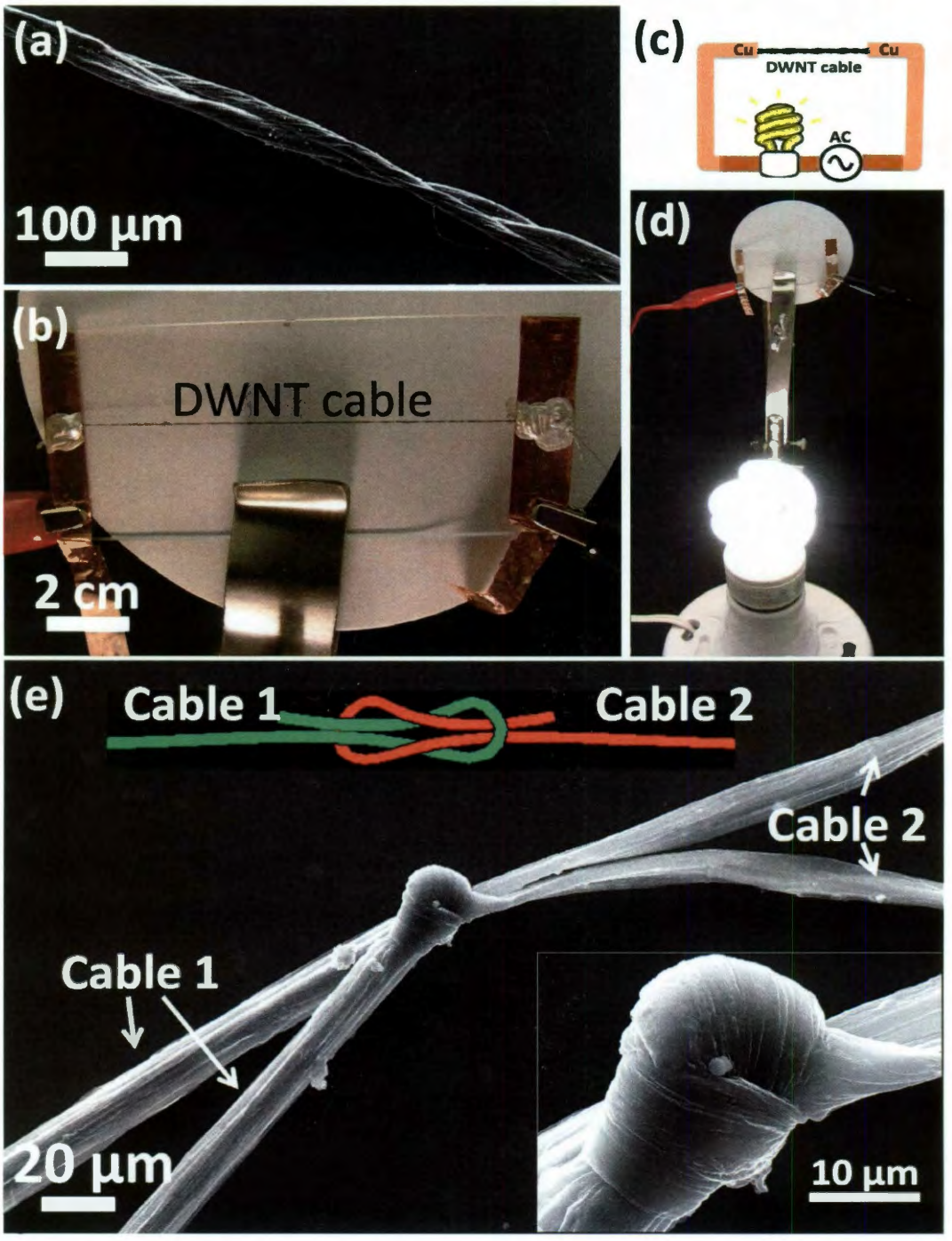

Figure 6.22. DWNT cables used in parallel and seires electrical circuits. (a) SEM image of two cables twisted in a parallel configuration. (b) The image of the twisted cable. (c) Schematics of the circuit (d) The cable as a segment of conductive media connected with the household power supply and loaded with a light bulb (9 watts, 0.15A, 120V). (e) SEM images shows that cable 1 and 2 can be knotted and joined. Inset is a higher magnification SEM image of the tie.

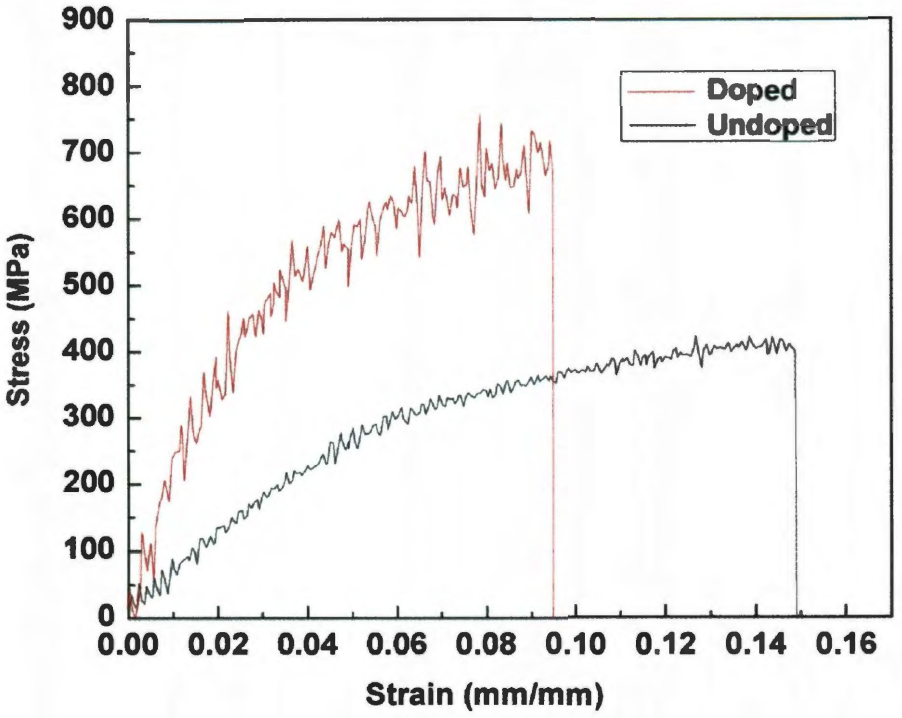

Figure 6.23. Strain-stress curves for the undoped and doped fibers.

6.4 Conclusions

In summary, we have made double-walled carbon nanotube cables that outperform Cu and Al in specific electrical conductivity. Iodine doping effectively increases the conductivity of the cables, as well as their tensile strength. Using cables as the building blocks and employing different assembly methods, larger and longer wires and cables can be created and we have used this approach to demonstrate a nanotube wire circuit to power a household light bulb. These lightweight nanotube cables could be serious contenders for replacing metal wires in electrical transmission as they would have intrinsic advantages to metals such as high temperature stability and chemical resistance.

Chapter 7: Conclusions and Future Work

Homogeneously dispersion of the nanotubes and a strong interface between the nanotubes and the epoxy matrix were simultaneously achieved in the BOC-nanotube/epoxy composite. As a result, the BOC-nanotube reinforced composite showed improvement in both ultimate tensile strength and toughness compared to the control sample reinforced by the raw nanotubes. Although the functionalization enabled nanotubes be a good mechanical reinforcement in the epoxy matrix, meanwhile, the electrical conductivity of the nanotubes were greatly degraded. From this work, we learned that functionalization could be a double-edged sword. Whether or not and in what occasions it would be applied are determined by what function of the composite is majorly pursued. "Function-oriented" processing is necessary.

Other than functionalization, another route was invented to realizing dispersion of nanotubes in a polymer matrix. In the MDPE/HiPco nanotube composite, the key step for achieving dispersion is creating the unique porous structure on MDPE. The porous MDPE were prepared by etching the MDPE powder in toluene under the high pressure. The pore size was adjusted to be as small as about 1 micron, which was slightly larger than the length of HiPco nanotubes. HiPco nanotubes readily penetrated into the pores assisted by the sonic agitation in DMF. Due to achiving homogeneous dispersion when using the raw HiPco nanotubes, both the good mechanical and electrical performance had been realized in the porous MDPE/HiPco nanotube composite.

To advance conductivity to the uplimit in composite systems, the Bayer nanotube/HDPE composite wires at high loading ratios upto 40 wt% were studied. A variety of strategies had been attempted to improve conductivity such as doping and annealing. However,

resistivity reached the bottleneck at the level of 10^{-2} ohm.cm. It was found that the polymer wrapped around nanotube's surface was the major orgin of the resistance.

To realize the final goal that making a microscopic wire of competitive conductivity to metals, pure DWNT cables were prepared by the solid spinning. The cable outperformed Cu and Al in specific electrical conductivity (conductivity/density). Iodine doping further increased the conductivity of the cables, as well as their tensile strength. The highest conductivity had been reached in the doped DWNT cable was $6.6*10^6$ S/m, which was still lower than conductivity of copper, $6.0*10^7$ S/m.

The DWNT cable was not yet in an ideal condition. Many aspects can be improved such as alignment, densification, contacts as well as nanotubes themselves. Through optimize some or all of these aspects; a mascroscopic nanotube-based conductor can be prepared. This conductor can be a serious contender to copper and have large application in transmission lines and low-dimensinal connection wires. Future work will be focus on improving these aspects. More specficically,

- Alignment
    - Build a take-up system attached with the growth chamber. By applying the pulling force, nanotubes could be better aligned in a certain direction.
    - Couple the growth chamber with an electrical field, in-situ application of the electrical force on the nanotubes as they are growing.
    - Make the DWNT cable by solution spinning. In this case, the nanotubes would be aligned by the laminar flow.
- Densification

  - Find a solvent with high tension stress and good wettability with the nanotubes.

- Contacts
  - Longer overlapping length, smaller inter-tube distance and better alignement are critical to build good contacts. Apply the nanotubes with higher aspect ratio to make cables.
  - Metallic-to-metallic nanotube contacts are ideal. Use pure metallic nanotubes to prepare cables.
- Nanotubes
  - Grow nanotubes with high aspect ratio.
  - Improve the degree of graphitization of nanotubes.
  - Grow pure metallic nanotubes.

References

[1] P. M. Ajayan and J. M. Tour, "Materials Science: Nanotube composites," *Nature*, vol. 447, no. 7148, pp. 1066-1068, Jun. 2007.

[2] J. Zhu, J. Kim, H. Peng, J. L. Margrave, V. N. Khabashesku, and E. V. Barrera, "Improving the Dispersion and Integration of Single-Walled Carbon Nanotubes in Epoxy Composites through Functionalization," *Nano Letters*, vol. 3, no. 8, pp. 1107-1113, 2003.

[3] J. Zhu et al., "Reinforcing Epoxy Polymer Composites Through Covalent Integration of Functionalized Nanotubes," *Advanced Functional Materials*, vol. 14, no. 7, pp. 643-648, Jul. 2004.

[4] E. T. Thostenson, Z. Ren, and T.-W. Chou, "Advances in the science and technology of carbon nanotubes and their composites: a review," *Composites Science and Technology*, vol. 61, no. 13, pp. 1899-1912, Oct. 2001.

[5] R. Saito, G. Dresselhaus, M. S. Dresselhaus, and others, *Physical properties of carbon nanotubes*, vol. 3. Imperial College Press London, 1998.

[6] A. Hirsch, "Functionalization of single-walled carbon nanotubes," *Angewandte Chemie International Edition*, vol. 41, no. 11, pp. 1853–1859, 2002.

[7] M. Holzinger et al., "Sidewall functionalization of carbon nanotubes," *Angewandte Chemie International Edition*, vol. 40, no. 21, pp. 4002–4005, 2001.

[8] Y. Lin, B. Zhou, K. A. S. Fernando, P. Liu, L. F. Allard, and Y. P. Sun, "Polymeric carbon nanocomposites from carbon nanotubes functionalized with matrix polymer," *Macromolecules*, vol. 36, no. 19, pp. 7199–7204, 2003.

[9] C. A. Mitchell, J. L. Bahr, S. Arepalli, M. James, and R. Krishnamoorti, "Dispersion of functionalized carbon nanotubes in polystyrene," *Macromolecules*, vol. 35, no. 23, pp. 8825–8830, 2002.

[10] M. Moniruzzaman and K. I. Winey, "Polymer nanocomposites containing carbon nanotubes," *Macromolecules*, vol. 39, no. 16, pp. 5194–5205, 2006.

[11] K. Balasubramanian and M. Burghard, "Chemically functionalized carbon nanotubes," *Small*, vol. 1, no. 2, pp. 180–192, 2005.

[12] J. L. Bahr and J. M. Tour, "Covalent chemistry of single-wall carbon nanotubes," *J. Mater. Chem.*, vol. 12, no. 7, pp. 1952–1958, 2002.

[13] Y. Zhao and E. V. Barrera, "Asymmmetric Diamino Functionalization of Nanotubes Assisted by BOC Protection and Their Epoxy Nanocomposites," *Advanced Functional Materials*, vol. 20, no. 18, pp. 3039-3044, Sep. 2010.

[14] V. P. Veedu et al., "Multifunctional composites using reinforced laminae with carbon-nanotube forests," *Nature materials*, vol. 5, no. 6, pp. 457–462, 2006.

[15] R. H. Baughman, A. A. Zakhidov, and W. A. De Heer, "Carbon nanotubes–the route toward applications," *Science*, vol. 297, no. 5582, p. 787, 2002.

[16] A. Buldum and J. P. Lu, "Contact resistance between carbon nanotubes," *Physical Review B*, vol. 63, no. 16, p. 161403, 2001.

[17] M. S. Fuhrer et al., "Crossed nanotube junctions," *Science*, vol. 288, no. 5465, p. 494, 2000.

[18] P. L. McEuen, M. S. Fuhrer, and H. Park, "Single-walled carbon nanotube electronics," *Nanotechnology, IEEE Transactions on*, vol. 1, no. 1, pp. 78–85, 2002.

[19] A. R. Bhattacharyya et al., "Crystallization and orientation studies in polypropylene/single wall carbon nanotube composite," *Polymer*, vol. 44, no. 8, pp. 2373–2377, 2003.

[20] L. Valentini, J. Biagiotti, M. A. López-Manchado, S. Santucci, and J. M. Kenny, "Effects of carbon nanotubes on the crystallization behavior of polypropylene," *Polymer Engineering & Science*, vol. 44, no. 2, pp. 303–311, 2004.

[21] B. P. Grady, F. Pompeo, R. L. Shambaugh, and D. E. Resasco, "Nucleation of polypropylene crystallization by single-walled carbon nanotubes," *The Journal of Physical Chemistry B*, vol. 106, no. 23, pp. 5852–5858, 2002.

[22] M. L. Minus, H. G. Chae, and S. Kumar, "Single wall carbon nanotube templated oriented crystallization of poly (vinyl alcohol)," *Polymer*, vol. 47, no. 11, pp. 3705–3710, 2006.

[23] L. Li, C. Y. Li, C. Ni, L. Rong, and B. Hsiao, "Structure and crystallization behavior of Nylon 66/multi-walled carbon nanotube nanocomposites at low carbon nanotube contents," *Polymer*, vol. 48, no. 12, pp. 3452–3460, 2007.

[24] L. M. Ericson et al., "Macroscopic, neat, single-walled carbon nanotube fibers," *Science*, vol. 305, no. 5689, p. 1447, 2004.

[25] B. Vigolo et al., "Macroscopic fibers and ribbons of oriented carbon nanotubes," *Science*, vol. 290, no. 5495, p. 1331, 2000.

[26] A. B. Dalton et al., "Super-tough carbon-nanotube fibres," *Nature*, vol. 423, no. 6941, p. 703, Jun. 2003.

[27] M. Zhang, K. R. Atkinson, and R. H. Baughman, "Multifunctional carbon nanotube yarns by downsizing an ancient technology," *Science*, vol. 306, no. 5700, p. 1358, 2004.

[28] M. Motta, Y. L. Li, I. Kinloch, and A. Windle, "Mechanical properties of continuously spun fibers of carbon nanotubes," *Nano letters*, vol. 5, no. 8, pp. 1529–1533, 2005.

[29] R. Annamalai, J. D. West, A. Luscher, and V. V. Subramaniam, "Electrophoretic drawing of continuous fibers of single-walled carbon nanotubes," *Journal of applied physics*, vol. 98, p. 114307, 2005.

[30] K. Koziol et al., "High-performance carbon nanotube fiber," *Science*, vol. 318, no. 5858, p. 1892, 2007.

[31] S. Iijima and others, "Helical microtubules of graphitic carbon," *nature*, vol. 354, no. 6348, pp. 56–58, 1991.

[32] P. J. F. Harris, E. Hernández, and B. I. Yakobson, "Carbon nanotubes and related structures: new materials for the twenty-first century," *American Journal of Physics*, vol. 72, p. 415, 2004.

[33] M. M. J. Treacy, T. W. Ebbesen, and J. M. Gibson, "Exceptionally high Young's modulus observed for individual carbon nanotubes," 1996.

[34] R. S. Ruoff and D. C. Lorents, "Mechanical and thermal properties of carbon nanotubes," *Carbon*, vol. 33, no. 7, pp. 925–930, 1995.

[35] J. P. Salvetat et al., "Mechanical properties of carbon nanotubes," *Applied Physics A: Materials Science & Processing*, vol. 69, no. 3, pp. 255–260, 1999.

[36] B. Yakobson and P. Avouris, "Mechanical properties of carbon nanotubes," *Carbon Nanotubes*, pp. 287–327, 2001.

[37] J. Hone et al., "Electrical and thermal transport properties of magnetically aligned single wall carbon nanotube films," *Applied physics letters*, vol. 77, p. 666, 2000.
[38] M. S. Dresselhaus and P. C. Eklund, "Phonons in carbon nanotubes," 2000.
[39] J. Che, T. Cagin, and A. G. William III, "Thermal conductivity of carbon nanotubes," *Nanotechnology*, vol. 11, p. 65, 2000.
[40] J. Hone et al., "Thermal properties of carbon nanotubes and nanotube-based materials," *Applied Physics A: Materials Science & Processing*, vol. 74, no. 3, pp. 339–343, 2002.
[41] P. Kim, L. Shi, A. Majumdar, and P. L. McEuen, "Thermal transport measurements of individual multiwalled nanotubes," *Physical Review Letters*, vol. 87, no. 21, p. 215502, 2001.
[42] H. Dai, "Carbon nanotubes: synthesis, integration, and properties," *Accounts of chemical research*, vol. 35, no. 12, pp. 1035–1044, 2002.
[43] T. W. Ebbesen, H. J. Lezec, H. Hiura, J. W. Bennett, H. F. Ghaemi, and T. Thio, "Electrical conductivity of individual carbon nanotubes," 1996.
[44] S. Li, Z. Yu, C. Rutherglen, and P. J. Burke, "Electrical properties of 0.4 cm long single-walled carbon nanotubes," *Nano Letters*, vol. 4, no. 10, pp. 2003–2007, 2004.
[45] H. Dai, E. W. Wong, and C. M. Lieber, "Probing electrical transport in nanomaterials: Conductivity of individual carbon nanotubes," *Science*, vol. 272, no. 5261, p. 523, 1996.
[46] M. Su, B. Zheng, and J. Liu, "A scalable CVD method for the synthesis of single-walled carbon nanotubes with high catalyst productivity," *Chemical Physics Letters*, vol. 322, no. 5, pp. 321–326, 2000.
[47] M. Meyyappan, L. Delzeit, A. Cassell, and D. Hash, "Carbon nanotube growth by PECVD: a review," *Plasma Sources Science and Technology*, vol. 12, p. 205, 2003.
[48] J. H. Hafner et al., "Catalytic growth of single-wall carbon nanotubes from metal particles," *Chemical Physics Letters*, vol. 296, no. 1-2, pp. 195–202, 1998.
[49] T. Guo, P. Nikolaev, A. Thess, D. T. Colbert, and R. E. Smalley, "Catalytic growth of single-walled manotubes by laser vaporization," *Chemical Physics Letters*, vol. 243, no. 1-2, pp. 49–54, 1995.
[50] J. Kong, A. M. Cassell, and H. Dai, "Chemical vapor deposition of methane for single-walled carbon nanotubes," *Chemical Physics Letters*, vol. 292, no. 4-6, pp. 567–574, 1998.
[51] P. Nikolaev et al., "Gas-phase catalytic growth of single-walled carbon nanotubes from carbon monoxide," *Chemical Physics Letters*, vol. 313, no. 1-2, pp. 91–97, 1999.
[52] W. Z. Li et al., "Large-scale synthesis of aligned carbon nanotubes," *Science*, vol. 274, no. 5293, p. 1701, 1996.
[53] S. Fan, M. G. Chapline, N. R. Franklin, T. W. Tombler, A. M. Cassell, and H. Dai, "Self-oriented regular arrays of carbon nanotubes and their field emission properties," *Science*, vol. 283, no. 5401, p. 512, 1999.
[54] Z. F. Ren et al., "Synthesis of large arrays of well-aligned carbon nanotubes on glass," *Science*, vol. 282, no. 5391, p. 1105, 1998.
[55] S. Ghosh, A. K. Sood, and N. Kumar, "Carbon nanotube flow sensors," *Science*, vol. 299, no. 5609, p. 1042, 2003.

[56] J. Li, Y. Lu, Q. Ye, M. Cinke, J. Han, and M. Meyyappan, "Carbon nanotube sensors for gas and organic vapor detection," *Nano Letters*, vol. 3, no. 7, pp. 929–933, 2003.

[57] H. W. C. Postma, T. Teepen, Z. Yao, M. Grifoni, and C. Dekker, "Carbon nanotube single-electron transistors at room temperature," *Science*, vol. 293, no. 5527, p. 76, 2001.

[58] T. Rueckes, K. Kim, E. Joselevich, G. Y. Tseng, C. L. Cheung, and C. M. Lieber, "Carbon nanotube-based nonvolatile random access memory for molecular computing," *science*, vol. 289, no. 5476, p. 94, 2000.

[59] K. H. An et al., "Electrochemical properties of high-power supercapacitors using single-walled carbon nanotube electrodes," *Advanced functional materials*, vol. 11, no. 5, pp. 387–392, 2001.

[60] A. Star, J. C. P. Gabriel, K. Bradley, and G. Gr\üner, "Electronic detection of specific protein binding using nanotube FET devices," *Nano Letters*, vol. 3, no. 4, pp. 459–463, 2003.

[61] C. Niu, E. K. Sichel, R. Hoch, D. Moy, and H. Tennent, "High power electrochemical capacitors based on carbon nanotube electrodes," *Applied Physics Letters*, vol. 70, p. 1480, 1997.

[62] M. S. Fuhrer, B. M. Kim, T. D\ürkop, and T. Brintlinger, "High-mobility nanotube transistor memory," *Nano Letters*, vol. 2, no. 7, pp. 755–759, 2002.

[63] J. Kong et al., "Nanotube molecular wires as chemical sensors," *Science*, vol. 287, no. 5453, p. 622, 2000.

[64] P. J. F. Harris, "Carbon nanotube composites," *International Materials Reviews*, vol. 49, no. 1, pp. 31–43, 2004.

[65] A. K. T. Lau and D. Hui, "The revolutionary creation of new advanced materials–carbon nanotube composites," *Composites Part B: Engineering*, vol. 33, no. 4, pp. 263–277, 2002.

[66] J. Liu et al., "Fullerene pipes," *Science*, vol. 280, no. 5367, p. 1253, 1998.

[67] A. G. Rinzler et al., "Large-scale purification of single-wall carbon nanotubes: process, product, and characterization," *Applied Physics A: Materials Science & Processing*, vol. 67, no. 1, pp. 29–37, 1998.

[68] R. Andrews et al., "Nanotube composite carbon fibers," *Applied Physics Letters*, vol. 75, p. 1329, 1999.

[69] Y. L. Li, I. A. Kinloch, and A. H. Windle, "Direct spinning of carbon nanotube fibers from chemical vapor deposition synthesis," *Science*, vol. 304, no. 5668, p. 276, 2004.

[70] A. B. Dalton et al., "Continuous carbon nanotube composite fibers: properties, potential applications, and problems," *J. Mater. Chem.*, vol. 14, no. 1, pp. 1–3, 2003.

[71] F. L. & R. Matthews and Matthews, F.L. & Rawlings, R.D., *Composite Materials: Engineering and Science*. Boca Raton: CRC Press, 1999.

[72] J. N. Coleman, U. Khan, and Y. K. Gun'ko, "Mechanical reinforcement of polymers using carbon nanotubes," *Advanced materials*, vol. 18, no. 6, pp. 689–706, 2006.

[73] J. N. Coleman, U. Khan, W. J. Blau, and Y. K. Gun'ko, "Small but strong: A review of the mechanical properties of carbon nanotube-polymer composites," *Carbon*, vol. 44, no. 9, pp. 1624–1652, 2006.

[74] L. S. Schadler, S. C. Giannaris, and P. M. Ajayan, "Load transfer in carbon nanotube epoxy composites," *Applied Physics Letters*, vol. 73, p. 3842, 1998.
[75] S. B. Sinnott et al., "Model of carbon nanotube growth through chemical vapor deposition," *Chemical Physics Letters*, vol. 315, no. 1-2, pp. 25–30, 1999.
[76] E. F. Kukovitsky, S. G. L'vov, N. A. Sainov, V. A. Shustov, and L. A. Chernozatonskii, "Correlation between metal catalyst particle size and carbon nanotube growth," *Chemical physics letters*, vol. 355, no. 5-6, pp. 497–503, 2002.
[77] Y. Y. Wei, G. Eres, V. I. Merkulov, and D. H. Lowndes, "Effect of catalyst film thickness on carbon nanotube growth by selective area chemical vapor deposition," *Applied Physics Letters*, vol. 78, p. 1394, 2001.
[78] Z. P. Huang, D. Z. Wang, J. G. Wen, M. Sennett, H. Gibson, and Z. F. Ren, "Effect of nickel, iron and cobalt on growth of aligned carbon nanotubes," *Applied Physics A: Materials Science & Processing*, vol. 74, no. 3, pp. 387–391, 2002.
[79] D. Chattopadhyay, I. Galeska, and F. Papadimitrakopoulos, "A route for bulk separation of semiconducting from metallic single-wall carbon nanotubes," *Journal of the American Chemical Society*, vol. 125, no. 11, pp. 3370–3375, 2003.
[80] A. R. Harutyunyan et al., "Preferential growth of single-walled carbon nanotubes with metallic conductivity," *Science*, vol. 326, no. 5949, p. 116, 2009.
[81] R. Krupke, F. Hennrich, H. L\öhneysen, and M. M. Kappes, "Separation of metallic from semiconducting single-walled carbon nanotubes," *Science*, vol. 301, no. 5631, p. 344, 2003.
[82] S. Ghosh, S. M. Bachilo, and R. B. Weisman, "Advanced sorting of single-walled carbon nanotubes by nonlinear density-gradient ultracentrifugation," *Nature Nanotechnology*, vol. 5, no. 6, pp. 443–450, 2010.
[83] M. C. Hersam, "Progress towards monodisperse single-walled carbon nanotubes," *Nature Nanotechnology*, vol. 3, no. 7, pp. 387–394, 2008.
[84] E. T. Thostenson, W. Z. Li, D. Z. Wang, Z. F. Ren, and T. W. Chou, "Carbon nanotube/carbon fiber hybrid multiscale composites," *Journal of Applied Physics*, vol. 91, p. 6034, 2002.
[85] C. S. Tang, B. Shi, W. Gao, and J. Liu, "Single fiber pull-out test and the determination of critical fiber reinforcement length for fiber reinforced soil [J]," *Rock and Soil Mechanics*, vol. 30, no. 8, pp. 2225–2230, 2009.
[86] A. A. Grant and E. H. Greener, "Whisker reinforcement of polymethyl methacrylate denture base resins," *Australian Dental Journal*, vol. 12, no. 1, pp. 29–33, 1967.
[87] T. Lacroix, B. Tilmans, R. Keunings, M. Desaeger, and I. Verpoest, "Modelling of critical fibre length and interfacial debonding in the fragmentation testing of polymer composites," *Composites science and technology*, vol. 43, no. 4, pp. 379–387, 1992.
[88] R. Andrews and M. C. Weisenberger, "Carbon nanotube polymer composites," *Current Opinion in Solid State and Materials Science*, vol. 8, no. 1, pp. 31–37, 2004.
[89] M. K. Yeh, N. H. Tai, and J. H. Liu, "Mechanical behavior of phenolic-based composites reinforced with multi-walled carbon nanotubes," *Carbon*, vol. 44, no. 1, pp. 1–9, 2006.

[90] X. Xu, M. M. Thwe, C. Shearwood, and K. Liao, "Mechanical properties and interfacial characteristics of carbon-nanotube-reinforced epoxy thin films," *Applied physics letters*, vol. 81, p. 2833, 2002.
[91] H. D. Wagner and R. A. Vaia, "Nanocomposites: issues at the interface," *Materials today*, vol. 7, no. 11, pp. 38–42, 2004.
[92] H. Daniel Wagner, "Nanotube-polymer adhesion: a mechanics approach," *Chemical Physics Letters*, vol. 361, no. 1-2, pp. 57–61, 2002.
[93] F. Dalmas, R. Dendievel, L. Chazeau, J. Y. Cavaillé, and C. Gauthier, "Carbon nanotube-filled polymer composites. Numerical simulation of electrical conductivity in three-dimensional entangled fibrous networks," *Acta materialia*, vol. 54, no. 11, pp. 2923–2931, 2006.
[94] C. Li, E. T. Thostenson, and T. W. Chou, "Dominant role of tunneling resistance in the electrical conductivity of carbon nanotube–based composites," *Applied Physics Letters*, vol. 91, p. 223114, 2007.
[95] C. Li, E. T. Thostenson, and T. W. Chou, "Effect of nanotube waviness on the electrical conductivity of carbon nanotube-based composites," *Composites Science and Technology*, vol. 68, no. 6, pp. 1445–1452, 2008.
[96] K. K. Mohanty, "The near-term energy challenge," *AIChE journal*, vol. 49, no. 10, pp. 2454–2460, 2003.
[97] G. Che, B. B. Lakshmi, E. R. Fisher, and C. R. Martin, "Carbon nanotubule membranes for electrochemical energy storage and production," *Nature*, vol. 393, no. 6683, pp. 346–349, 1998.
[98] J. M. Tarascon and M. Armand, "Issues and challenges facing rechargeable lithium batteries," *Nature*, vol. 414, no. 6861, pp. 359–367, 2001.
[99] B. E. Conway, "Transition from 'supercapacitor' to 'battery' behavior in electrochemical energy storage," *Journal of the Electrochemical Society*, vol. 138, p. 1539, 1991.
[100] C. T. White and T. N. Todorov, "Carbon nanotubes as long ballistic conductors," *Nature*, vol. 393, no. 6682, pp. 240–242, 1998.
[101] C. Dekker and others, "Carbon nanotubes as molecular quantum wires," *Physics Today*, vol. 52, pp. 22–30, 1999.
[102] S. J. Tans et al., "Individual single-wall carbon nanotubes as quantum wires," *Nature*, vol. 386, no. 6624, pp. 474–477, 1997.
[103] S. Badaire et al., "Correlation of properties with preferred orientation in coagulated and stretch-aligned single-wall carbon nanotubes," *Journal of applied physics*, vol. 96, no. 12, pp. 7509–7513, 2004.
[104] J. Steinmetz, M. Glerup, M. Paillet, P. Bernier, and M. Holzinger, "Production of pure nanotube fibers using a modified wet-spinning method," *Carbon*, vol. 43, no. 11, pp. 2397–2400, 2005.
[105] M. E. Kozlov, R. C. Capps, W. M. Sampson, V. H. Ebron, J. P. Ferraris, and R. H. Baughman, "Spinning Solid and Hollow Polymer-Free Carbon Nanotube Fibers," *Advanced Materials*, vol. 17, no. 5, pp. 614–617, 2005.
[106] E. Y. Jang et al., "Macroscopic Single-Walled-Carbon-Nanotube Fiber Self-Assembled by Dip-Coating Method," *Advanced materials*, vol. 21, no. 43, pp. 4357–4361, 2009.

[107] X. H. Zhong et al., "Continuous multilayered carbon nanotube yarns," *Advanced Materials*, vol. 22, no. 6, pp. 692–696, 2010.
[108] X. Zhang et al., "Strong carbon-nanotube fibers spun from long carbon-nanotube arrays," *Small*, vol. 3, no. 2, p. 244, 2007.
[109] K. Liu et al., "Scratch-Resistant, Highly Conductive, and High-Strength Carbon Nanotube-Based Composite Yarns," *ACS nano*, 2010.
[110] C. A. May, *Epoxy resins: chemistry and technology*. CRC, 1988.
[111] L. Valentini, I. Armentano, D. Puglia, and J. M. Kenny, "Dynamics of amine functionalized nanotubes/epoxy composites by dielectric relaxation spectroscopy," *Carbon*, vol. 42, no. 2, pp. 323-329, 2004.
[112] L. Ci and J. B. Bai, "The reinforcement role of carbon nanotubes in epoxy composites with different matrix stiffness," *Composites Science and Technology*, vol. 66, no. 3-4, pp. 599–603, 2006.
[113] S. B. Sinnott, "Chemical functionalization of carbon nanotubes," *Journal of Nanoscience and Nanotechnology*, vol. 2, no. 2, pp. 113–123, 2002.
[114] S. Banerjee, T. Hemraj-Benny, and S. S. Wong, "Covalent surface chemistry of single-walled carbon nanotubes," *Advanced Materials*, vol. 17, no. 1, pp. 17–29, 2005.
[115] A. Kuznetsova et al., "Oxygen-containing functional groups on single-wall carbon nanotubes: NEXAFS and vibrational spectroscopic studies," *Journal of the American Chemical Society*, vol. 123, no. 43, pp. 10699–10704, 2001.
[116] Y. Ying, R. K. Saini, F. Liang, A. K. Sadana, and W. E. Billups, "Functionalization of carbon nanotubes by free radicals," *Organic letters*, vol. 5, no. 9, pp. 1471–1473, 2003.
[117] Y. Liu, Z. Yao, and A. Adronov, "Functionalization of single-walled carbon nanotubes with well-defined polymers by radical coupling," *Macromolecules*, vol. 38, no. 4, pp. 1172–1179, 2005.
[118] V. N. Khabashesku, W. E. Billups, and J. L. Margrave, "Fluorination of single-wall carbon nanotubes and subsequent derivatization reactions," *Accounts of chemical research*, vol. 35, no. 12, pp. 1087–1095, 2002.
[119] M. X. Pulikkathara, O. V. Kuznetsov, and V. N. Khabashesku, "Sidewall covalent functionalization of single wall carbon nanotubes through reactions of fluoronanotubes with urea, guanidine, and thiourea," *Chemistry of Materials*, vol. 20, no. 8, pp. 2685–2695, 2008.
[120] L. Zeng, L. Zhang, and A. R. Barron, "Tailoring Aqueous Solubility of Functionalized Single-Wall Carbon Nanotubes over a Wide pH Range through Substituent Chain Length," *Nano Letters*, vol. 5, no. 10, pp. 2001-2004, Oct. 2005.
[121] E. A. Englund, H. N. Gopi, and D. H. Appella, "An efficient synthesis of a probe for protein function: 2, 3-Diaminopropionic acid with orthogonal protecting groups," *Organic Letters*, vol. 6, no. 2, pp. 213–215, 2004.
[122] D. M. Shendage, R. Fr\öhlich, and G. Haufe, "Highly efficient stereoconservative amidation and deamidation of α-amino acids," *Organic Letters*, vol. 6, no. 21, pp. 3675–3678, 2004.
[123] T. W. Greene, P. G. M. Wuts, and I. NetLibrary, "Protective groups in organic synthesis," 1999.

[124] M. S. Strano et al., "Electronic structure control of single-walled carbon nanotube functionalization," *Science*, vol. 301, no. 5639, p. 1519, 2003.
[125] J. L. Hudson, M. J. Casavant, and M. James, "Water-soluble, exfoliated, nonroping single-wall carbon nanotubes," *Journal of the American Chemical Society*, vol. 126, no. 36, pp. 11158–11159, 2004.
[126] M. F. Budyka, T. S. Zyubina, A. G. Ryabenko, S. H. Lin, and A. M. Mebel, "Bond lengths and diameters of armchair single wall carbon nanotubes," *Chemical physics letters*, vol. 407, no. 4-6, pp. 266–271, 2005.
[127] P. M. Ajayan, L. S. Schadler, C. Giannaris, and A. Rubio, "Single-walled carbon nanotube–polymer composites: strength and weakness," *Advanced Materials*, vol. 12, no. 10, pp. 750–753, 2000.
[128] L. E. Nielsen and R. F. Landel, *Mechanical properties of polymers and composites*, vol. 90. CRC Press, 1994.
[129] Y. Wang, F. Wei, G. Luo, H. Yu, and G. Gu, "The large-scale production of carbon nanotubes in a nano-agglomerate fluidized-bed reactor," *Chemical Physics Letters*, vol. 364, no. 5-6, pp. 568–572, 2002.
[130] Y. Wang, F. Wei, G. Gu, and H. Yu, "Agglomerated carbon nanotubes and its mass production in a fluidized-bed reactor," *Physica B: Condensed Matter*, vol. 323, no. 1-4, pp. 327–329, 2002.
[131] F. Wei et al., "The mass production of carbon nanotubes using a nano-agglomerate fluidized bed reactor: A multiscale space-time analysis," *Powder Technology*, vol. 183, no. 1, pp. 10–20, 2008.
[132] A. Jorio, G. Dresselhaus, and M. S. Dresselhaus, *Carbon nanotubes: advanced topics in the synthesis, structure, properties and applications*, vol. 111. Springer Verlag, 2008.
[133] T. McNally et al., "Polyethylene multiwalled carbon nanotube composites," *Polymer*, vol. 46, no. 19, pp. 8222–8232, 2005.
[134] P\ötschke, A. R. Bhattacharyya, and A. Janke, "Melt mixing of polycarbonate with multiwalled carbon nanotubes: microscopic studies on the state of dispersion," *European polymer journal*, vol. 40, no. 1, pp. 137–148, 2004.
[135] P\ötschke, H. Br\ünig, A. Janke, D. Fischer, and D. Jehnichen, "Orientation of multiwalled carbon nanotubes in composites with polycarbonate by melt spinning," *Polymer*, vol. 46, no. 23, pp. 10355–10363, 2005.
[136] P. P\ötschke, A. R. Bhattacharyya, and A. Janke, "Morphology and electrical resistivity of melt mixed blends of polyethylene and carbon nanotube filled polycarbonate," *Polymer*, vol. 44, no. 26, pp. 8061–8069, 2003.
[137] R. Haggenmueller, J. E. Fischer, and K. I. Winey, "Single wall carbon nanotube/polyethylene nanocomposites: nucleating and templating polyethylene crystallites," *Macromolecules*, vol. 39, no. 8, pp. 2964–2971, 2006.
[138] B. Z. Tang and H. Xu, "Preparation, alignment, and optical properties of soluble poly (phenylacetylene)-wrapped carbon nanotubes," *Macromolecules*, vol. 32, no. 8, pp. 2569–2576, 1999.
[139] M. Eder and A. Wlochowicz, "Kinetics of non-isothermal crystallization of polyethylene and polypropylene," *Polymer*, vol. 24, no. 12, pp. 1593–1595, 1983.

[140] B. P. Grady, F. Pompeo, R. L. Shambaugh, and D. E. Resasco, "Nucleation of polypropylene crystallization by single-walled carbon nanotubes," *The Journal of Physical Chemistry B*, vol. 106, no. 23, pp. 5852–5858, 2002.

[141] J. Yang et al., "Direct Formation of Nanohybrid Shish-Kebab in the Injection Molded Bar of Polyethylene/Multiwalled Carbon Nanotubes Composite," *Macromolecules*, vol. 42, no. 18, pp. 7016–7023, 2009.

[142] J. F. Vega et al., "Rheology, Processing, Tensile Properties, and Crystallization of Polyethylene/Carbon Nanotube Nanocomposites," *Macromolecules*, vol. 42, no. 13, pp. 4719–4727, 2009.

[143] L. Hubert, L. David, R. Seguela, G. Vigier, C. Degoulet, and Y. Germain, "Physical and mechanical properties of polyethylene for pipes in relation to molecular architecture. I. Microstructure and crystallisation kinetics," *Polymer*, vol. 42, no. 20, pp. 8425–8434, 2001.

[144] K. Cho, B. H. Lee, K. M. Hwang, H. Lee, and S. Choe, "Rheological and mechanical properties in polyethylene blends," *Polymer Engineering & Science*, vol. 38, no. 12, pp. 1969–1975, 1998.

[145] W. Bauhofer and J. Z. Kovacs, "A review and analysis of electrical percolation in carbon nanotube polymer composites," *Composites Science and Technology*, vol. 69, no. 10, pp. 1486–1498, 2009.

[146] Q. Zhang, S. Rastogi, D. Chen, D. Lippits, and P. J. Lemstra, "Low percolation threshold in single-walled carbon nanotube/high density polyethylene composites prepared by melt processing technique," *Carbon*, vol. 44, no. 4, pp. 778–785, 2006.

[147] W. Tang, M. H. Santare, and S. G. Advani, "Melt processing and mechanical property characterization of multi-walled carbon nanotube/high density polyethylene (MWNT/HDPE) composite films," *Carbon*, vol. 41, no. 14, pp. 2779–2785, 2003.

[148] S. Zhang, M. L. Minus, L. Zhu, C. P. Wong, and S. Kumar, "Polymer transcrystallinity induced by carbon nanotubes," *Polymer*, vol. 49, no. 5, pp. 1356–1364, 2008.

[149] Y. Wang, H. Shan, R. H. Hauge, M. Pasquali, and R. E. Smalley, "A highly selective, one-pot purification method for single-walled carbon nanotubes," *The Journal of Physical Chemistry B*, vol. 111, no. 6, pp. 1249–1252, 2007.

[150] C. A. Martin et al., "Formation of percolating networks in multi-wall carbon-nanotube-epoxy composites," *Composites Science and Technology*, vol. 64, no. 15, pp. 2309–2316, 2004.

[151] Z. Ounaies, "Electrical properties of single wall carbon nanotube reinforced polyimide composites," *Composites Science and Technology*, vol. 63, no. 11, pp. 1637-1646, Aug. 2003.

[152] A. Allaoui, S. Bai, H. M. Cheng, and J. B. Bai, "Mechanical and electrical properties of a MWNT/epoxy composite," *Composites Science and Technology*, vol. 62, no. 15, pp. 1993-1998, Nov. 2002.

[153] J. Sandler, M. S. P. Shaffer, T. Prasse, W. Bauhofer, K. Schulte, and A. H. Windle, "Development of a dispersion process for carbon nanotubes in an epoxy matrix and the resulting electrical properties," *Polymer*, vol. 40, no. 21, pp. 5967-5971, Oct. 1999.

[154] J. K. W. Sandler, J. E. Kirk, I. A. Kinloch, M. S. P. Shaffer, and A. H. Windle, "Ultra-low electrical percolation threshold in carbon-nanotube-epoxy composites," *Polymer*, vol. 44, no. 19, pp. 5893-5899, Sep. 2003.

[155] Y. Yu, G. Song, and L. Sun, "Determinant role of tunneling resistance in electrical conductivity of polymer composites reinforced by well dispersed carbon nanotubes," *Journal of Applied Physics*, vol. 108, p. 084319, 2010.

[156] C. L. Kane et al., "Temperature-dependent resistivity of single-wall carbon nanotubes," *Europhysics Letters (EPL)*, vol. 41, no. 6, pp. 683-688, Mar. 1998.

[157] J. E. Fischer et al., "Metallic resistivity in crystalline ropes of single-wall carbon nanotubes," *Physical Review B*, vol. 55, no. 8, pp. 4921–4924, 1997.

[158] A. B. Kaiser, G. D\üsberg, and S. Roth, "Heterogeneous model for conduction in carbon nanotubes," *Physical Review B*, vol. 57, no. 3, p. 1418, 1998.

[159] P. Sheng, "Fluctuation-induced tunneling conduction in disordered materials," *Physical Review B*, vol. 21, no. 6, p. 2180, 1980.

[160] V. K. Ksenevich et al., "Localization and nonlinear transport in single walled carbon nanotube fibers," *Journal of Applied Physics*, vol. 104, no. 7, pp. 073724-073724-7, Oct. 2008.

[161] A. L. Efros and B. I. Shklovskii, "Electronic properties of doped semiconductors," *Springer Series in Solid-State Sciences, Springer, Berlin*, 1984.

[162] M. Sahimi, *Applications of percolation theory*. CRC Press, 1994.

[163] D. Stauffer and A. Aharony, *Introduction to percolation theory*. CRC, 1994.

[164] D. S. McLachlan, M. Blaszkiewicz, and R. E. Newnham, "Electrical resistivity of composites," *Journal of the American Ceramic Society*, vol. 73, no. 8, pp. 2187–2203, 1990.

[165] Z. Ounaies, C. Park, K. E. Wise, E. J. Siochi, and J. S. Harrison, "Electrical properties of single wall carbon nanotube reinforced polyimide composites," *Composites Science and Technology*, vol. 63, no. 11, pp. 1637–1646, 2003.

[166] R. Haggenmueller, H. H. Gommans, A. G. Rinzler, J. E. Fischer, and K. I. Winey, "Aligned single-wall carbon nanotubes in composites by melt processing methods," *Chemical Physics Letters*, vol. 330, no. 3-4, pp. 219–225, 2000.

[167] S. Hooshmand, A. Soroudi, and M. Skrifvars, "Electro-conductive composite fibers by melt spinning of polypropylene/polyamide/carbon nanotubes," *Synthetic Metals*, vol. 161, no. 15-16, pp. 1731-1737, Aug. 2011.

[168] Z. Li, G. Luo, F. Wei, and Y. Huang, "Microstructure of carbon nanotubes/PET conductive composites fibers and their properties," *Composites Science and Technology*, vol. 66, no. 7-8, pp. 1022-1029, Jun. 2006.

[169] T. E. Chang, A. Kisliuk, S. M. Rhodes, W. J. Brittain, and A. P. Sokolov, "Conductivity and mechanical properties of well-dispersed single-wall carbon nanotube/polystyrene composite," *Polymer*, vol. 47, no. 22, pp. 7740–7746, 2006.

[170] B. H. Cipriano et al., "Conductivity enhancement of carbon nanotube and nanofiber-based polymer nanocomposites by melt annealing," *Polymer*, vol. 49, no. 22, pp. 4846–4851, 2008.

[171] I. Alig, D. Lellinger, S. M. Dudkin, and P. P\ötschke, "Conductivity spectroscopy on melt processed polypropylene-multiwalled carbon nanotube composites: Recovery after shear and crystallization," *Polymer*, vol. 48, no. 4, pp. 1020–1029, 2007.

[172] U. Dettlaff-Weglikowska et al., "Effect of SOCl2 treatment on electrical and mechanical properties of single-wall carbon nanotube networks," *Journal of the American Chemical Society*, vol. 127, no. 14, pp. 5125–5131, 2005.

[173] V. Skakalova, U. Dettlaff-Weglikowska, and S. Roth, "Electrical and mechanical properties of nanocomposites of single wall carbon nanotubes with PMMA," *Synthetic metals*, vol. 152, no. 1-3, pp. 349–352, 2005.

[174] C. K. Najeeb, J. H. Lee, J. Chang, and J. H. Kim, "Evaluation of SOCl2 Doping Effect on Electrical Conductivity of Thin Films of SWNTs and SWNT/PEDOT-PSS Composites," *Journal of Nanoscience and Nanotechnology*, vol. 11, no. 7, pp. 5839–5844, 2011.

[175] M. Breza, "Model studies of SOCl2 adsorption on carbon nanotubes," *Journal of Molecular Structure: THEOCHEM*, vol. 767, no. 1-3, pp. 159–163, 2006.

[176] X. Zhang et al., "Ultrastrong, stiff, and lightweight carbon-nanotube fibers," *Advanced Materials*, vol. 19, no. 23, pp. 4198–4201, 2007.

[177] H. G. Chae and S. Kumar, "Making strong fibers," *Science*, vol. 319, no. 5865, p. 908, 2008.

[178] V. A. Davis et al., "True solutions of single-walled carbon nanotubes for assembly into macroscopic materials," *Nature Nanotechnology*, vol. 4, no. 12, pp. 830–834, 2009.

[179] M. Naraghi, T. Filleter, A. Moravsky, M. Locascio, R. O. Loutfy, and H. D. Espinosa, "A Multiscale Study of High Performance Double-Walled Nanotube-Polymer Fibers," *ACS nano*, 2010.

[180] J. Wei et al., "Preparation of highly pure double-walled carbon nanotubes," *Journal of Materials Chemistry*, vol. 13, no. 6, pp. 1340–1344, 2003.

[181] L. Ci et al., "Double wall carbon nanotubes promoted by sulfur in a floating iron catalyst CVD system," *Chemical physics letters*, vol. 359, no. 1-2, pp. 63–67, 2002.

[182] Z. Zhou et al., "Controllable growth of double wall carbon nanotubes in a floating catalytic system," *Carbon*, vol. 41, no. 2, pp. 337–342, 2003.

[183] V. Georgakilas et al., "Purification of HiPCO carbon nanotubes via organic functionalization," *Journal of the American Chemical Society*, vol. 124, no. 48, pp. 14318–14319, 2002.

[184] R. S. Lee, H. J. Kim, J. E. Fischer, A. Thess, and R. E. Smalley, "Conductivity enhancement in single-walled carbon nanotube bundles doped with K and Br," *Nature*, vol. 388, no. 6639, pp. 255–256, 1997.

[185] L. Grigorian et al., "Reversible intercalation of charged iodine chains into carbon nanotube ropes," *Physical review letters*, vol. 80, no. 25, pp. 5560–5563, 1998.

[186] J. E. Fischer, "Chemical doping of single-wall carbon nanotubes," *Accounts of chemical research*, vol. 35, no. 12, pp. 1079–1086, 2002.

[187] S. Niyogi et al., "Chemistry of single-walled carbon nanotubes," *Accounts of Chemical Research*, vol. 35, no. 12, pp. 1105–1113, 2002.

[188] L. Kumari, V. Prasad, and S. V. Subramanyam, "Effect of iodine incorporation on the electrical properties of amorphous conducting carbon films," *Carbon*, vol. 41, no. 9, pp. 1841–1846, 2003.

[189] J. Cambedouzou, J. L. Sauvajol, A. Rahmani, E. Flahaut, A. Peigney, and C. Laurent, "Raman spectroscopy of iodine-doped double-walled carbon nanotubes," *Physical Review B*, vol. 69, no. 23, p. 235422, 2004.

[190] K. R. Kissell, K. B. Hartman, P. A. W. Van der Heide, and L. J. Wilson, "Preparation of I2@ SWNTs: synthesis and spectroscopic characterization of I2-loaded SWNTs," *The Journal of Physical Chemistry B*, vol. 110, no. 35, pp. 17425–17429, 2006.

[191] T. Michel et al., "Structural selective charge transfer in iodine-doped carbon nanotubes," *Journal of Physics and Chemistry of Solids*, vol. 67, no. 5-6, pp. 1190–1192, 2006.

[192] F. Khoerunnisa et al., "Electronically modified single wall carbon nanohorns with iodine adsorption," *Chemical Physics Letters*, vol. 501, no. 4-6, pp. 485-490, Jan. 2011.

[193] W. Zhou et al., "Raman scattering and thermogravimetric analysis of iodine-doped multiwall carbon nanotubes," *Applied physics letters*, vol. 80, p. 2553, 2002.

[194] W. I. Choi, J. Ihm, and G. Kim, "Modification of the electronic structure in a carbon nanotube with the charge dopant encapsulation," *Applied Physics Letters*, vol. 92, p. 193110, 2008.

[195] R. Pfeiffer, T. Pichler, Y. Kim, and H. Kuzmany, "Double-wall carbon nanotubes," *Carbon Nanotubes*, pp. 495–530, 2008.

[196] Y. A. Kim, H. Muramatsu, T. Hayashi, M. Endo, M. Terrones, and M. S. Dresselhaus, "Fabrication of High-Purity, Double-Walled Carbon Nanotube Buckypaper," *Chemical Vapor Deposition*, vol. 12, no. 6, pp. 327–330, 2006.

[197] U. S. B. of Standards, *Copper wire tables*. Government Printing Office, 1914.

[198] B. Q. Wei, R. Vajtai, and P. M. Ajayan, "Reliability and current carrying capacity of carbon nanotubes," *Applied Physics Letters*, vol. 79, p. 1172, 2001.

[199] J. Ma, J. Tang, H. Zhang, N. Shinya, and L. C. Qin, "Ultrathin Carbon Nanotube Fibrils of High Electrochemical Capacitance," *ACS nano*, vol. 3, no. 11, pp. 3679–3683, 2009.

[200] R. Murali, Y. Yang, K. Brenner, T. Beck, and J. D. Meindl, "Breakdown current density of graphene nanoribbons," *Applied Physics Letters*, vol. 94, p. 243114, 2009.

[201] Preece, W.H. *Royal Soc. Proc.* **36**, 464, (1884).

Appendix

Appendix A:

We suggest that there are majorly two reasons for the enhancement of conductivity of nanotubes by the iodine doping. First, the energy band of DWNT is altered by the iodine doping. Second, the iodine doping increases density of mobile holes. In the iodine doped DWNT fiber, the iodine as acceptors form $(I_3)^-$ and $(I_5)^-$ polyiodide chains in the intercalated sites, meanwhile, mobile holes are created in the DWNTs [Grigorian, L. et al. Phys. Rev. Letts. **80** (25), 5560-5563 (1998)]. In addition, the dominant charge carriers are holes in the DWNT sample. Therefore the iodine doping increases density of mobile holes and hence enhances conductivity of the DWNT fibers.

XRD spectra were collected for both the iodine doped and the undoped cables (figure 6.18). After doping, the (002) peak at $2\theta \sim 10.86^{o}$ corresponding to the inter-layer spacing between the outer and inner walls shifts to the higher angle. The shift indicates suppression of the inter-layer spacing from 3.76 Å to 3.63 Å. XRD data could be direct indication of charge transfer and covalent bond formation.

The peak corresponding to the tube-tube distances overlaps the peak corresponding to the inter-layer spacing, but is much smaller in magnitude (figure A1 gives the explanation).

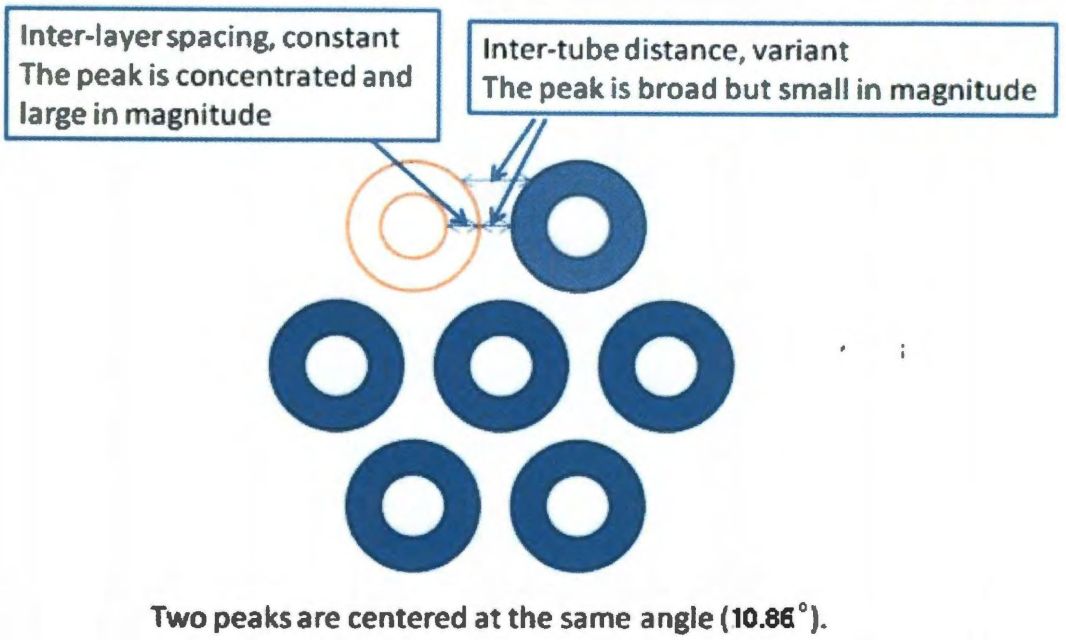

Figure A1. Schematics of the DWNT bundle, which gives the explanation of the XRD pattern.

In this thesis, Mo target was used to generate the X-ray, which has wavelength of 0.7107 Å. The x-ray spectrum of the raw DWNTs shown in this thesis is consistent with the result reported by Futaba DN etc. (J. AM. Chem. Soc. 2011, 133, 5716-5719) as shown in figure A2. In their research, Cu Kα is the X-ray source (λ = 1.5418 Å). The peak with 2θ at around 26° is corresponding to the crystal lattice of 3.6 Å. The peak was decomposed into two peaks. The one with lower intensity (indicated by dotted red line) is attributed to the inter-tube spacings (broad and relatively low in intensity). The other one with higher intensity (indicated by solid blue line) is ascribed to the inter-layer spacings. The finding gives a good explanation why not a single peak corresponding to inter-tube spacings can be separately identified.

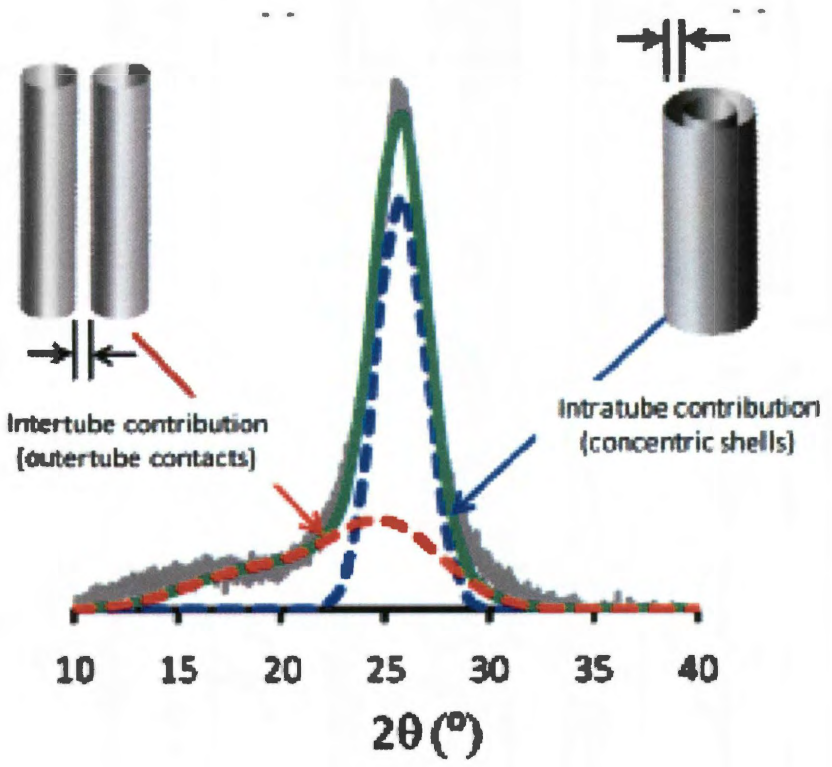

Figure A2. Conceptual illustration of the decomposition of the total (002) peak (green) into the two basic contributions: (red) intertube structure (outer-wall contacts) and (blue) intratube structure (concentric shells).

Appendix B:

The electronic mean free path of the nanotube cable can be calculated by the formula [S. Datta, Electronic transport in mesoscopic systems. Cambridge Univ Pr, 1997.] :

$$R = \frac{h}{2e^2 N}\frac{L}{\lambda} \qquad (1)$$

, where h is the Planck constant, L is the length of the cable, R is the resistance of the cable, N is the number of the conductance channels, and λ is electronic mean free path.

Take the cable (as shown in figure 6.7) as an example, whose resistance R is 114 Ω, length L is 0.65 cm and diameter is 4.22 μm.

From the TEM image, we know that the average diameter of the DWNTs is about 2.5 nm. If assume that every single nanotube contributes a conductance channel and all the nanotubes are densely packed in a hexagonal fashion. The number of conductance channels, N can be calculated as:

$$N = \frac{\pi D^2}{\pi d^2}\eta \qquad (2)$$

, where D is diameter of the cable, d is the average diameter of the DWNTs, and η is the packing ratio for dense hexagonal packing.

$$N = \frac{\pi(4.22\ \mu m)^2}{\pi(2.5\ nm)^2} \times 0.906 = 2.58 * 10^6$$

Plug R = 114 Ω, L = 0.65 cm and N = $2.58*10^6$ into the equation (1), we can obtain electronic mean free path

$$\lambda \approx 0.29\ \mu m$$

In the real nanotube cable, the number of conductance channels is less than that in the assumed scenario because the packing density is not as high as that in the dense hexagonal packing and not every tube-tube junction can be a conductance channel. Therefore, the real electronic mean free path could be a few times larger than 0.29 μm. This finding is consistent with the mean free path as 1.6 μm measured by J.Y.Park et al. for a metallic single-walled carbon nanotube [J. Y. Park et al., "Electron-phonon scattering in metallic single-walled carbon nanotubes," *Nano Letters*, vol. 4, no. 3, pp. 517–520, 2004.].

Appendix C:

Compare current carrying capacity between the DWNT cable and the copper wire of the same diameter.

W. H. Preece gave the equation for calculating the fuse current for wires in air, $I = A*D^{3/2}$, where A is a constant depending on the metal and D is the diameter for the wire [W.H.Preece, Royal Soc. Proc., 36, pp. 464, 1884.]. For copper, A = 80 (D in mm). Plug D = 4.2 microns into the formula, we get I = 21.8 mA and current carrying capacity as $1.57*10^5$ A/cm^2.

Compared to the cable as shown in figure 6.7 (diameter = 4.2 microns, fuse current = 22.5 mA and current carrying capacity = $1.62*10^5$ A/cm^2), the copper wire of the same diameter has slightly smaller current carrying capacity than that of the DWNT cable.

Appendix D:

Instruction for the following table:

In the name column, the samples are named in the format: D******_#, where "******" indicates the date when the samples were prepared and "#" indicates the sample number.

In the doping column, "U" indicates that the sample was not doped. "D" indicates that the sample was doped by iodine.

In the batch column, "TH_w1" and "TH_w2" individually indicate the nanotubes were grown in Tsinghua University during the week from July, 1st to July, 8th and the other week from July, 9th to July 16th. "TH_old" indicates that nanotubes what were brought by Professor Jinquan Wei from Tsinghua University.

Name	Resistance (Ohm)	Length (mm)	Diameter (microns)	Resistivity (Ohm.cm)	Doping	Batch	Solution used for shrinking the fibers	Other treatment
D092111_1	408	25.5	12.0	1.81E-04	U	TH_w1	H2O	
D092111_2	6.2	27.5	130.0	2.99E-04	U	TH_w1	H2O	
D092511_1	50	12.9	19.0	1.10E-04	D	TH_w2	H2O	
D092511_2	16.6	5.2	20.0	1.00E-04	D	TH_w2	H2O	
D092511_3	38	7.8	16.0	9.80E-05	D	TH_w2	H2O	
D092511_4	60	8.4	13.0	9.48E-05	D	TH_w2	H2O	
D092511_5	55	9.3	21.0	2.05E-04	D	TH_w2	H2O	
D093011_1	233	7.8	6.0	8.45E-05	u	TH_w2	H2SO4	
D093011_2	185	6	8.5	1.75E-04	u	TH_w2	H2SO4	
D093011_3	297	5	5.5	1.41E-04	u	TH_w2	H2SO4	
D093011_4	335	7.5	5.6	1.10E-04	u	TH_w2	H2SO4	
D093011_5	132	5.45	8.0	1.22E-04	u	TH_w2	H2SO4	
D093011_6	230	4.6	5.0	9.82E-05	u	TH_w2	H2SO4	
D100111_1	90.5	11.4	7.3	3.32E-05	D	TH_w2	H2SO4	
D100111_2	104	10	8.8	6.33E-05	D	TH_w2	H2SO4	
D100111_3	242	9.75	10.0	1.95E-04	D	TH_w2	H2SO4	
D100311_2	472	7.98	6.5	1.96E-04	u	TH_w2	DMSO	
D100311_3	288	22.72	7.5	5.60E-05	u	TH_w2	DMSO	
D100611_1	190	5.93	6.0	9.06E-05	u	TH_w2	DMSO	
D100611_2	68.8	9.38	12.0	8.30E-05	u	TH_w2	DMSO	
D101011_1	104	8.44	8.0	6.19E-05	D	TH_w2	DMSO	

D101011_2	156	10.68	9.5	1.04E-04	D	TH_w2	DMSO	
D101011_3	153	9.35	7.5	7.23E-05	D	TH_w2	DMSO	
D101011_1	5600	15.61	2.0	1.13E-04	u	TH_w2	DMSO	
D101011_2	2484	8.82	2.5	1.38E-04	u	TH_w2	DMSO	
D110110_1	450	7	4.2	8.91E-05	u	TH_old	H2O	
D110110_2	125	5	5.5	5.94E-05	u	TH_old	H2O	
D110110_3	115	5	6.5	7.63E-05	u	TH_old	H2O	
D110110_4	268	7	4.5	6.09E-05	u	TH_old	H2O	
D110110_5	57	6.8	10.0	6.58E-05	u	TH_old	H2O	
D111510_1	213	6.5	4.9	6.18E-05	u	TH_old	H2O	
D111510_2	162	6.5	6.5	8.27E-05	u	TH_old	H2O	
D111510_3	114	6.5	6.9	6.56E-05	u	TH_old	H2O	
D111510_4	149	6.5	7.4	9.86E-05	u	TH_old	H2O	
D111510_5	276	6.5	7.5	1.88E-04	u	TH_old	H2O	
D111510_6	441	6.5	4.5	1.08E-04	u	TH_old	H2O	
D120310_1	86	6.5	8.2	6.99E-05	D	TH_old	H2SO4	
D120310_2	44	6.5	8.2	3.57E-05	D	TH_old	H2SO4	
D120310_3	226	6.5	4.1	4.59E-05	D	TH_old	H2SO4	
D120310_4	41	6.5	12.8	8.12E-05	D	TH_old	H2SO4	
D120710_1	32	6.5	7.7	2.29E-05	D	TH_old	H2SO4	
D120710_5	62	6.5	8.5	5.41E-05	D	TH_old	H2SO4	
D120710_6	62	6.5	12.0	1.08E-04	D	TH_old	H2SO4	
D120710_7	32	6.5	9.0	3.13E-05	D	TH_old	H2SO4	
D122510_1	30	80	60.0	1.06E-04	D	TH_old	H2SO4	
D011611_1	37	1.4	5.9	7.23E-05	D	TH_old	H2SO4	
D011611_2	96.3	6.8	5.1	2.89E-05	D	TH_old	H2SO4	
D011611_3	42.8	6.8	5.6	1.55E-05	D	TH_old	H2SO4	
D011611_4	13	1.3	11.5	1.04E-04	D	TH_old	H2SO4	
D020311_1	94.3	6.5	8.5	8.23E-05	u	TH_old	H2SO4	
D020311_2	177.4	6.6	7.0	1.03E-04	u	TH_old	H2SO4	
D020311_3	51.58	6.6	16.0	1.57E-04	u	TH_old	H2SO4	
D020311_4	73.02	6.6	16.0	2.22E-04	u	TH_old	H2SO4	
D020311_5	31.12	6.5	12.0	5.41E-05	u	TH_old	H2SO4	
D020311_6	88.7	6.5	10.0	1.07E-04	u	TH_old	H2SO4	
D020311_7	100.7	7.5	11.5	1.39E-04	D	TH_old	H2SO4	
D020311_8	109	7.5	11.5	1.51E-04	D	TH_old	H2SO4	
D020311_9	43.99	7	13.0	8.34E-05	u	TH_old	H2SO4	
D020311_10	66.3	6.5	11.0	9.69E-05	u	TH_old	H2SO4	
D031311_1	114	6.5	4.2	2.43E-05	u	TH_old	H2SO4	
D031311_2	279	11.5	4.3	3.46E-05	u	TH_old	H2SO4	
D032311_1	525	13.25	7.0	1.52E-04	u	TH_old	H2SO4	

D032311_2	581	17.5	8.1	1.70E-04	u	TH_old	H2SO4	
D032311_3	1140	21.9	7.0	2.00E-04	u	TH_old	H2SO4	
D032311_4	949	14.7	6.5	2.14E-04	u	TH_old	H2SO4	
D032311_5	504	16.5	7.0	1.18E-04	u	TH_old	H2SO4	
D032311_6	859	19.4	8.0	2.23E-04	u	TH_old	H2SO4	
D032311_7	823	6.9	7.0	4.59E-04	u	TH_old	H2SO4	Annealed
D032311_8	441	10.6	7.0	1.60E-04	u	TH_old	H2SO4	Annealed
D032311_9	1130	15.1	8.1	3.84E-04	u	TH_old	H2SO4	Annealed
D032311_10	3610	18.2	7.0	7.63E-04	u	TH_old	H2SO4	Annealed
D032311_11	1200	11	7.0	4.20E-04	u	TH_old	H2SO4	Annealed
D032311_12	1338	8	7.0	6.44E-04	u	TH_old	H2SO4	Annealed
D032311_13	2833	12.8	8.1	1.13E-03	u	TH_old	H2SO4	Annealed
D032311_14	4341	15.9	7.0	1.05E-03	u	TH_old	H2SO4	Annealed
D032311_15	1130	9.3	7.0	4.68E-04	u	TH_old	H2SO4	Annealed
D032611_01	1161	20.8	4.4	8.37E-05	u	TH_old	Chloroform	
D032611_02	1560	20.6	7.8	3.62E-04	u	TH_old	Chloroform	
D032611_03	820	18	6.0	1.29E-04	u	TH_old	Chloroform	
D032611_04	676	17	3.6	4.05E-05	u	TH_old	Chloroform	
D032611_05	593	10.1	4.0	7.38E-05	D	TH_old	Chloroform	
D032611_06	502	7.33	3.8	7.77E-05	D	TH_old	Chloroform	
D032611_07	729	13.2	4.4	8.28E-05	D	TH_old	Chloroform	
D032611_08	714	13.1	7.8	2.60E-04	D	TH_old	Chloroform	
D032611_09	304	10.6	6.0	8.11E-05	D	TH_old	Chloroform	
D032611_10	558	9.6	3.6	5.92E-05	D	TH_old	Chloroform	
D041211_1	432	6.39	4.5	1.08E-04	u	TH_old	H2SO4	
D041211_2	1285	8.9	2.5	7.09E-05	u	TH_old	H2SO4	
D041211_3	259	6.68	8.0	1.95E-04	u	TH_old	H2SO4	
D041211_4	473	8.35	9.0	3.60E-04	u	TH_old	H2SO4	
D041211_5	488	9.45	6.0	1.46E-04	u	TH_old	H2SO4	
D041511_2	248	9	7.5	1.22E-04	u	TH_old	H2SO4	
D041511_3	2360	8.58	4.5	4.37E-04	u	TH_old	H2SO4	
D041911_1	1954	7.15	8.0	1.37E-03	u	TH_old	H2SO4	
D041911_2	1064	5.72	7.9	9.12E-04	u	TH_old	H2SO4	
D041911_3	1675	8.62	6.2	5.87E-04	u	TH_old	H2SO4	
D041911_4	2505	12.9	7.2	7.91E-04	u	TH_old	H2SO4	
D042511_1	425	6.67	5.0	1.25E-04	u	TH_old	H2SO4	
D042511_2	396	18.8	5.0	4.14E-05	D	TH_old	H2SO4	
D042511_3	360	9.28	5.0	7.62E-05	D	TH_old	H2SO4	
D052711_1	480	15.2	5.0	6.20E-05	D	TH_old	H2SO4	
D052711_2	460	11.3	7.5	1.80E-04	u	TH_old	H2SO4	
D052711_3	36	27	35.0	1.28E-04	u	TH_old	H2SO4	